OXIDATION OF COMMERCIALLY PURE Ti AND Ti ALLOYS

By

Mokhotjwa Simon Dhlamini

B.Sc Hons.

This dissertation is presented in fulfilment of the requirements for the degree

Magister Scientiae

In the Faculty of Natural and Agricultural Sciences

Department of Physics

at the

University of the Free State

Bloemfontein

Study leader: Prof. HC Swart

Co-study leader: Dr. JJ Terblans

December 2004

Dedicated to Nonhlanhla Dhlamini and the family

ACKNOWLEDGEMENTS

The author wishes to express his gratitude and special thanks to the following people:

- The all Mighty God, for making impossible things possible for him in this study.
- My parents, sisters and brothers for their support and encouraging me when things were tough.
- My close friends (**"Thabang"**, Sello, Mamale, Mofokeng, George and Ditaba) and fellow students, for being there for me in good and tough times.
- Prof. HC Swart, the author's study leader, for his great ideas and knowledge in the field of the subject.
- Dr. JJ Terblans, the author's co-study leader, for his advice on the subject and making sure that the ESCA system is operating well.
- Prof. WD Roos, from the department of Physics (UFS), for his assistance with fixing the ESCA system.
- Dr. CJ Terblanche, from SOMCHEM, for his contribution in the project.
- Mr. JKO Asante, from the department of Physics (UFS), for his assistance in the extraction of the Auger yield contributions from the combined APPH of the overlapping peaks and his advice and support.
- The National Research Foundation (NRF), the University of the Free State, SOMCHEM and ARMSCOR, for their financial assistance in this research.
- The personnel of the Physics Department (UFS), for their assistance and support.
- The Instrumentation division and Electronics, for their assistance.

ABSTRACT

The surface temperature and composition of commercially pure Ti, Ti6Al4V and Ti3Al8V6Cr4Zr4Mo were monitored during oxidation with AES (Auger electron spectroscopy). Theory suggested the release of large amount of heat by titanium during oxidation process at high oxygen pressures. The AES surface technique was used to investigate if the increase in the surface temperature due to oxidation at lower oxygen pressures is measurable.

The respective samples were cut into specially designed shapes to enable the surface temperature change measurements without affecting the temperature of the sample due to factors other than an exothermic oxidation reaction. Two thermocouples were used in this study, the one spot-welded to the base of the sample and the second one on the surface. There was about 100 °C – 200 °C temperature difference at equilibrium between the base of the sample and the surface temperature. The time delay in temperature change between the surface and base made it possible to measure the changes in surface temperature. The specimens were exposed to oxygen at various temperatures and pressures. The Auger peak-to-peak heights for the specified elements in the specimens were measured as a function of time.

The amount of heat generated during the oxidation was infinitesimally small and no significant change in the surface temperature was measured. However, the theoretical calculated amount of heat generated during the reaction of Ti atoms with oxygen to form TiO_2 layer is 939.7 KJ. The change in the surface temperature for the single layer due to the reaction was calculated to be 34450 °C. For the sample thickness used, 0.9 mm, the calculated amount of heat generated was 0.011°C. The effect of both the electron and the ion beams on the surface temperature was also monitored and it is clear that there was an increase in temperature due to heating by electron beam and ion beam.

The segregation of the impurities (C and S) at the very low oxygen pressures (5×10^{-8} Torr) was also observed. The decrease in the oxidation rate at higher temperatures and lower pressures due to the segregating species and the mean surface lifetime of oxygen on the surface was apparent. No clear difference in the oxidation behaviour amongst the different samples was found. The initial reaction for the three samples followed the parabolic rate law.

The impurity segregation profiles at different constant temperatures (400 °C - 800 °C) and linear heating ramp (0.05 °C/s) were experimentally investigated. It was found that mainly C and S segregated at 400 °C and Cl and S at higher temperatures for the pure Ti sample. Sulfur was however the main segregating specie for all three samples. Aluminium segregation was measured at 800 °C for the Ti6Al4V sample. But due to strong interaction between the S and Al segregating species the surface was immediately covered by S. The linear least square fit method was used to determine the contributions of pure titanium and titanium carbide from the measured APPH's. The AES peak fitting was done and confirmed the formation of TiC on the surface at temperatures 400 °C to 500 °C.

Contents

3. Ignition and explosions of Ti and its alloys

4. Experimental setup

5. Results and discussions

Chapter 1

An overview of Ti and Ti alloys

1.1 Introduction

Titanium, the most abundant element in the earth's crust, has long been of service to mankind. The existence of titanium was first recognised in 1791 by William McGregor, an English mineralogist while analysing black sand from Menachan in Cornwall. He produced a white metallic oxide from the mineral mechanite, a variety of ilmenite, and named the new element menachite. The German chemist, Martin Heinrich Klaproth, in 1795, realised the closely coincided description of the oxide with the properties of an oxide that he had isolated from the sample of Hungarian rutile. Klaproth named the metallic element in the oxide titanium. Impure titanium was prepared by Nilson and Pettersson in 1887; however, the pure metal was not isolated until 1910 when Mathew A. Hunter in the USA produced titanium by the reduction of titanium tetrachloride ($TiCl_4$) with sodium [1].

Titanium tetrachloride is produced by mixing rutile (TiO_2) or ilmenite ($FeTiO_3$) with coke or tar and charged in a chlorinator [1, 2, 3]. Heat is then applied and chlorine gas is passed through the charge. The metal was a laboratory curiosity until Kroll [2, 3, 4] in 1937, in Luxembourg, showed that titanium could be produced commercially by reducing $TiCl_4$ with molten magnesium under an argon atmosphere.

Titanium is not found as a pure metal in nature; it is mainly in chemical combination with oxygen and occurs in some 60 minerals. The most important economical minerals are ilmenite $FeTiO_3$ and the titanium dioxide minerals, rutile, anatase and brookite, which although they have same formula, differ in their crystal structure. The mineral, rutile (TiO_2), is found mainly in sand on beaches along the eastern coast of Australia, estuaries in Sierra Leone and along the coast of northern Natal in South Africa. Since 1940's, its relatively low density (4.505 $Mg.m^{-3}$), high melting point (1678°C), high specific strength, thermal and electrical conductivity, good high temperature properties, corrosion and resistance has led to many applications in the aerospace industry, submarine environments, chemical processing equipment, heat-conducting tubes in vapour generators, nuclear reactors, biomedical implants and food processing and packaging [1 - 8].

An adherent, protective TiO_2 film is said to provide excellent resistance to corrosion, wear and contamination below 535 °C. Above 535 °C, the oxide film breaks down and small atoms such as carbon, nitrogen, and hydrogen embrittle the titanium. Due to its high affinity for oxygen [1, 2, 3, 4, 7], all melting and casting processes have to be carried out under vacuum. Combined with nitrogen, carbon or boron it forms ultra-hard ceramics that can be coated onto cutting tool steels, automotive parts and surgical instruments. The most interesting and useful application is the implantation of pure titanium and titanium alloys into the human body.

Solid materials substitutes for embrittled body parts have given extended moveability and therefore an improved quality of life to the human. At first such aids were only used as external support tools, but with the

advancements in modern medicine during the last century body parts could be substituted internally. Initially, the more commonly known metals were used, but soon modern lightweight metals and alloys were selected for their strength, durability and biocompatibility with the human body. Successful clinical performance of machined commercially pure Ti implants has resulted in a wide spread usage of them [10].

Titanium is allotropic [4, 11], with an hcp crystal structure (α) at low temperatures and a bcc structure (β) above 882 °C. Alloying elements provide solid solution strengthening and change the allotropic transformation temperature. If titanium is doped with elements that improve its strength properties, juvenile fragments are heated to higher temperatures resulting in a decrease in the oxygen pressure at which these fragments can be ignited [4]. The alloying elements can be divided into four groups. Addition of tin (Sn) and zirconium (Zr) provide solid strengthening without affecting the transformation temperature. Aluminium, oxygen, hydrogen, and other alpha stabilising elements increase the temperature at which α transforms to β. Beta stabilisers such as vanadium, tantalum, molybdenum, and niobium lower the transformation temperature causing β to be stable at room temperature.

Finally manganese, chromium, and iron produce a eutectoid reaction, reducing the temperature at which the α-β transformation occurs and producing a two-phase structure at room temperature. α+β Ti alloys present good formability and cold strength at temperatures under 300 °C [12, 13]. In this group, Ti6Al4V has been the main alloy for mechanical components. Aluminium has a strong solid-solution hardening effect on titanium; vanadium stabilizes β phase at room temperature, and makes the alloy more ductile during high temperature processing [12, 14]. Ti-alloy and its products are required to have excellent corrosion resistance to work safely for prolonged periods in high temperatures [15]. Several categories of titanium and its alloys are; commercially pure titanium, alpha titanium alloys, beta alloys and alpha-beta titanium alloys.

1.2 General applications of Ti and Ti alloys

1.2.1 Industrial applications

Titanium and titanium alloys are currently finding increasingly widespread use in many industries due to their combination of very good mechanical properties allied to excellent corrosion and erosion resistance [6, 16]. Titanium alloys capable of operating at temperatures from sub zero to 600 ^{o}C are used in aircraft engines, for discs, computer circuit boards [17], blades, shafts and castings from the front fan to the last stage of the high pressure compressor, and at the rear end of the engine for lightly loaded fabrications such as plug and nozzle assemblies [5]. Alloys with strength up to 1200 MPa are used in a wide variety of airframe applications from small fasteners weighing a few grams to landing gear trucks and large wing beams weighing up to 1 ton. Titanium alloys are also appropriate for application at elevated temperatures [16]. It is difficult to imagine how current levels of performance; engine power to weight ratios; airframe strength; aircraft speed and range and other critical factors could be achieved without titanium.

In military services, it was noted that many military vehicles are heavy due to use of rolled steel armour plating. By use of titanium parts, the weight was reduced at high cost [18]. The use of titanium parts for armoured vehicles was described with examples given of shaping and ballistic performance.
Titanium is also used in the fabrication of the front head covers for missiles as shown in figure 1.1 below [19].

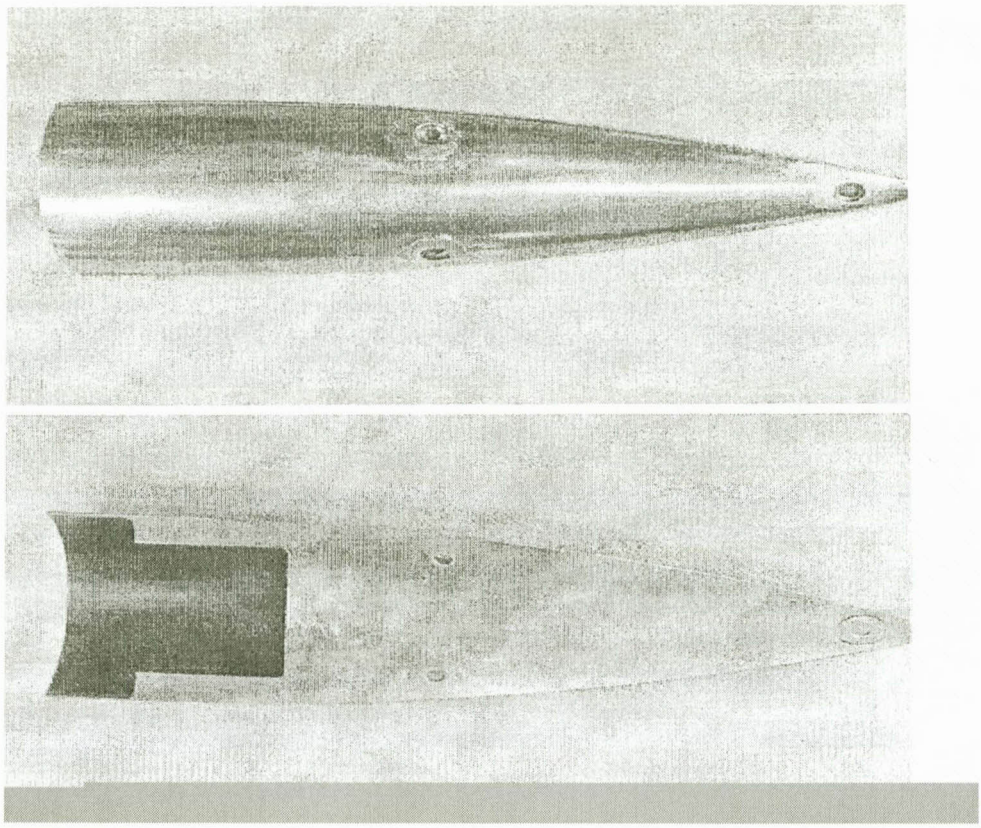

Figure 1.1: The front view and back view of the front-head covers for missiles made of Ti6Al4V, respectively [19].

1.2.2 Biomedical applications

Amongst conventional biomaterials, pure titanium as well as Ti6Al4V alloy exhibit excellent properties for surgical implant applications [20, 21, 22]. The performance of the implanted material depends mostly upon the nature of the tissue-implant interface, the load bearing capabilities of the implant, and the overall resistance to chemical and physiological degradation in the aggressive aqueous environment. Due to its good mechanical, chemical properties, high corrosion resistance and good compatibility with biological materials, titanium and its alloys has had considerable applications as dental implants [23]. The good corrosion resistance and biocompatibility properties are attributed to the existence of the stable and passivating air-formed surface oxide layer of near stoichiometric TiO_2 [24] that is always present on the alloys. The coatings are

of interest in biomedical applications of titanium, since they impede release of metal ions and assist tissue development [25]. This oxide layer regrows very rapidly if removed or mechanically damaged and it can attain the thickness of about 10 Å [12] in seconds on a freshly exposed metal. The use of titanium and titanium alloys as bearing surfaces in total human joint replacements, like artificial hip and knee joints was widespread during the 1970's [20, 26, 27]. Titanium and its alloys have received exploitation in medical implant application for more than 30 years.

1.3 Structure and composition of the passivating oxide layer

The characterization of layers on the surface of titanium, but mostly Ti6Al4V alloy specimens revealed that irrespective of the surface preparation condition, the layer consists predominantly of tetravalent titanium in the form of TiO_2 [15,28-30]. The oxide layer is built up of a combination of TiO, TiO_2, Ti_2O_3 and Ti_3O_4 [20, 31].

Oxides from the alloying constituents [32] have been found in the oxide layer. Aluminium (Al_2O_3) has a large negative free energy [28] of formation, higher than that of titanium oxide, and there will thus be a larger driving force towards the formation of Al_2O_3 than TiO_2. TiO_2 has a high dielectric constant, charges are well screened, and the driving force for migration is minimised. However, Al_2O_3 has a much lower dielectric constant and a lower isolating effect exists. Ion flow is therefore increased, and the combination of higher driving force for ion migration and the smaller more mobile aluminium ion may result in a proportionally higher aluminium release from the substrate. This explains why Al has been found at the outermost surface, and through the inner regions of the oxide layer on Ti6Al4V. The measurements performed on oxidized titanium and Ti6Al4V surfaces [22] showed that the titanium sub-oxides are closer to the metal-oxide interface, which agrees with the location of these components in thermally produced oxides.

In both air- and steam-passivated surface layers the dominant specie is an oxide in tetravalent state, TiO_2, with no evidence of the presence of other

oxide species. Titanium oxide in lower oxidation states was also found, although it was concluded that titanium dioxide on pure Ti and Ti6Al4V is solely in the 4^+ oxidation state [32]. TiO_2 (rutile) can be grown on a single crystal TiC [33] substrate with different orientation. The analysis of XRD spectra and XRD texture measurements have shown that growth of the TiO_2 layers on TiC substrate is strongly influenced by the crystallographic orientation of the substrate. It was found that the growth of thin and adherent oxide layer would improve the chemical stability of the refractory carbides without affecting their mechanical properties [33]. The SEM analysis of the oxidized samples also revealed that the edges are mostly oxide free. The thickness of the edge oxide appears to be not uniform and thinner than the oxide on the surface directly exposed to the gas stream.

The rutile has a tetragonal structure [33, 34] with lattice parameters **a** = 0.45933 nm and **b** = 0.29592 nm. The titanium atoms lie in the positions (0,0,0) and (1/2,1/2,1/2) whereas the oxygen atoms are located in four sites, at ± (0.31,0.31,0), and ±(0.31+1/2,1/2-0.31,1/2). For the TiO_2 structure only the titanium layers are perfectly flat and the oxygen atoms lie slightly above and below the reference plane. Little or no studies were done on the alloy, Ti3Al8V6Cr4Zr4Mo. It is a beta (β) alloy, with established spring applications.

1.4 The objective of the study

The main objective of this study is to establish the effects of oxidation on the surface temperature of the commercially pure titanium and its alloys (Ti6Al4V and Ti3Al8V6Cr4Zr4Mo). That is, to determine if the increase in surface temperature of pure Ti and its alloys during oxidation is measurable. Thermal oxidation will be done on titanium and its alloys, and at the same time the surface temperature will be monitored using a chromel-alumel thermocouple. Two thermocouples will be used in this study, the first one to control the temperature of the specimen and the second one to monitor the surface temperature. The impurity segregation profiles will be measured.

1.5 The outline

The thesis consists of five chapters. The chapters are divided as follows:

Chapter 2 deals with the basic theory of oxidation. In this chapter, the effects of oxidation on the physical properties will be discussed. The oxidation mechanisms at the surface metal as well as the oxide film formation and oxide crystal structure will be dealt with. Pre-oxidation, chemical structure of the oxide layer and the thermodynamics of Ti and Ti alloys will be looked into.

Chapter 3 explores the conditions of ignition and explosions of titanium and its alloys. Finally, the literature review on the effects of oxidation on the surface temperature of the materials will also be discussed.

In chapter 4, the experimental set-up is given. The sample preparations, apparatus used and the experimental procedures followed are discussed.

After the measurements had been taken, the results and discussions are contained in chapter 5. This chapter includes the analysis and discussions of all the experimental data points in graphical form.

Finally, in chapter 6, the conclusions are made and a summary is given with some suggestions for future work.

Chapter 2

OXIDATION THEORY

It is important to first understand the theory behind the processes involved in the oxidation of Ti and Ti alloys. The question of how does the layer form, the thermodynamics processes involved in the formation of the layer, effects of oxidation on the surface properties, and the structure of the layer. This chapter deals with the theoretical information about the oxidation process of Ti and Ti alloys.

2.1 Introduction

Oxidation in the simplest and most rigorous way is defined as the loss of electrons from an atom, compound or molecule. In general use, the term is applied to a chemical reaction of a substance with oxygen or an oxygen-containing material which adds oxygen atoms to the compound being oxidized. Whenever something is oxidized, something else must undergo the opposite, reduction. Metals also oxidised and lose electrons when they go from one valency to a higher one. Oxygen is said to be very corrosive/erosive to most materials, especially at high temperatures and since operation at high temperatures mandate the use of refractory metals, ceramics and composite,

most of which oxidize rapidly and therefore require oxidation protection [35]. Oxidation and reduction go hand in hand, you can not have one without the other. During an oxidation-reduction reaction the oxidizer (oxidant) is reduced and the reducing agent (reductant) is always oxidized. This particular reaction produces a large amount of energy in the form of heat [36]. The reaction in which energy or heat is given off to the surroundings is known to be an exothermic reaction. Many common materials undergo exothermic reactions. The heat that a chemical reaction gives off can quickly heat the surrounding area to a very high temperature. As the temperature increases, the rate of chemical reactions generally increases as well. Once an exothermic reaction begins, it can quickly run away, accelerating its rate because of the heat produced. This can be dangerous, especially if the material reaches its flash point or autoignition temperature, at which point a fire or explosion could occur. Therefore, it is very important to know when a chemical reaction can generate excess heat and to take appropriate measures to deal with this.

Materials of all types may react with oxygen and other gases. These reactions can, like corrosion, alter the composition, properties, or integrity of a material [4]. Metals may react with oxygen to produce an oxide layer at the surface. Oxidation of the materials involves the diffusion [1-36] of oxygen into the bulk of the material and the formation of an oxide on the surface. Since pure titanium is a highly reactive material [1-36], it easily reacts with oxygen and forms a protective TiO_2 layer, which is said to be very stable and corrosion/wear resistant. Oxidation of titanium can occur spontaneously or by means of some mechanical means. Titanium and its alloys oxidise more rapidly when it is exposed to air at elevated temperatures. Different oxidation mechanisms of titanium and its alloys include thermal, air, glow-discharge, furnace treatments, plasma treatments, anodic polarization and microarc oxidation.

The rate at which oxidation occurs depends on the access of oxygen to the metal atoms [37]. In titanium oxidation the overall rate of oxidation depends on the method used and on the growth rates of the various oxide regions that form either as layers or agglomerates [37]. The growth rates of the oxide

regions depend on the rate of titanium-oxygen reaction at the gas-solid interface and on the rates of diffusion of oxygen through the regions. The type of oxide film influences the rate at which oxidation occurs [4]. Temperature also affects the rate of oxidation. In many metals, the rate of oxidation is controlled by the rate of diffusion of oxygen or metal ions through the oxide layer. If oxygen diffusion is more rapid, oxidation occurs between the oxide and the metal; if metal ion diffusion is more rapid, oxidation occurs at the oxide-atmosphere interface [37].

The mathematical description for the rates of titanium oxidation consists of diffusion equations for oxygen in each oxide region as well as equations for the displacement of each interface between regions. It was found that the concentration dependence of diffusion coefficients is less important than their temperature dependence [37]. So it was considered reasonable to represent diffusion of oxygen by Fick's law with diffusion coefficient that depends only on temperature [37]. Consequently, we would expect oxidation rates to follow an Arrhenius relationship, increasing exponentially as the temperature increases.

2.2 Effects of oxidation on physical properties

Titanium and its alloys exhibit excellent mechanical properties and a very high strength-to-weight ratio [17], but unfortunately showed relatively poor creep, wear resistance and contact corrosion properties [38]. This together with a sudden change in emphasis from manned aircraft to guided weapons, led to a slump in interest in Ti consumption during 1957-58. The high oxygen affinity of titanium can be used to improve the surface hardness (properties) and wear resistance of titanium and titanium alloy components by means of thermal treatments [1-9, 38].

Titanium and its alloys react with oxygen to form an oxide layer on top of its surface. It was concluded that the oxide layer formed on the surface is responsible for affording Ti and Ti alloys with excellent corrosion resistance and assures their excellent biocompatibility [20, 21, 23, 24, 27]. Titanium alloys pick up oxygen and nitrogen from the atmosphere easily.

Wei Zhou et al. [39] discovered in their study on the effect of welding on impact toughness of butt-joints in a titanium alloys that the increase in O and H concentrations increases the strength but at the expense of toughness. It was also discovered that Ti and its alloys pick up oxygen and nitrogen from the atmosphere easily during welding which increases their strength. The alloy Ti6Al4V, in contrast to pure Ti, is a two phase alloy at room temperature, and due to the presence of the two alloying elements and associated microstructure, some differences between the surface oxides on pure Ti and on the Ti6Al4V alloy may be expected which in turn could influence the performance of the material.

2.3 Mechanisms of oxidation on metal surface

2.3.1 Initial stages of oxidation

Oxidation process, at its initial stages depends on the cleanliness of the surface, which in turn depends on the gaseous environment and the purity of the metal [40]. One crucial factor which determines how long a surface can be maintained clean or, alternatively, how long it takes to build-up a certain surface concentration of the adsorbed species, is the number of gas molecules impacting on the surface from the gas phase. This is the incident molecular flux on the surface, which is also said to be the number of incident molecules per unit time per unit area of the surface. If ΔN is the total number of molecules arriving from all directions and with all speeds at one side of a specimen of surface area ΔA during time interval Δt, the molecular flux ϕ at the surface is defined as [41];

$$\phi = \frac{\Delta N}{\Delta A \Delta t} \qquad (2.1)$$

It was found that even under conventional high vacuum, surfaces are exposed to constant interaction with atoms and molecules in the residual vacuum, so that monolayers of contamination can form in the course of the measurements. From the kinetic theory of gases [41, 42], the arrival rate of N molecules $cm^{-2}s^{-1}$ of molecular weight M at a temperature T K at a pressure of p Torr is given by;

$$N = 2.89 \times 10^{22} p(MT)^{1/2} \text{ molecules } cm^{-2} s^{-1} \qquad (2.2)$$

The flux does not take account of the angle of incidence; it is merely a summation of all the arriving molecules over all possible incident angles. Another factor is the gas exposure, which is the measure of the amount of gas that a surface has been subjected to. Gas exposure is quantified by taking the product of the pressure of the gas above the surface and time of exposure [40].

$$(\text{Exposure/L}) = 10^6 \times (\text{Pressure/Torr} \times \text{Time/s}) \qquad (2.3)$$

The sticking coefficient also plays a major role in the surface cleanliness of the material. It is a measure of the fraction of incident molecules that adsorb upon the surface. It is a probability and lies in the range 0 – 1 [40, 42], where the limits correspond to no adsorption and complete adsorption of all incident molecules respectively. Sticking coefficient depends on many variables i.e. surface coverage, temperature and crystal face. The surface coverage of an adsorbed species may be specified as the number of adsorbed species per unit area of surface. Relative to the atom density in the topmost atomic layer of the substrate, surface coverage is define as:

$$\theta = \frac{Actual\ surface\ coverage}{\text{Saturation surface coverage}} \qquad (2.4)$$

A monolayer of adsorbate is taken to correspond to the maximum attainable surface concentration of adsorbed species bound to the substrate. The time or period that a clean surface will take to become covered with complete monolayer of adsorbate is dependent upon the flux of gas phase molecules incident upon the surface, the actual coverage corresponding to the monolayer and the coverage-dependent sticking probability. It is, however, possible to get a minimum estimate of time required by assuming a unit sticking probability and noting that monolayer coverages are generally of the order of 10^{15} per cm^2 or 10^{19} per cm^2 [42].

The process, oxidation, also critically depends on the surface orientation and roughness. Further complexities are introduced after the growth of a continuous layer of oxide on the metal surface, since the oxide provides a barrier between the reactants. These include the process of adsorption of oxygen onto the metal, the incorporation of the oxygen into the metal with the formation of some type of metal-oxygen structure, the process of nucleation and growth of the oxide and the solution of oxygen in the metal. Gas-metal interactions may be classified in terms of physical adsorption, chemisorption, and solution (absorption) or bulk compound formation [28]. Oxygen molecules from the gas must first contact the metal surface to be adsorbed. The molecules may be incorporated in the metal by a process of place exchange [28]. The overall equation for the chemical reaction involved in the oxidation of a metal is [4, 28]:

$$nM + mO_2 \rightarrow M_nO_{2m} \qquad (2.5)$$

where M is the atom or molecular mass, n is the number of metal atoms in the oxide and m is the number of oxygen atoms in the oxide. The thermodynamic driving force for this oxidation reaction on a metal surface to occur can be considered as the change in the standard free energy resulting from the formation of the oxide from the reactants, and is negative for all metals. It was noted that the formation of the oxide depends on the oxygen

pressure [28] being higher than the dissociation pressure, **p**, of the oxide in equilibrium with the metal, where:

$$p = \exp\left(\frac{\Delta G}{RT}\right) \tag{2.6}$$

and ΔG is the Gibbs free energy of formation of the oxide per mole of oxygen consumed. The growth of such a film must be preceded by the adsorption of molecules from the gas, their dissociation and ionization, their rearrangement to form oxide nuclei, and the lateral growth of the nuclei until they impinge on each other to form a complete layer of oxide [43].

The progress of reaction is in most cases determined by phase boundary reactions and diffusion processes that are usually very complex. If the layer is compact, diffusion processes dominate and in the case of porous oxide the reaction may be controlled by phase-boundary processes. The initial stage of oxidation, if a continuous oxide layer is already present, is still adsorption of the gaseous species. The type of the oxide layer formed on the surface during oxidation is described by the Pilling-Bedworth (P-B) ratio [4].

The Pilling-Bedworth (P-B) ratio is defined as:

$$\text{P-B ratio} = \frac{\text{oxide volume per metal atom}}{\text{metal volume per metal atom}}$$

$$= \frac{(M_{oxide})(\rho_{metal})}{n(M_{metal})(\rho_{oxide})} \tag{2.7}$$

If the Pilling-Bedworth ratio is less than one, the oxide occupies a smaller volume than the metal from which it formed; the coating is therefore porous and oxidation continues rapidly – typical of metals such as magnesium. If the ratio is one or two, the volumes of the oxide and metal are similar, and considerable oxygen solution occur which may eventually lead to the formation of ordered, adherent, nonporous, protective superlattice domains or

sub-oxide films – typical of aluminium and titanium. If the ratio exceeds two, the oxide occupies a large volume and may flake from the surface, exposing fresh metal that continues to oxidise – typical of iron.

The rate at which oxidation occurs depends on the access of oxygen to the metal atoms [4, 44]. A linear rate of oxidation occurs when the oxide is porous and oxygen has continued access to the metal surface;

$$y = kt \tag{2.8}$$

where y is the thickness of the oxide, t is the time, and k is a constant that depends on the metal and temperature. A parabolic relationship is observed when diffusion of ions or electrons through a nonporous oxide layer is the controlling factor;

$$y = \sqrt{kt} \tag{2.9}$$

Finally, a logarithmic relationship is observed for the growth of thin oxide films that are particularly protective, as for aluminium, titanium and possibly chromium;

$$y = k\ ln(ct+1) \tag{2.10}$$

where k and c are constants for a particular temperature, environment, and composition. These three rate laws are shown in figure 2.1 below.

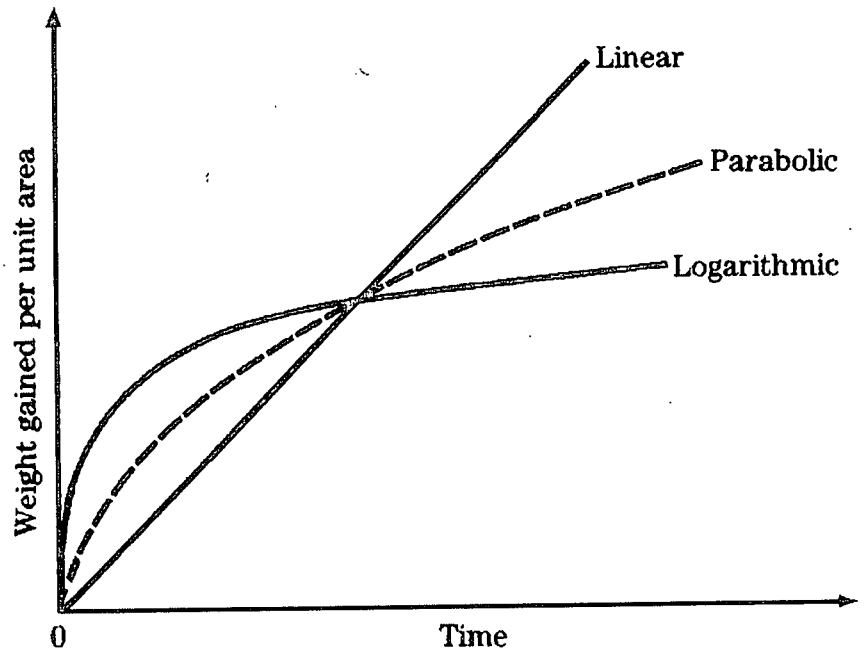

Figure 2.1: Schematic representation of the three rate laws [44].

The transfer of an electron from the metal proceeds relatively quickly, with the simultaneous dissociation of molecular oxygen to atoms. The incorporation of the oxygen into the oxide generally depends on the defect structure of the oxide. Diffusion of cations and anions across the oxide film is much slower than the electron transfer and can lead to space-charge layers that may modify the transport process. The driving force for the diffusion of metal or oxygen ions may be either the strong electric field set up across thin films of oxide, and/or the chemical potential gradient across thicker oxide films or scales [28]. The reaction mechanism will normally also be a function of temperature, oxygen pressure and the crystal structure and physical properties of the oxide on the metal.

2.3.2 Low temperature oxidation

According to literature, much work has been done on oxidation at elevated temperatures, but there is insufficient data in lower temperature oxidation. R.W. Rogers et al. [37], in an effort to quantify oxidation and diffusion behaviour at lower temperatures, conducted Ti oxidation experiments in oxygen ambients of 3 to 700 Torr, at temperatures from 373 to 773 K. The interface was examined by looking at the pressure dependence of oxidation, and discovered that the oxidation rate is independent of oxygen pressure in the pressure range of 3 to 300 Torr. The oxide film growth was much faster at higher temperatures than at lower temperatures.

At lower temperatures, the thermal activation energy for atomic motion is small. At these temperatures, nucleation at surface defects and the existence of small domains or island structures explain the nucleation of sub-oxide surface structures [28]. Nucleation of an oxide is an activated process and at low pressures and temperatures is expected to occur at sites of high chemical potential (i.e. surface defects). The possibility that nucleation of an oxide will take place at any site on a surface increases when the partial pressure of oxygen is increased. It is expected that at atmospheric pressure nucleation would occur very fast at all points on a surface, leading to the formation of a continuous relatively uniform oxide film [28]. In nature, the oxide film was found not homogeneous, with crystallites varying from 2-8 nm in diameter and large regular shaped oxide particles of up to 300 nm in diameter. The nucleus density varies with crystal face and is the highest at grain boundaries. Oxidation of a number of metals such as aluminium, silicon, tantalum, and niobium at low temperatures leads to the formation of an amorphous oxide.

The movement through a film at very low temperatures is impossible, only a chemi-adsorbed oxygen film is produced. Due to help from an electric field, movement through a film is possible at low temperatures, and this lead to a film which almost ceases thicken after it has reached a certain range of thickness. At low temperatures oxidation is parabolic being controlled by diffusion of oxygen through a compact scale and at intermediate

temperatures it is parabolic until the compact scale reaches the critical thickness, when it suddenly breaks down, giving a porous scale so that further thickening follows a linear law. The films on titanium are more protective at low temperatures than at high temperatures.

2.3.3 High temperature oxidation

Oxidation at elevated temperatures has been proved for most metals [28, 37]. At a certain pressure and temperature, the following three successive periods in the growth of oxide may be distinguished:

i) An induction period: this last until oxide nuclei are first observable on the metal surface.

ii) A period of lateral growth of the oxide nuclei: only last until the surface is completely covered by oxide.

iii) The period of uniform growth of the continuous oxide film.

Induction period depends on the oxygen pressure, and decrease with an increase in oxygen pressure. The effects of temperature on the induction period vary with crystal orientation of the surface. For a number of metals, induction period is associated with the solution of oxygen in the metal. The induction period was observed to be the result of oxygen going into solution until the oxygen concentration on the surface reaches a critical value which vary with crystal plane and then oxide nuclei formed by a precipitation process [45].

In lateral directions, the nuclei grow rapidly and slowly normal to the surface. The particle density on the surface remains constant until the particles start to grow together to a continuous film. After the initial growth, no new nuclei are formed and this is due to that the initial precipitation of oxide removes much of the oxygen which was in solution and additional oxygen adsorbing on the surface can react more easily with nuclei already formed. The oxide nuclei will contact one another and form a continuous oxide layer on the metal because of their lateral growth. The lateral growth is dependent upon migration or surface diffusion of the adsorbent specie towards the nuclei. The

layer will have a defect structure in terms of grain boundaries associated with it and the details depend on the conditions of temperature and pressure used for the oxidation process.

At high temperatures, the film thickening is also parabolic and in this temperature range, the stresses that would cause the break-down are relieved by annealing and sintering, so that the film remains relatively protective. The stresses mentioned above result from the growth of fresh oxide at the interface between scale and metallic (ore). At this temperature range, movement through the film is possible without help, but in the absence of a field or gradient it would proceed at random, the field or gradient directs it in one direction, so that thickening occurs according to the parabolic law. The diffusion process determines the rate lateral growth. The diffusion coefficient, D, depends on temperature and can be defined by the equation:

$$D = D_o \exp(-Q/kT) \qquad (2.11)$$

where D_o is a constant that depends on temperature, Q is the activation energy needed for diffusion to take place and T is the temperature.

2.3.4 Pre-oxidation

To improve the corrosion resistance of titanium alloys has been a subject of concern. Many methods have been used to modify the surface properties of titanium alloys in order to improve the corrosion and wear resistance [46]. Ion implantation of Nb was found to be able to improve the oxidation resistance of Ti-65Nd alloys at 650 °C. Ion implantation of Nb^+ and Al^+ coating on Ti60 alloy can affect the oxidation and corrosion resistance remarkably. Nb coating on pure titanium and titanium alloy, Ti6Al4V, also changes their sulfidation and oxidation behaviour. Another method discovered was the pre-oxidation [14, 46] of titanium alloys. From the slope of the oxidation curve, it was concluded that the pre-oxidation used, increased the oxidation resistance of the Ti-alloy. The method is discussed in the next section.

2.3.4.1 Oxidation kinetics

Zu Xiaotao et al. [46] successfully studied the effects of pre-oxidation of Ti2Al2.5Zr. The sample was oxidised in an alkaline steam at 300 °C and the results were analysed by SEM, XRD, XPS and in situ AES. It was observed that the oxidation of pre-oxidised Ti2Al2.5Zr and the controlled sample follow quasi-parabolic kinetics [46]. The reaction was found to be fast during the first period, but decreased greatly afterwards. A compact protective layer was found to have formed on the surface of the specimen. It is apparent that the pre-oxidised Ti2Al2.5Zr exhibited lower weight gains than the controlled samples. The oxidation kinetics after 1000 h showed a little difference between the pre-oxidised and controlled samples of the Ti2Al2.5Zr.

2.3.4.2 Microstructure of the oxidised surface

There was an apparent difference between the oxide scale on the Ti-alloy with and without pre-oxidation. From the surface morphology of the pre-oxidised samples [46], the grains were to be very fine, compact and homogenising, but those of the controlled samples were bulky and dispersed. It was concluded that a dense TiO_2 layer was formed on the pre-oxidised samples. The composition of the oxide scale on the Ti2Al2.5Zr with and without pre-oxidation oxidised at 300 °C was examined, and the Brookite-TiO_2, the ternary oxide $Al_2TiO_5(Al_2O_3.TiO_2)$, Ti_3O_5 and Ti_2O_3 were observed to have formed during oxidation. The peaks of pure titanium also appeared in the XRD pattern, and this was due to the penetration depth of the X-rays (7-35 μm) being greater than the thickness of the oxide scale. The XRD pattern also showed that the peaks of Ti_3O_5, Brookite-TiO_2 and $Al_2TiO_5(Al_2O_3.TiO_2)$ on the pre-oxidised specimen were much higher than those for the sample without pre-oxidation. That indicated that the thickness of the oxide scale of the pre-oxidised sample was thicker than that of the specimen without pre-oxidation. It was concluded that the pre-oxidation increases the oxidation resistance of the Ti-alloy. The analysis of the oxide scale showed that the chemical state of Ti as determined by XPS changes with depth.

The percentages of the distribution of the states are: Ti^{4+} 100%, Ti^{3+} 0% and Ti^{2+} 0%. As the depth increases, Ti^{3+} (Ti_2O_3) and Ti^{2+} (TiO) appear. At first the percentages of Ti^{3+} are higher than Ti^{2+}, then there is more Ti^{2+} than Ti^{3+} when the depth is increased. The AES results showed that the whole thickness of the pre-oxidised sample is thinner than that of the controlled one, but the stable oxide scale is just the reverse, the pre-oxidised sample being much thicker [14, 46]. From this it was concluded that the stable oxide scale provides a barrier to oxygen diffusion. It is well known that the oxide scales on Ti alloys grow through oxygen diffusion from the environment side to the oxide/metal interface. Before the discussion of the effect of the oxide scale formed first on the later oxidation behaviour, the atomic percentage of O was converted into the concentration of O. From Fick's second law, the diffusion coefficients of O were calculated to be [46]:

$$D_{pre} = 0.225\ cm^2/s,\ D_{control} = 0.426\ cm^2/s$$

where D_{pre} and $D_{control}$ are the diffusion coefficients of the pre-oxidised and the control samples respectively. It is apparent that D_{pre} is much smaller than $D_{control}$ and probably, this is another factor that leads to the better oxidation resistance of the pre-oxidised sample. The results obtained from the investigations on Ti2Al2.5Zr agree with the results obtained in the investigations on Ti6Al4V.

2.3.5 Oxygen solubility in metals

Oxygen solubility in different solid materials varies from negligible amounts in metals like Cr, W, and Mo, moderate solubility in V, Nb and Ta, while up to 20-30 at.% in Hf, Zr and Ti [28]. Since Ti is such a reactive element, the oxygen-deficient surfaces are expected to react with oxygen. Oxygen atoms become adsorbed on the surface of the oxide-film, and by attracting electrons from the metal, become converted into oxygen ions. The oxygen ions attract metallic cations from the outer layer of the oxide into new places where they constitute an additional oxide layer together. This leaves vacancies at places previously occupied by these cations and such vacancies migrate inwards

under the electrical or chemical potential gradient, and may either be accumulated at the metal-oxide interface or enter the metal and become annihilated at the end of dislocations. When it reaches the metal-oxide interface, part of it enters the metal in solid solution and part of it is used to form fresh and thus increase the thickness of the film.

When a surface with 8% vacancies is exposed to oxygen at cryogenic temperatures, the saturation coverage is about three times the vacancy concentration. The solubility of oxygen varies highly with temperature. Oxygen dissolved in the group IV(A) (Ti, Zr and Hf) and V(A) (V, Nb and Ta) metals is generally presumed to be located in octahedral interstitial positions. At higher temperatures, the effects of oxygen solution on the total oxidation process for IV (A) and V (A) metals may be very large.

Large solubilities of oxygen are reported for the hexagonal α-phases of Ti (30 at%) at temperatures below 900 ^{o}C, owing to the larger internal space, while the solubility is reduced to the order of several atomic per cent in the β-phase body centred cubic region at higher temperatures. The metals such as V, Nb and Ta with bcc structures, showed oxygen solubilties of the order of 1-3 at. % at temperatures between 1000-2000 ^{o}C [23].

2.4 Oxide film formation

As soon as a thin continuos oxide film has formed on a metal surface, the metal and gaseous reactants are separated by a barrier and the reactions can continue only if cations, anions or both and electrons diffuse through the oxide layer. The rate-determining step in the oxidation reaction may be mass or charge transport through the oxide layer, mass or charge transport across one of the interfaces or a process associated with the chemisorption of oxygen. This is shown in figure 2.2.

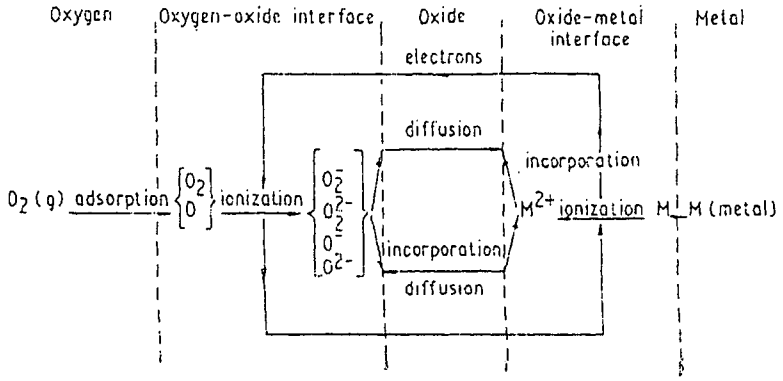

Figure 2.2: Schematic diagram of possible reaction paths.

The thickness of the oxide film ranges around some microns depending on the oxidation conditions, such as temperature, oxygen partial pressure and time [29]. Experimentally, logarithmic, inverse-logarithmic, cubic and quartic rate laws have been observed at low to moderate temperatures. The parabolic and linear laws normally observed at elevated temperatures.

2.4.1 Chemisorption on oxide films

When an oxide film is present on the surface of a metal, the chemical reaction between the solid and a gas is initiated by chemisorption of the gas on the oxide. The process of chemisorption is influenced by the presence of lattice defects, the distribution of electrons and holes, as well as traps in and near the surface of the oxide. Oxygen is actually chemisorbed dissociatively with essentially zero activation energy on most clean surfaces. Since most of the oxides are semiconductors, the chemisorption process for a gas on a semiconducting oxide proceeds by the transfer of an electron from the semiconductor to the gaseous molecule. The direction of electron transfer can be determined from the conductivity measurements. It is being agreed that in TiO_2, an electron is transferred from the valence band to the conduction band by adsorption of a photon, and the resulting hole pair reacts with molecules on the surface of the semiconductor [47].

A decrease in conductivity for n-type oxide [28] implies that electrons have been transferred from the conduction band of the semiconductor to adsorbed gas molecule. The transfer of electrons from a p-type semiconductor to a gas on the surface leads to an increase in conductivity owing to an increase in positive holes. These two types of chemisorption processes are known as depletive and comulative chemisorption respectively. The oxygen molecule has a positive electron affinity of 8-13 $kJ.mol^{-1}$ [28], so it is natural to expect oxygen to be adsorbed as negative ions (either as O^-, O^{2-} or O_2^-). At coverages exceeding a certain concentration of adsorbed charged oxygen species, neutral oxygen can also be adsorbed.

For the oxide to form the negative ions for an n-type semiconductor, electrons must initially come from the partly filled conduction band. As more atoms are adsorbed, more electrons must be transferred and these must come from deeper impurity levels in the oxide. The process causes the build-up of a space charge boundary layer and the development of a potential barrier to electron transfer, so that adsorption should stop when only a fraction of a monolayer of adsorbed gas has formed. In p-type semiconductors, there are sufficient electrons in the conducting band such that oxygen adsorption using electrons near the surface is not limited to a fraction of a monolayer. Chemisorption process creates more holes and the conductivity is observed to increase.

Space charge boundary layers will be formed because of the different distributions of ion and electron defects which are established near the oxide surface as a result of different chemical potentials for the ions and electrons in equilibrium with the adsorbed oxygen. These charge layers set up an electric field which tends to counteract the adsorption process. The conductivity and work function of the oxide may under certain conditions play an important role in oxidation. The chemisorption of oxygen with the development of a surface charge and the resulting bending of the energy bands near the surface and shift of the Fermi level causes changes in both the conductivity and work function.

2.5 Oxide crystal structure

A knowledge of the relationship between the atomic surface structure and other physical and chemical properties of the oxide at all stages of oxidation process is of the most important achievement in surface science. This knowledge is essential for the understanding of oxidation kinetics and mechanisms. Due to the mixed ionic and covalent bonding in metal oxide systems, the surface structure has a stronger influence on local surface chemistry as compared to metals or semiconductors.

Titanium dioxide crystallizes in three major different structures; rutile (tetragonal, **a** = **b** = 4.584 Å, **c** = 2.953 Å), anatase (tetragonal, **a** = **b** = 3.782 Å, **c** = 9.502 Å) and brookite (rhombohedrical, **a** = 5.436 Å, **b** = 9.166 Å, **c** = 5.135 Å) [33,34]. In the applications of the titanium dioxide, only rutile and anatase play a role and are of most interest as they have been studied with surface science techniques. Modern techniques for the determination of oxide structures have shown that perfect crystalline order and likewise perfect stoichiometry are almost non-existent in oxide films on metals. For the kinetics and mechanisms of physical and chemical transformations, the thermodynamic defects corresponding to a state of minimum free energy, and non-thermodynamic defects that belong to a non-equilibrium state may be important.

The unit cells of both rutile and anatase are shown in figures 2.3 and 2.4. In both structures, the basic building block consists of a titanium atom surrounded by six oxygen atoms in a more or less distorted octahedral configuration. In each structure, the two bonds between the titanium and the oxygen atoms at the aspices of the octahedron are slightly longer. A sizeable deviation from a 90° bond angle is observed in anatase. In rutile, neighbouring octahedral share one corner along <110>-type directions, and are stacked with their long axis alternating by 90°. In anatase the corner-sharing octahedral form (001) planes. They are connected with their edges

with the plane of octahedral below. In all three titanium dioxide structures, the stacking of the octahedral results in threefold co-ordinated oxygen atoms.

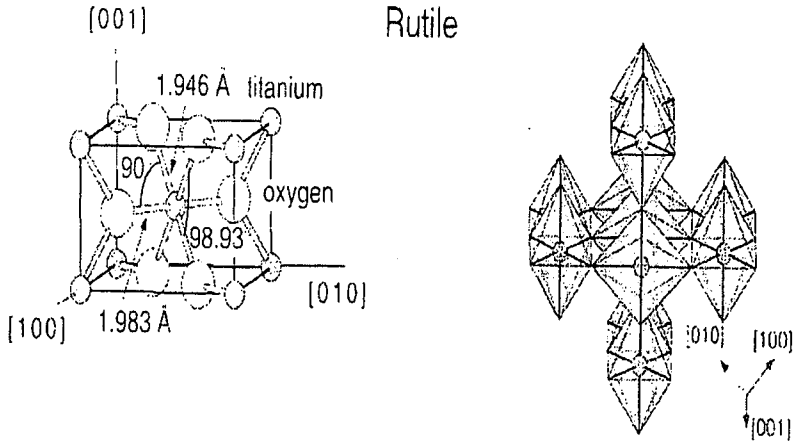

Figure 2.3: Tetragonal bulk unit cell of rutile

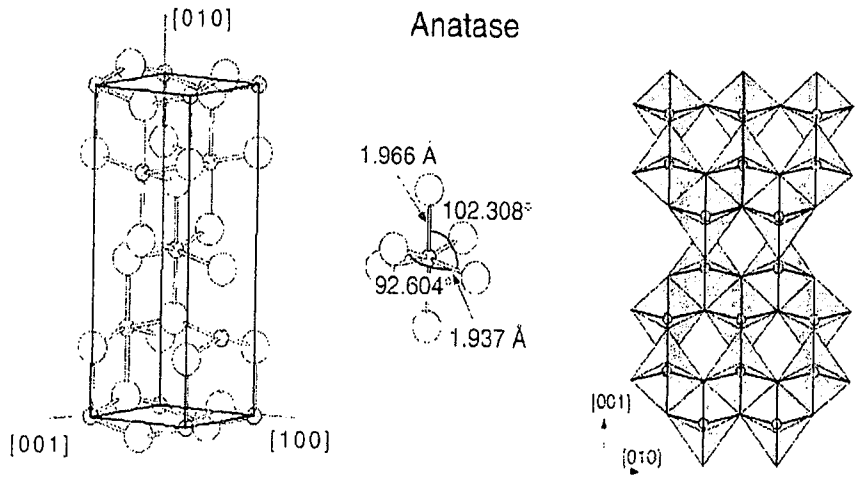

Figure 2.4: Tetragonal bulk unit cell of anatase.

The (110) oxide surface has the lowest surface energy, and the (001) surface the highest. This is also expected from considerations of surface stability based on electrostatic and dangling-bonds arguments. The thermodynamic stability of the (100) surface was found to be stable with respect to forming (110) facet [28]. The (001) surface was almost unstable with respect to

formation of microscopic (011) facets. For rutile, the (110), (001) and (100) surfaces were studied, with (110) being the most stable.

The (100) surface is non-polar (or charge neutral), which means the net charge in each atomic plane parallel to the surface is zero. If a surface oxygen ion is removed, the ligand co-ordination of the four adjacent cations is reduced from five to four and the cation directly below the vacancy becomes five-fold co-ordinated [28]. If a cation is removed from the (100) surface, a similar reduction in the co-ordination of surrounding oxygen ions occurs.

2.5.1 Rutile TiO_2 (110) surface structure

The rutile crystal structure has a tetragonal lattice and a composition of MO_2. The cations in the rutile lattice are in a 4^+ valence state and reside in slightly distorted O^{2-} octahedral. The rutile crystal face (110) surface is the most stable. The most stable surfaces are predicted to be those, which are auto-compensated, that is, excess charge from cation-derived dangling bonds compensates anion-derived dangling bonds. The result is that the cation-(anion) derived dangling bonds are completely empty (full) on stable surfaces. On this surface, two types of cations are present, the first one have five O^{2-} ligands and the other one has its full complement of six O^{2-}-ions. The rutile surface is not automatically flat due to the row of bridging O^{2-} ions, but it is non-polar [34]. The surface also contains two different types of titanium atoms. Along the [001] direction, rows of six-fold co-ordinated Ti atoms alternate with five-fold co-ordinated Ti atoms with one dangling bond perpendicular to the surface.

Two types of oxygen atoms are created as well. Within the main surface plane, they are threefold co-ordinated, and the other one corresponds to the removal of the bridging oxygen atoms to bond to Ti atom in the removed layer and are twofold co-ordinated. In the former case two of the six-fold surface cations have their co-ordination reduced to five-fold, while in the latter case two four-fold cations are formed in the surface plane. Cation-cation screening is greatly reduced at such sites. Due to their co-ordinative undersaturation,

atoms from the rows are thought to be removed easily by thermal annealing. The perfect (100) surface has all of its cations co-ordinated with five O^{2-}-ions, and are also non-polar.

It was observed that every surface relaxes to some extent. The main relaxations are said to occur perpendicular to the surface. Only the in-plane oxygens (4,5), as shown in figure 2.5 below, move laterally towards the five-fold co-ordinated Ti atoms. The bridging oxygen atoms (3) are measured to relax downwards considerably, and the six-fold co-ordinated Ti atoms upwards. The five-fold co-ordinated Ti (2) atoms move downwards and the neighbouring three-fold co-ordinated oxygen atoms (4,5) upwards causing the rumple appearance of the surface. The experimentally determined directions of atoms are illustrated in the figure below. The relaxations in the second TiO_2 layer are approximately a factor of two smaller.

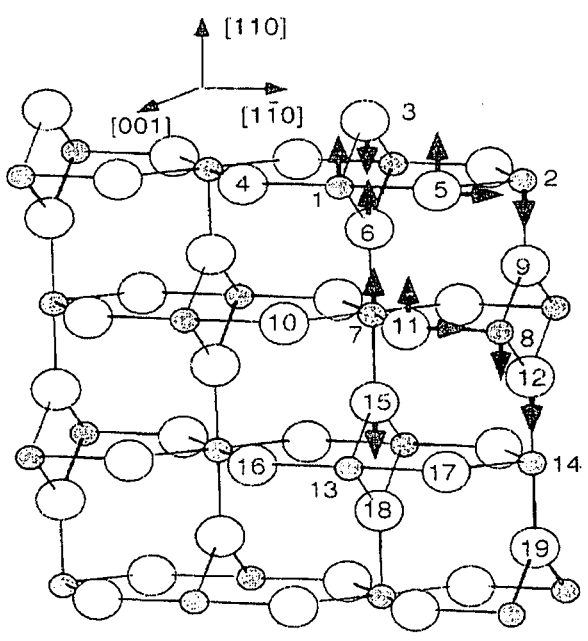

Figure 2.5: The relaxation of surface atoms.

In the experimentally determined co-ordinates, the most striking feature is the large relaxation of the bridging oxygen atoms (by -0.27 Å) [34]. The measured geometry indicated a very small bond length between the sixfold co-ordinated

Ti atom (1) and the bridging oxygens (3) of about 1.71 ± 0.07 Å which is much lesser than the expected one from the bulk structure.

Most of the oxidation mechanisms depend on the atomic or electronic transport properties of the oxide, which in turn depend on the types of structural and electronic defects in the oxide. Structural defects in crystals are classified into four groups: (1) point defects such as vacancies, interstitial or misplaced atoms, (2) line defects such as dislocations, (3) planar defects such as stacking faults or grain boundaries and (4) volume defects (clusters) such as large pores or voids [4, 28]. It is also known that associated defects, long-range ordering of defects and structural defects described in terms of crystallographic shear planes occur in a large number of metal oxides. The defect structure varies with oxygen deficiency that depends on temperature, gas pressure, and impurities.

As pointed out from the preceding discussions, most oxides are non-stoichiometric in composition, although the deviation may be infinitesimally small in some cases. Two important types of defect structures for stoichiometric compounds in oxides are Schottky and Frenkel pair defects [4, 28]. Frenkel defect corresponds to a vacancy-interstitial pair formed when an ion jumps from its original lattice point to occupy an interstitial site leaving a vacancy behind. Schottky defect involves a pair of vacancies in an ionically bonded material; both an anion and a cation must be missing from the lattice if electrical neutrality is to be maintained in the crystal. In this situation, the number of cations and anions is equivalent.

In non-stoichiometric oxides, two types of defect structures occur. These include (i) an oxygen deficiency or metal excess and (ii) a metal deficiency or oxygen excess with respect to the stoichiometric composition. For oxygen deficient oxides, the formula may be written as MO_{2-x} where oxygen vacancies are the predominant defect, or as $M_{1+y}O_2$ if interstitial cations are the major defect. In case of metal deficient oxides, the major defects may be either cation vacancies or interstitial oxygen ions, the formulas may be written

in the same way. The phase diagram of titanium-oxygen system is shown in the sketch below [34].

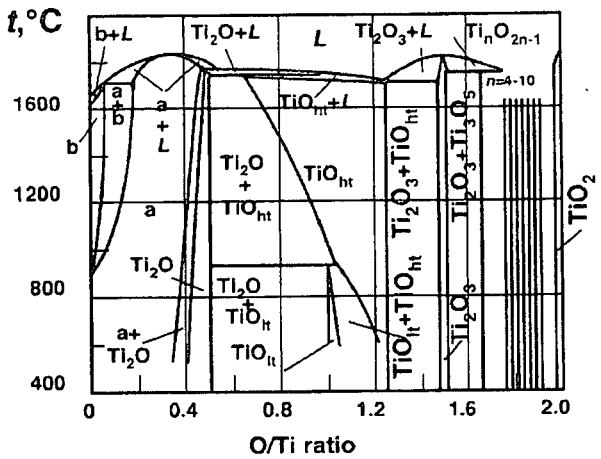

Figure 2.6: The phase diagram of Ti-O system. The region Ti_2O_3-TiO_2 contains Ti_2O_3, Ti_3O_5, seven discrete phases of homologous series Ti_nO_{2n-1} and TiO_2.

Extents of non-stoichiometry in oxides depend on the temperature and partial pressure of its components. For an oxygen deficient oxide, the non-stoichiometry increases with a decrease in oxygen pressure, and for oxygen excess oxides, it increases with an increase in oxygen pressure. Oxides showing much deviation from stoichiometry (including Ti and V) are made up of a series of intermediate phases of narrow homogeneity range, which results from defect ordering or the development of crystallographic shear structures. In metals which dissolve a considerable amount of oxygen (e.g. Ti, Ta, Nb, V), the formation of ordered metal-oxygen structures is often observed, particularly at lower temperatures. With increasing oxygen in the metal lattice, martensitic type shear transformations may occur, forming platelet sub-oxide structures. The initial sub-oxide may on further oxidation process be converted to higher sub-oxide and eventually to a stable form of oxide. Oxides formed on a metal surface are usually polycrystalline, with varying amounts of preferred orientation determined by the oxidation conditions. They can be characterised in terms of their degree and type of orientation, grain size and distribution of stresses and strains within the oxide.

2.5.2 Anatase surfaces

Most commercial titania powder catalyst are a mixture of rutile and anatase. For certain photocatalytic reactions and non-photoinduced catalysis such mixtures work best. There is growing evidence that anatase is more active than rutile for O_2 photo-oxidation [28], but not necessarily for all photocatalytic processes. It behaves differently than rutile in gas-sensing devices, and most photovoltaic cells are based on granular thin films with anatase structure. Both anatase and rutile show inherent particle size differences and this might cause some of the observed differences in chemical properties. Typically, surface planes, (101) and (100)/(010) are found together with some (001). The (101) face is the most thermodynamically stable surface. The average surface of an equilibrium-shape anatase crystal is smaller than the one of rutile, which might explain the fact that nanoscopic TiO_2 particles are less stable in the rutile phase.

Since anatase is a metastable phase, it transforms into rutile at relatively high or low temperatures, with the transition temperature dependent on impurities, crystal size, sample history, etc.

2.6 The thermodynamics of oxide formation

The changes in nature are due to the tendency of a system to reach a maximum stability leading to state of equilibrium. Once the equilibrium has been reached, the tendency toward further change disappears and the system is stable [41, 48]. The driving force for the reaction to take place is given by the change in the Gibbs free energy (ΔG). For a reaction taking place at constant temperature and pressure, the change in G between two states of a system will be;

$$\Delta G = G_2 - G_1 \qquad (2.11)$$

By substituting G by the relation, G = H – TS, ΔG is now given by the equation;

$$\Delta G = \Delta H - T\Delta S \qquad (2.12)$$

where;

ΔH: is the heat of formation of 1 mole of a substance from the elements.

ΔS: the change in entropy between the initial and final stages of the system.

T: the constant temperature at which the reaction takes place.

The free energy change for any process being the function of the initial and final states of the system, is a definite quantity at any given temperature and pressure and varies as these two variables are changed [41]. It was observed that in a reaction ΔG generally approach ΔH more closely as the temperature was reduced, even at quite high temperatures [41]. This is shown in figure 2.7 below.

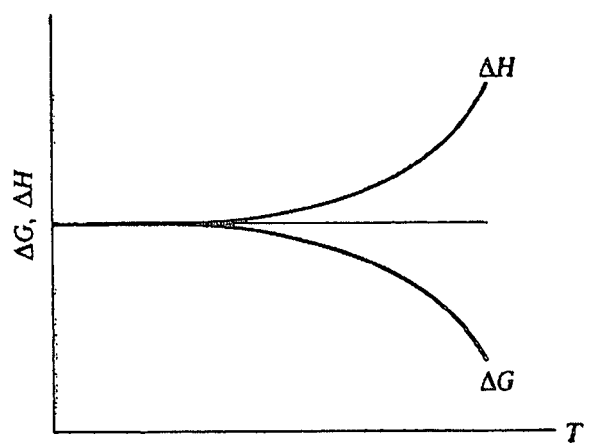

Figure 2.7: The temperature dependence of the change in the Gibbs function and in the enthalpy [41].

The absolute values of free energies of substances are not known and hence, only differences can be dealt with. The sign of the free energy change of a process is very important. A large negative free energy indicates a more stable oxide. When the driving tendency of a reaction is from the left to right, energy is emitted on reaction and the sign of ΔG is negative. A minus sign denotes that the reaction is spontaneous. If the net work equivalent to ΔG has to be adsorbed in order for a reaction to proceed in the direction indicated, ΔG is positive and the reaction is not spontaneous. When the system is in equilibrium, there is no tendency to proceed in either direction and ΔG is zero. This implies that the more negative ΔG is, the more spontaneous a process will proceed and take preference over a reaction with a less negative ΔG. The Gibbs free energy of formation (ΔG_f) can then be used to predict the oxide and sub-oxide formation sequence on the surface of a metal. If ΔG_f is calculated over a range of temperatures and a plot of ΔG_f versus temperature (Ellingham plot) is constructed, the relative stability of the oxides in a specific system and therefore the sequence of oxide formation can be obtained from the plot. The ease with which oxidation occurs is given by the free energy of formation for the oxide. The Ellingham plot of oxide formation was calculated, and is shown in figure 2.8 [28] below.

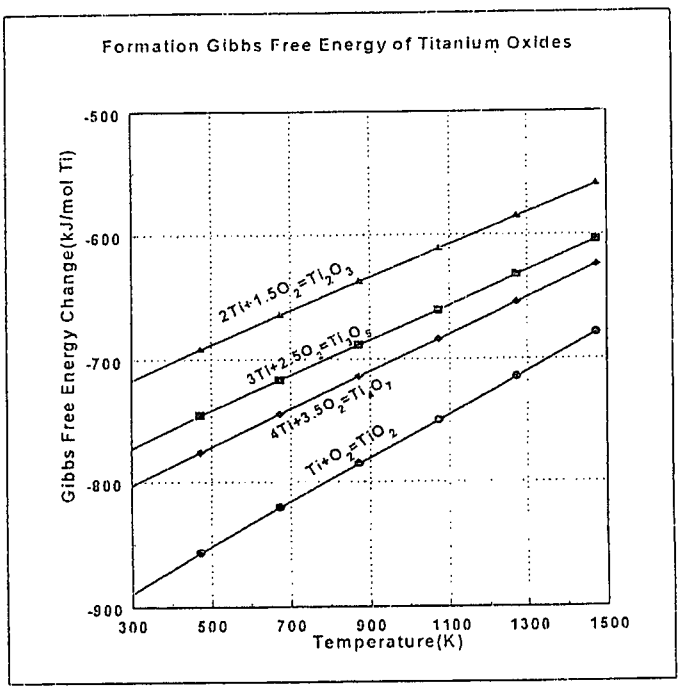

Figure 2.8: The formation Gibbs free energy vs temperature different Ti oxides.

The Ellingham plot for TiO was not included, as ΔG_f for TiO per mole Ti is positive at room temperature. It only becomes negative at a temperature of 573 °C and has a value of 164 kJ/mole at temperature of 1473 K. From the graph, the order of stability and therefore preferential equilibrium state Ti oxide formation is predicted as:

$$TiO_2 > Ti_4O_7 > Ti_3O_5 > Ti_2O_3 > TiO$$

The morphology and composition of oxide films on titanium alloys are also affected by the type of surface treatment applied. The phases been detected as the oxidation progresses and temperatures are increased are [28]:

$$Ti + O \rightarrow Ti\,(O) \rightarrow Ti_6O \rightarrow Ti_3O \rightarrow Ti_2O \rightarrow TiO_3 \rightarrow Ti_3O_5 \rightarrow TiO_2$$

The factors controlling the crystal structure that a phase of a given composition may adopt are the environmental factors, temperature and

pressure. All these are associated with the entropy term, TS, and the geometrical, energy band, chemical bond, and electrochemical factors resulting from the properties of the component atom, which relate mainly to the enthalpy term, H. The main contribution to the enthalpy in metals comes from nearest-neighbour interactions which might also be referred to as the chemical bonding. A contribution which is at least an order of magnitude smaller may be expected from the interactions between next nearest and further neighbours. On the energy band picture, the nearest-neighbour interactions or chemical bonds may be expected to correlate mainly with energy bands of valence electrons lying below the Fermi level, particularly in phases containing transition metals, whereas interactions involving next nearest neighbours probably correlate more with the electrons at the Fermi level.

For a TiAlV alloy, the Gibbs free energy of formation of oxygen anions at the surface, ΔG_f, for the various alloy constituents will then give an indication of the preferential oxide formation at certain temperature. Both Al and Ti have a high affinity of oxygen, however, Al_2O_3 has the largest free energy of formation per mole of O_2. At low temperatures and oxygen pressure, Al is expected to oxidize preferentially, followed by Ti and V. Oxidation process is very sensitive towards the oxygen pressure and during the competition for oxygen at the alloy surface, the suboxides can form preferentially and will only transform to highest valence state metal oxide when total equilibrium is reached. Al does not form any stable intermediate oxides and directly form an Al_2O_3 on the surface of the alloys at low temperature and oxygen pressure.

The change in the surface temperature during oxidation can be calculated from the equation below;

$$\Delta T = \frac{Q}{mc_s}, \tag{2.13}$$

where Q is the heat generated, m the mass and c_s the specific heat capacity.

CHAPTER 3

Ignition and Explosions of Ti and its alloys

3.1 Introduction

The ignition and explosion of titanium and its alloys is a very important aspect in this study, since the oxidation can lead us to it. Lives of valuable people could be lost due to ignition and explosion. So it is quite imperative to know the conditions at which ignition and explosion can take place. This chapter entails the literature review of ignition and explosions of Ti and Ti alloys.

3.2 Ignition and self ignition of Ti

The thermal decomposition and subsequent ignition of materials handled in industrial processes have resulted in numerous fires and dust explosions in a wide range of industries [50]. When the Ti is subsequently mixed with an oxidiser and heated, the thermal dissolution of the TiO_2 layer was suggested to control the ignition temperature of the composition [50]. The thermal ignition characteristics of Ti-based pyrotechnics are controlled by diffusion of oxygen from a surface coating into the bulk of the metal [37]. Technological applications

of Ti and its alloys are hindered by the potential risk of failure of titanium equipment due to the abnormal ignitability of titanium and its alloys in oxygen and oxygen mixtures. Self-ignition occurs only in the case of fracture of construction metal and contact of a juvenile metal surface with oxygen media at pressures higher than a certain critical pressure $\mathbf{p}^*$. Since such fracture cannot be ruled out during operation of reactors, equipment made of titanium and its alloys can be safely operated in an oxygen medium only if the process parameters exclude the possibility of self-ignition of the material with juvenile surfaces. The thickness of the oxide coating may also play a crucial role, and the ignition temperature is a strong function of the activation energy for the diffusion of oxygen into α-**Ti** [37].

Ignition is possible for various types of fracture, such as tension, flexure, as a result of friction, rupture by oxygen pressure, an electric spark discharge, and exposure of a specimen to a high-rate oxygen flow. It was found that the critical ignition pressure is different for each type of fracture. Ignition occurs only as a result of direct metal fracture, whereas elastic and plastic deformations under stresses smaller than fracture stress do not lead to ignition of a new juvenile surface [51]. Practically, all commercial titanium alloys tend to ignite and the critical pressures of ignition in oxygen for the same fracture type differ by more than an order of magnitude and vary from 0.7 MPa to 7.5 MPa [51].

The values of $\mathbf{p}^*$ for alloys depend on the character and relief of the fractured surface. The critical pressure of the alloy ignition in oxygen increases during transition from tough (uneven fracture) fracture to brittle fracture (flat fracture). Due to this reason, preliminary hydrogenation or nitration of titanium alloys and incision of specimen, which promotes transition to brittle fracture, lead to an increase in critical ignition pressure. Ignition occurs in both liquid and gaseous oxygen in temperature range of 90 K to 1273 K [51]. The value of $\mathbf{p}^*$ of alloys usually decrease as the experimental temperature $\mathbf{T_o}$ increases, but they can also increase sometimes.

Dilution of gaseous oxygen with inert gas or water vapour always leads to an increase in critical pressure. It was suggested that metallic materials (titanium, zirconium, and their alloys) are ignitable in oxygen only if their oxides are soluble in liquid metals [51]. According to the hypothesis, self-ignition occurs only if the initial reaction is intense enough to raise the surface temperature to the melting point for that metal. A contact of a pure (unoxidized) titanium surface with oxygen causes exothermic oxidation involving the formation of an oxide layer and release of a large amount of heat [36,37]. At higher oxidation rates, the heat of the reaction is accumulated and the metal is ignited. At lower oxidation rates, the heat of the reaction disperses into the ambient medium. It is believed that the main reason for titanium ignition in oxygen is a damage of an oxide film and free access of oxygen to the metal surface. Since the rate of titanium oxidation depends on oxygen pressure and the temperature in the system, a certain oxygen pressure corresponds to a certain oxygen temperature at which the critical oxidation rate is so high that the oxidation yields interaction products that have a random structure and do not prevent access to the juvenile surface.

Other metallic materials whose oxides are virtually insoluble in liquid metals, such as chromium-nickel alloys, steels, and iron, can ignite after fracture in oxygen. However, the explanations of exothermic oxidation and titanium ignition in oxygen are based on the fact that interaction of free titanium surface with oxygen leads to the formation of an oxide layer at the ignition moment. This interaction pattern is close to oxidation whose rate depends on oxygen pressure and at the same it is known that the rate of titanium oxidation over a wide temperature range is determined by the diffusion of oxygen through the TiO_2 layer and does not virtually depend on pressure.

The rate of interaction of titanium and its alloys with oxygen at room temperature, especially at cryogenic temperature, at which titanium ignites, is low. It only increases at temperatures above 623 K [51]. However, self-ignition at room temperature is at least possible only if the metal is fractured; that is if the metal is damaged, titanium does not ignite. Microscopic observations of specimens fractured in oxygen showed that fracture sites at which heat transfer to the depth of the specimen is obstructed are commonly the first to ignite. This leads to the conclusion that only those elements of juvenile surface that have been heated to a high temperature T^* by the moment of interaction with oxygen tend to ignite. Temperature T^* is the sum of the initial temperature T_o and the temperature increment ΔT due to heat release during metal fracturing:

$$T^* = T_o + \Delta T \tag{3.1}$$

The temperature T^* to which elements of a new juvenile surface are heated is a critical parameter that characterizes the ability of titanium alloy to ignite. For constant T_o, the parameter is the temperature increment ΔT due to the heat release during metal fracturing. It was found that, since the ability of titanium to ignite depends uniquely on critical pressures, the critical ignition pressure of the alloys is likely to depend on the critical ignition temperature T^* to which elements of the juvenile surface can be heated upon fracture. This can clearly be seen from the graph of critical pressure versus critical temperature below [51].

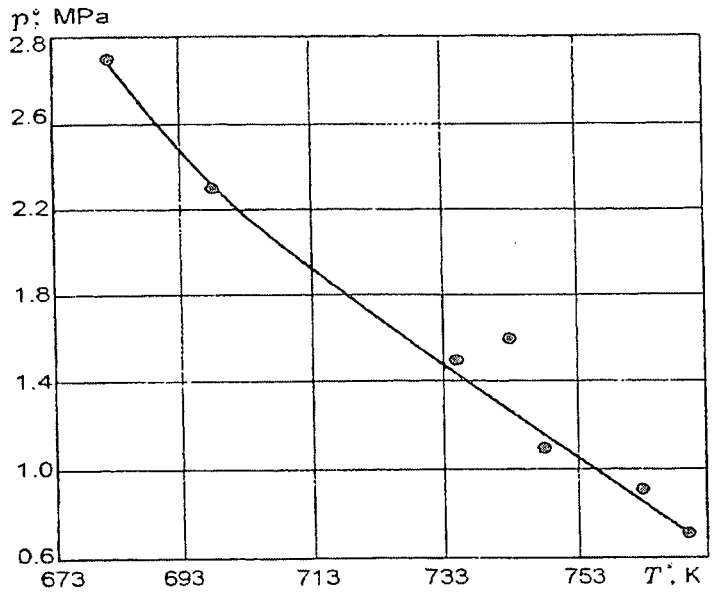

Figure 3.1: Critical ignition pressure of Ti alloys versus heating Temperature [51].

3.3 Effect of composition and properties of alloys on the critical pressure

It was found that with increase in the final temperature T^* (from 682 to 770 K) to which juvenile surface fragments can be heated, the critical oxygen pressure required to ignite the specimens decreases monotonically (from 2.9 to 0.7 MPa). At constant temperature T_o = 293 K, the heating of the specimens correlates with the critical pressure as ΔT increases from 405 to 407 K, the ignition pressure decreases from 2.3 to 0.9 MPa. Since ΔT depends on the fracture work, which in turn depends on the fracture stress, the critical ignition pressure depends upon the strength characteristics of the material. The higher the stress necessary for fracture of specimen, the lower the oxygen pressure at which the metal juvenile surface is ignited.

Due to this reason, material characterised by low strength, for example titanium iodide, is subjected to least heating during fracture compared with other alloys, and is extremely resistant to ignition. If titanium is doped with elements that improve its strength properties, juvenile surface fragments are heated to higher temperatures, resulting in a decrease in the oxygen pressure at which these fragments can be ignited.

3.4 Effect of test temperature on critical pressure and temperature

It was discovered that the effect of the test temperature T_o on the alloy pressure p^* is ambiguous because of the dual effect of T_o on the temperature T^*. Increase in T_o as a term of $T^* = T_o + \Delta T$, leads to an increase in temperature T^*, and on the other hand, it facilitates a decrease in T^* due to the degradation of strength properties and fracture work under heating. This leads to a decrease in the heating temperature term ΔT. Depending on which of the terms (T_o or ΔT) changes, the value of T^* with increase in T_o can either increase or decrease and the pressure p^* of the materials can decrease or increase accordingly. For commercial VT1-0 titanium (grade 2), the pressure p^* increases with increase in temperature T_o, which is due to a significant decrease in its ultimate strength and consequently, in ΔT and T^*. At the same time, the strength properties and heating (ΔT) of refractory OT4-1 alloy -decrease to a lesser degree with increase in test temperature, which leads to an increase in the total temperature T^* and, hence, a decrease in the alloy pressure p^*.

Figure 3.2 illustrates the dependencies of $T^* = f(T_o)$ and $p^* = f(T_o)$ for Ti alloys at higher test temperatures. As can be seen from figure 3.2, there is an apparent correlation between the dependencies studied; as the experimental temperature (T_o) increases, the temperature T^* increases and the pressure p^* decreases. Since $T^* = T_o + \Delta T$ and $\Delta T = f(S_k, c_p)$, where S_k is the strength properties and c_p the specific heat capacity, the comparison of curves in figure 3.2 show that the dependence $p^* = f(T_o)$ for any Ti alloy is determined by the dependence of S_k and

c_p of the alloy on temperature. The ultimate strength of commercial titanium reached 900 MPa at T_o = 90 K which leads to an increase in S_k to 2000 MPa and ΔT to 1500 K with preserved plasticity ($\Psi \cong 0.73$) [51]. The heating of titanium under the liquid oxygen was said to be sufficient to initiate self-ignition.

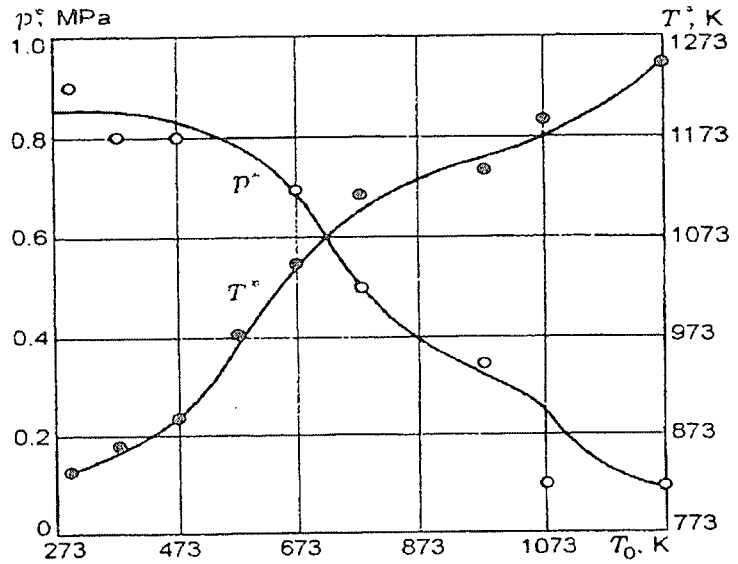

Figure 3.2: Critical ignition pressure and temperature of juvenile surfaces in oxygen versus test temperature [51].

3.5 Geometrical dimensions of specimen and fracture type effects on critical pressure

During transition from elastic fracture to brittle fracture, the work changes (decreases). As a result, the temperature T^* is lower for fractured incised titanium specimens and nitrated or hydrogenated specimen than for flat or initial specimens of the same alloy. This is realised from an increase in p^*. Another factor responsible for a rise in p^* during brittle fracturing of titanium alloys is a change in juvenile surface shape during transition from rough fracture to flat fracture. In this process, a decrease in the area subjected to oxidation is accompanied by improvement in heat transfer from fragments of fracture surface

into the depth of the specimen. As a result, these fragments are less heated by the moment of interaction with oxygen than in the case of a rough surface.

3.6 Explosions and fires

The ultra-light metals oxidise at constant rate as long as the heat evolved in the reaction is removed. Any failure to remove the whole of the heat, so that the temperature rises, will cause the reaction to proceed faster [52]. Thus metals of this class if heated in air from an external source may start to become hotter as a result of the oxidation, and eventually reaching the temperature at which the oxide layer burn in air. Some members of the class forming compact oxides do not normally burn in air. In this case oxidation rate, at constant temperature will fall off as the film thickens, even if in the opening stages the whole of the heat evolved is not removed, the slight increase in temperature will not compensate for the effect of film-thickening and thus, no burning of these metals in general. Titanium was observed to burn in air at about 1200 °C and in oxygen at 610 °C, and it was found to be the only element that burns in nitrogen at about 800 °C [53]. However, heavy metals can burn in air when present as a sponge, a fine powder or very thin wire.

Titanium and Zirconium are subject to hydrogen embrittlement, which is a matter that should receive a serious attention before deciding on their use. The highly protective character of the oxide-films on titanium and zirconium is almost certainly due to the fact that they are formed by the inward oxygen penetration so that the oxide contains a compressed stress parallel to the surface. These tend to close any fissures and the thin films are highly protective. If a certain thickness is exceeded, the strain energy per unit volume becomes greater than the work involved in detaching the metal and spalling or other failures occurs; thus the break-down of the films.

The sudden break-down of resistance on both metals has been the cause of fatal accidents and destructive fires. If a quantity of zirconium scrap in store is allowed to become damp, the film may approach the thickness at which spontaneous break-down would occur and relatively small amount of disturbance may supply sufficient additional force to break the film at a few points and causing a sudden hydrogen evolution along with much heat which may cause local explosion of the hydrogen-air mixture present in the interstices of the scrap. Violent explosion of titanium occurred during the testing of specimens in red fuming nitric acid. The reagent usually produces little attack on titanium, but occasionally some slight movement or impact has caused a disastrous explosion, leading to the loss of valuable life. The explosions generally seem to be preceded by an attack on the metal leading to pyrophoric material. When titanium is placed in hydrochloric acid, its potential first declines, indicating the destruction of the air-formed film, but then rises again, apparently owing to the formation of a secondary film which is more resistant than its predecessor.

It was observed that the reaction of the red acid with titanium, leading to pyrophoric material, is much more violent in experiments carried out in sealed flasks [52]. The lessened danger associated with open flasks has been attributed to the access of oxygen or up-take of moisture that would certainly tend to slow down the reaction. The difference on the two may really be due to the fact that the use of closed flasks prevents the escape of nitrogen peroxide, which is possibly needed for the setting up of an autocatalytic cycle. The danger of red nitric acid increases with the concentration of NO_2 in the original reagent. The relative safety is obtained at the higher H_2O contents and lower NO_2 contents, and so the probability of disaster diminishes as the NO_2 content diminishes and as H_2O content increases.

The rare explosion occurrences seem to depend on some unusual conditions. The danger is increased if there are internal stresses in the type of metal which will keep opening out cracks and thus exposing the film-free surfaces more quickly than films can be formed by the oxidizing action of the acid. The danger is also increased if the rapidly evolved oxides of nitrogen can form a gas space around the metal, so that it becomes dry, then starts to burn reaching the temperatures exceeding the melting-point. Explosion will only occur when three different conditions are spontaneously fulfilled. These include (1) internal stress, (2) crevices favourable to an autocatalytic cycle, and (3) geometry suitable for the formation of a gas pocket next metal. Some friction between the particles when material has reached the sensitive condition may be necessary. Combustion in oxides of nitrogen will cause more heat than combustion in air.

Chapter 4

EXPERIMENTAL SETUP

4.1 Introduction

In this chapter a brief description of the AES technique is given. It is followed by a detailed sample preparation and mounting procedure. Brief descriptions of the oxidation and segregation procedure are also given. The use of AES analytical surface technique in this study is due to its high surface sensitivity and ability to give information regarding the composition of the specimen to depth of a few monolayers.

4.2. Instrumentation

4.2.1. AES system

Auger Electron Spectroscopy was developed in the late 1960's, deriving its name from the effect first observed by Pierre Auger [54], a French Physicist, in the mid-1920's. It is based on the measurement of the kinetic energies of the emitted Auger electrons.

Auger electron spectroscopy, which is capable of identifying individual elements and with a shallow depth of about five monolayers from which data is taken, is particularly suited for surface analysis. In the Auger process, a high-energy (2-10 keV) primary electron hits and liberates a core level electron thereupon ionising the atom. The ionised atom that remains after the removal of the core hole electron is in a highly excited state and will rapidly relax back to a lower energy state. For this atom to reorganise itself to a lower energy state, an electron from the higher level will drop to the lower level to fill the void caused by the liberated electron. The energy released in the transition is either emitted as a photon or given to another electron in the higher level. If the energy is sufficient, this electron can be ejected from the surface and detected as an Auger secondary electron.

Due to the specific energy levels involved in the transition and the energy of the detected Auger electron, the atom from which the electron was ejected can be identified. Auger Spectroscopy can also be used for depth profiling with the use of an ion gun as part of the vacuum system. As the ion gun etches away the material, the electron probe focused on the same spot can give information about the composition of the surface layers with sputter depth. A detailed discussion of the Auger process can be obtained from other sources [42, 54].

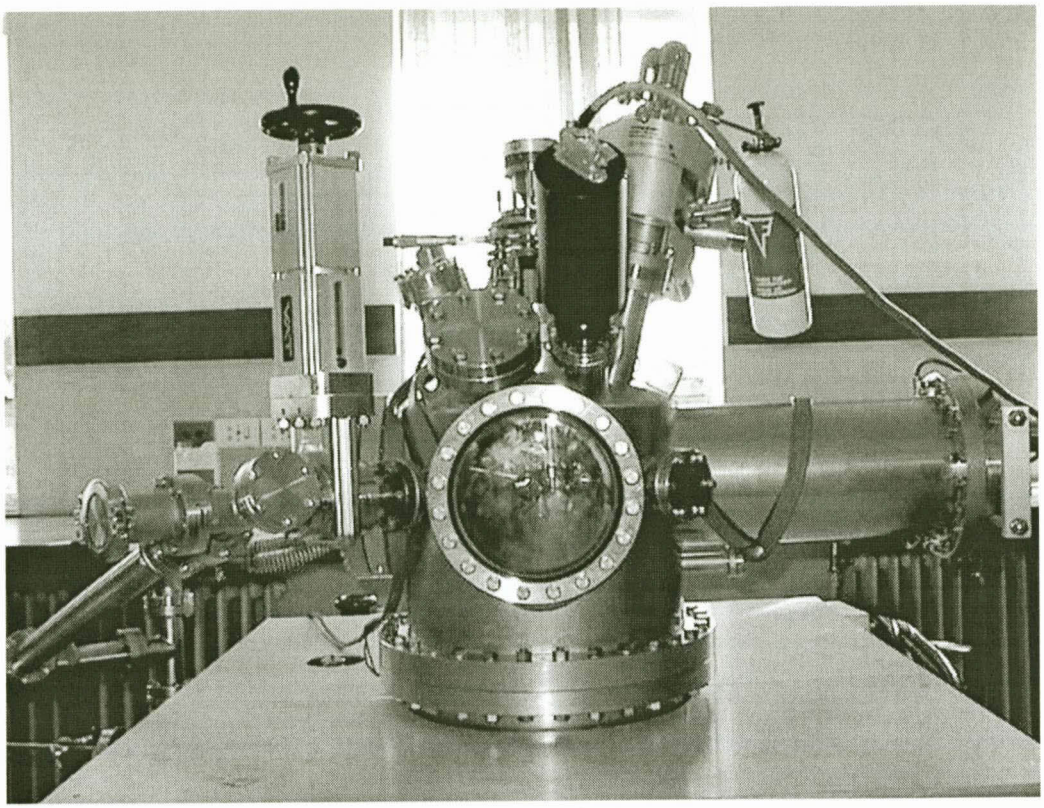

Figure 4.1: A photo of a PHI Model 549 ESCA system.

4.2.2. Ultra High Vacuum Chamber

The vacuum chamber is equipped with a turbo molecular pump and a rotary vain pump to attain pressures down to 10^{-6} Torr. An ion pump and a Titanium sublimation pump (TSP) are also attached to the system and are used to attain ultrahigh vacuum, < 10^{-9} Torr in the chamber. The AES apparatus is housed inside a vacuum chamber and all experiments are performed under ultrahigh vacuum conditions. The base pressure for this study was < 2 x 10^{-9} Torr.

The vacuum chamber is divided into a lower and an upper chamber. The upper chamber contains the AES apparatus, the ionisation pressure gauge, the gas analyser, differentially pumped ion gun, and the sample carousel. The lower chamber houses the ion pump and the titanium sublimation pump. These two chambers are separated by a pop-up valve. A leak valve is

attached to the lower chamber via a bellows enabling the inlet of gases such as oxygen.

4.2.3. Control Unit Settings

Attached to the AES system are several control units. In this study, the control units for the different parameters used during the measurements were set as shown in Table 4.1 below.

Electron Gun	
V_P	2 keV
I_B	7 μA
Ion Gun	
V_{ION}	2 keV
I_{ION}	0.6 μA
Gas	Ar
Raster size (cleaning)	2x2 mm
Spectrometer	
Scan rate	4 eV/s
Modulation energy (peak to peak)	4 eV
Time constant	0.03
$V_{MULTIPLIER}$	1800V

Table 4.1: The AES settings.

The peak shapes in the selected energy intervals with time are measured using a multiplexer. In the selection of the energy intervals in the multiplexer, the peaks of all the basic contaminant elements and the elements of major concern were included. The energy selection of the multiplexer used are given in Table 4.2 below.

Element	Lower limit (eV)	Upper limit (eV)
TiAl	15	100
C	250	295
Cl	170	195
CrO	480	580
CMo	173	295
O	490	535
S	135	160
SCl	153	195
Ti	360	457
V	457	484
SZr	105	168

Table 4.2: Multiplexer energy interval settings for different elements.

Due to the large number of elements to be analysed on the surface in the samples, Ti6Al4V and Ti3Al6Cr4Zr4Mo, some of the elements energy intervals were set to the same energy interval. After the measurements were completed, the appropriate software developed in the department was used to separate the different peaks.

4.2.4. Heater Unit

The sample holder used in this study contains a filament and a chromel-alumel thermocouple. The heater control unit regulates the current through the filament and thus controls the temperature of the sample. The figure below contains the photographs of the sample holder used in this study.

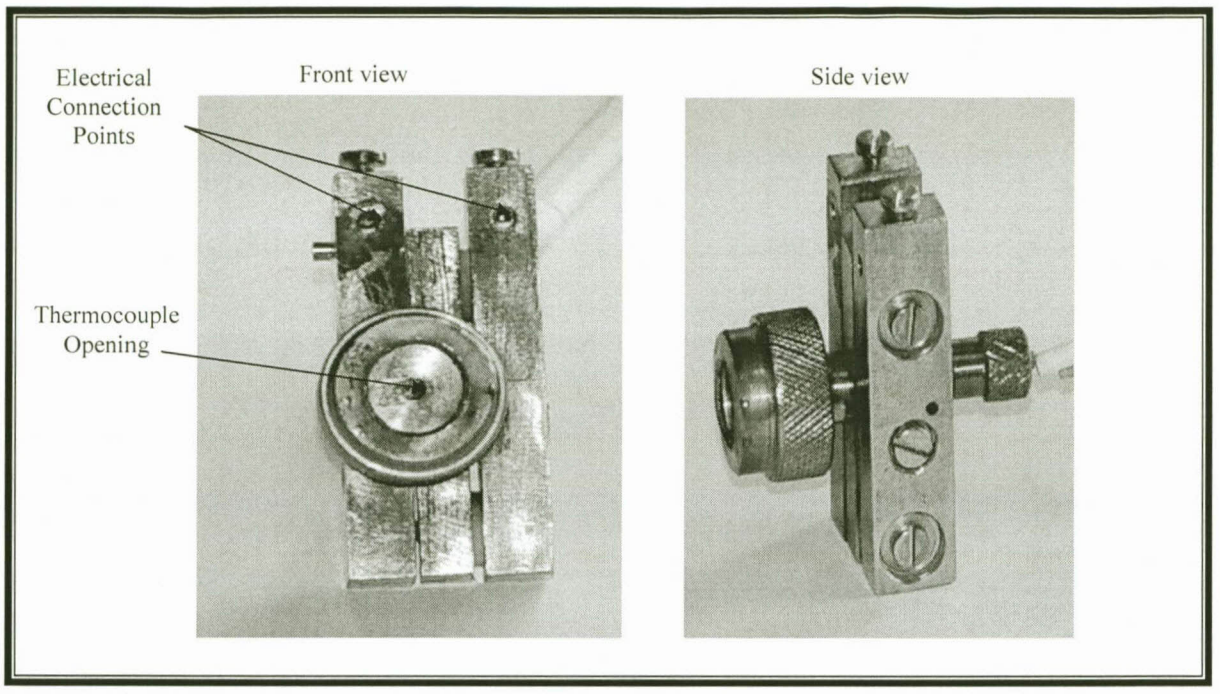

Figure 4.2: Photographs of the sample holder and heating unit.

4.2.5. Samples

Three different samples were used in this study.

	Ti	Al	V	Cr	Mo	Zr	S	P	Si
Commercially pure-Ti	98.980	0.030	0.210	0.030	0.020	0.110	0.010	0.010	0.030
Ti6Al4V	89.060	5.820	4.390	0.040	0.010	0.100	0.000	0.030	0.050
Ti3Al8V6Cr4Zr4Mo	73.370	2.950	8.760	5.450	4.300	4.130	0.000	0.000	0.040

Table 4.3: The impurity concentration in atomic percentage for the three samples.

All samples were obtained from the SOMCHEM in Somerset-west, Cape Town, South Africa.

The samples were polished to a mirror-like finish, to remove scratches from the surface. The polishing was done using diamond paste. After polishing, the samples were rinsed thoroughly with acetone.

4.3. Experimental procedure

4.3.1. Sample preparation

To make it possible to monitor the surface temperature, the samples were cut into the designed shape to make sure that the effect of the change in the surface temperature will take enough time before it can affect the control temperature. Two chromel-alumel thermocouples measuring within ±5 °C tolerance were spot-welded to each sample as shown in figure 4.3 below, with one at the steel disc edge between the heater and the back (2) of sample to control the sample's temperature and the other one on the sample surface (1) to monitor the temperature changes. The spot to be analysed for the temperature change was the one next to the thermocouple on the sample surface. There was a temperature difference of about 100 – 200 °C between the control and the surface temperatures which made it possible to monitor the change in the surface temperature. The samples were fitted into the sample holder and mounted on the sample carousel in the vacuum chamber.

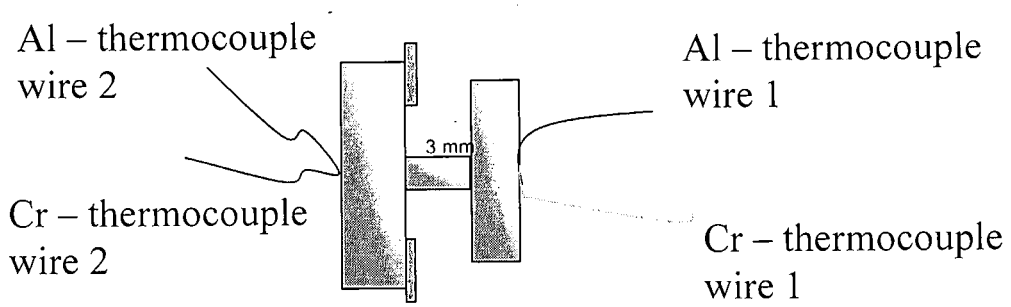

Figure 4.3: Side view of the sample. Thermocouple 1 was used to monitor the temperature of the surface, while thermocouple 2 was used to control the sample temperature.

Because of the high chemical reactivity of titanium and titanium alloys, atmospheric gettering generated a substantial oxygen and carbon

contamination layer. The source of high initial concentrations of O and C is due to exposure to atmospheric gases or present during sample manufacturing. The contaminants were removed from the surface by Ar^+ sputtering, but they were still present after sputtering because of the continual uptake of the background gases.

4.3.2. Oxidation and segregation run

In this study, great care was taken to keep the experimental conditions constant for the oxidation of the various samples. The filaments were switched on an hour before the measurements commenced to allow them to stabilise. The same procedure was followed for the oxidation of the three samples.

The oxidation procedure can be divided into the following steps:

1. The sample was sputter cleaned using the parameters as given in Table 4.1.
2. An Auger spectrum of the sputter cleaned sample surface was taken.
3. During sputtering, the sample temperature was increased to the desired oxidation temperature.
4. The valve between the upper and the lower chambers was closed partially to decrease the pump rate and ensure a constant gas flow.
5. As soon as the valve was closed, and the temperature was stable, the sputtering was stopped and the Ar^+ gas leak valve was closed completely. The Ar^+ gas was pumped out of the chamber and the oxygen gas at a desired pressure was allowed into the system and the measurements were started.
6. Another Auger spectrum after oxidation was taken.

The effects of both the electron and ion beams on the surface temperature were also measured. In the oxidation of Ti3Al8V6Cr4Zr4Mo, the surface temperature was not studied since no increase due to oxidation in the other samples was measured. During the oxidation process at the lower

oxygen pressures, the decrease in the rate of oxidation as the oxidation temperature increases was observed. As a result, oxidation rate measurements at constant oxygen pressures 5 x 10^{-8} Torr and 5 x 10^{-7} Torr and different temperatures for the commercially pure titanium were performed. Finally the impurity segregation measurements at both constant temperatures and linear heating ramp were done.

The following procedure for the segregation studies was followed:

1. The sample was sputter cleaned using the parameters as given in Table 4.1.
2. An Auger spectrum of the sputter cleaned sample surface was taken.
3. During sputtering, the sample temperature was increased to the desired temperature.
4. As soon as the temperature was stable, simultaneously the sputtering was stopped and the measurements were started.
5. An Auger spectrum after the segregation process was taken.

4.4. Linear Least Square Fit

In this investigation, during the annealing process, the titanium carbide (TiC), titanium oxide (TiO) and titanium nitrite (TiN) formed due to the reaction between carbon, oxygen, nitrogen and titanium. However, because the Ti, TiC, TiO and TiN peaks do overlap in the energy regions where their characteristic spectra are, and since the peaks cannot be monitored separately with conventional Auger peak-to-peak heights (APPH) measurements, the linear least squares (LLS) [55,56] method is used to determine the fraction that the Ti and TiC, Ti and TiO, and Ti and TiN contribute to the measured APPH. The need for this technique arises from the common practice to store only the APPH of a selected peak of each element that is studied during depth profiling or a temperature run, instead of storing the peak shapes at each time step. The method decompose the combined peak into the spectra of the two standards with weighted least squares fit and explain features in a measured APPH's containing both chemical states.

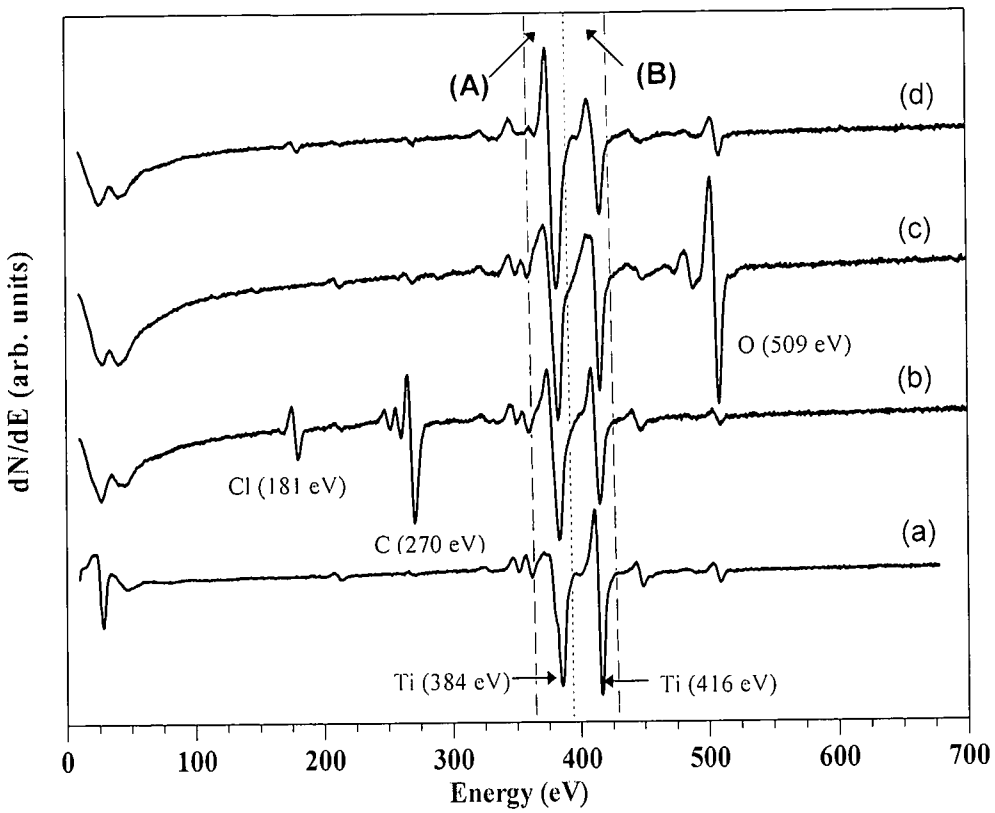

Figure 4.4: The standard AES spectra for; (a) commercially pure Ti, (b) TiC, (c) TiO and (d) TiN.

In figure 4.4, the two energy regions where the peaks overlap are chosen as 355 – 396 eV and 396 – 430 eV respectively.

The APPH-functions of the combined peaks in the two energy intervals could be defined as:

$$I_{(A)}(\alpha,\beta) = Apph_{(A)}(\alpha f_{Ti} + \beta f_{TiC}) \quad (4.1)$$

$$I_{(B)}(\alpha,\beta) = Apph_{(B)}(\alpha f_{Ti} + \beta f_{TiC}) \quad (4.2)$$

where α and β are true yield of Ti and TiC respectively in the APPH. The subscripts (A) and (B) denote the two energy intervals where the peaks overlap. Each has to be evaluated computationally in the following way: it

combines the spectra of the standards in the specified region and using weights α and β, then finds the maximum and minimum of the combination computationally and supplies the minimised difference between the maximum and minimum as output.

In order to determine the contributions, α (Ti) and β (TiC/TiO/TiN) for each measured value of t, equation 4.3 below was used.

$$g(\alpha,\beta,t) = [I_{(A)}(\alpha,\beta) - I_{(A)}^{me}(t)]^2 + [I_{(B)}(\alpha,\beta) - I_{(B)}^{me}(t)]^2 \qquad (4.3)$$

where $I_{(A)}(\alpha,\beta)$ and $I_{(B)}(\alpha,\beta)$ are the APPH's of the standards in the intervals (A) and (B). And $I_{(A)}^{me}(t)$ and $I_{(B)}^{me}(t)$ are the measured APPH's in the energy intervals (A) and (B).

The parameters can be easily determined by a MATLAB code for the script file which loops through all the time steps and calculates the correct contributions. The method is well explained in Asante et al [60].

Chapter 5

Results and discussion

5.1. Introduction

The oxidation behaviour of titanium can be used as reference point to establish the influence of the alloying elements on the oxidation behaviour of Ti6Al4V and Ti3Al8V6Cr4Zr4Mo samples. The oxidation behaviour of the commercially pure Ti at different temperatures and pressures is presented and discussed in this chapter and followed by the discussion on the oxidation behaviour of Ti6Al4V and Ti3Al8V6Cr4Zr4Mo. The oxidation rate of pure Ti at a constant pressure and different temperatures is dealt with. The effect of both electron and ion beams on the surface temperature is also discussed. Finally the impurities segregation from the bulk of the three samples at different constant temperatures as well as heating with a linear heating ramp will be discussed. A linear least square (LLS) method was used to determine the contributions of titanium (Ti), titanium oxide (TiO), titanium carbide (TiC) and titanium nitrite (TiN) from the measured Auger profiles.

5.2. Oxidation of commercially pure Ti

5.2.1. Room temperature oxidation

The sample was sputter cleaned using the parameters in Table 4.1 before it was exposed to the O environment. The AES spectra before and after oxidation are shown in the figure 5.1 below.

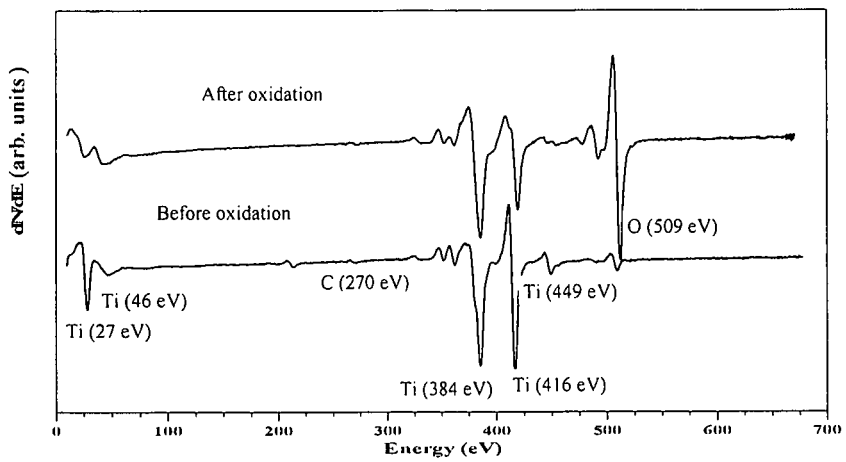

Figure 5.1: The AES spectra of pure Ti before and after oxidation.

The Auger spectrum after sputter cleaning (with argon Ar^+) before oxidation was taken and indicates the presence of O and C contaminants on the surface, which could not be removed completely by sputtering. As soon as the O was released into the system, the low energy (20-50) Ti as well as the high energy (370-450) Ti peaks shifted and changes in shape are also recorded. The O peak also increased rapidly as O was admitted into the system.

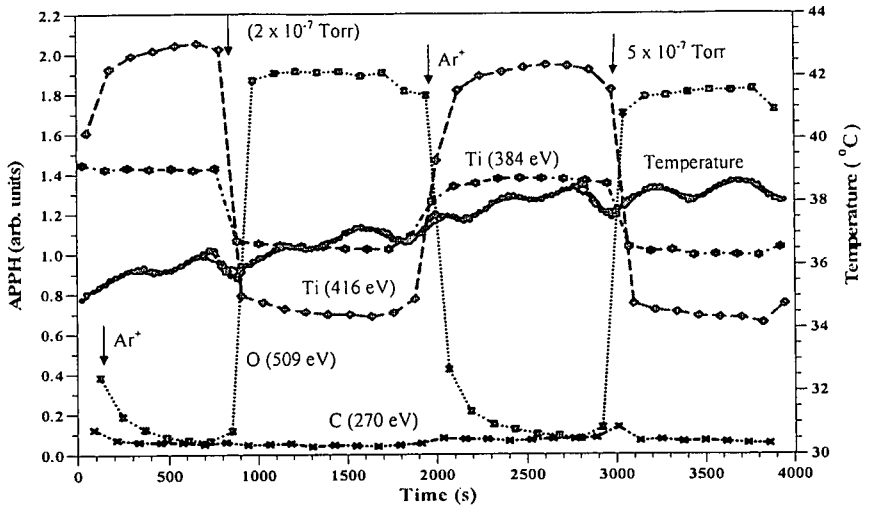

Figure 5.2: The room temperature APPH changes during sputtering and oxidation at 2 x 10^{-7} Torr and 5 x 10^{-7} Torr oxygen pressures.

Figure 5.2 shows the room temperature APPH changes during sputtering and oxidation of pure commercial Ti at 2 x 10^{-7} Torr and 5 x 10^{-7} Torr oxygen pressures as a function of time. The O peak increased immediately when O was leaked into the system at the different pressures and the rate of oxidation was observed to be pressure depended, the oxidation rate increases with the increase in O pressure. The oxidation rate followed the parabolic rate law [4,52] and the type of the oxide layer formed on the surface (compact) can be used to explain the oxidation behaviour. Both titanium peaks, Ti (384 eV and 416 eV), decreased as the O peak increased, with Ti (416 eV) peak decreasing more severe than the Ti (384 eV) peak, which is expected for Ti oxidation. The C peak showed no important features accept a slight increase at 5 x 10^{-7}. Torr. The fluctuation in temperature of about 0.5 °C as discussed in section 5.6 was measured. No increase in surface temperature was measured during the oxidation process.

5.2.2. Oxidation of commercially pure Ti at different Temperatures as function of time

During sputter cleaning, the temperature was increased to the required value and allowed to stabilise. Once the temperature was stable, sputtering was stopped, simultaneously the O was leaked into the system to the desired oxidation pressure as soon as Ar was removed and the measurements were started.

The oxidation measurements were repeated at the different temperatures (300, 400, 500 and 630 °C) and oxygen pressures (5 x 10^{-8}, 5 x 10^{-7} and 2 x 10^{-6} Torr). The same oxidation procedures were followed for all three samples.

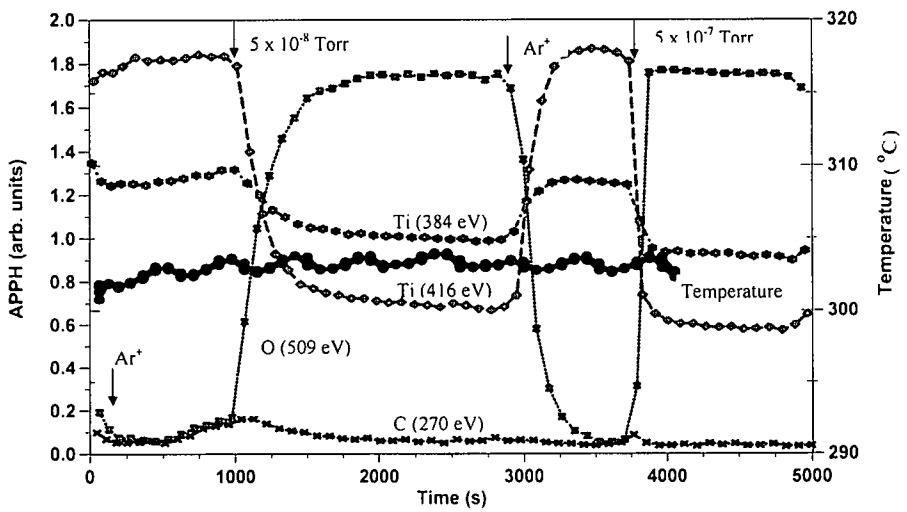

Figure 5.3: The 300 °C APPH changes during sputtering and oxidation at 5 x 10^{-8} Torr and 5 x 10^{-7} Torr oxygen pressures.

Figure 5.3 shows the 300 °C APPH changes during sputtering and oxidation of commercially pure Ti at 5 x 10^{-8} Torr and 5 x 10^{-7} Torr oxygen pressures. The O peak as in the case of room temperature oxidation increased immediately when O was leaked into the system at the different temperatures and pressures. Both the titanium peaks, Ti (384 eV and 416 eV), decreased

as the O peak increased, with Ti (416 eV) peak still showing a more severe decrease than the Ti (384 eV) peak. The rate at which the Ti peaks are decreasing increases with the increase in the O pressure. The C signal showed a slight increase as the O peak increased at 5 x 10^{-8} Torr but decreased after a few seconds. No increase in surface temperature was measured during the oxidation process.

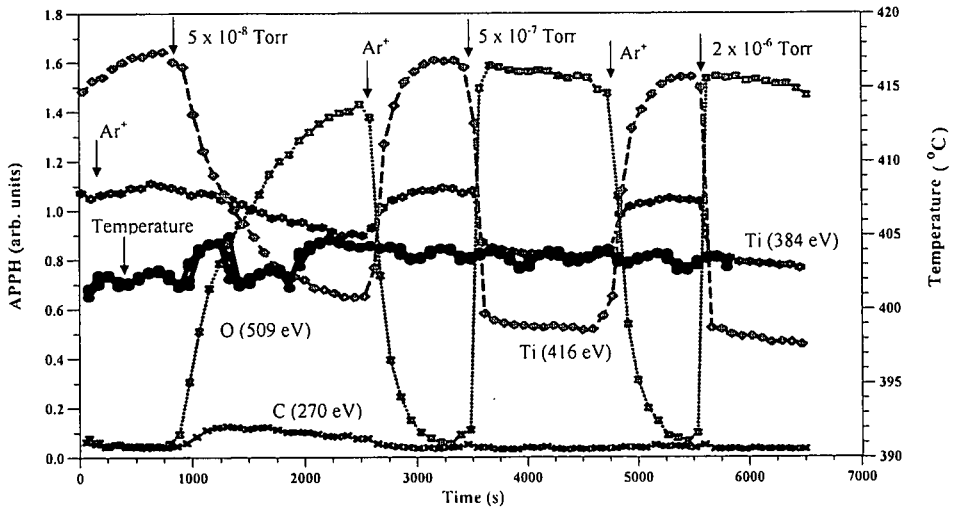

Figure 5.4: The 400 °C APPH changes during sputtering and oxidation at 5 x 10^{-8} Torr, 5 x 10^{-7} Torr and 2 x 10^{-6} Torr oxygen pressures.

Figure 5.4 shows the 400 °C APPH changes during sputtering and oxidation of commercially pure Ti at 5 x 10^{-8} Torr, 5 x 10^{-7} Torr and 2 x 10^{-6} Torr oxygen pressures. The Ti (384 eV) showed a slower decreasing rate at 5 x 10^{-8} Torr compared to the other lower temperatures oxidation. The C peak also showed a slight increase as the O peak increased at 5 x 10^{-8} Torr. No increase in surface temperature was measured during the oxidation process.

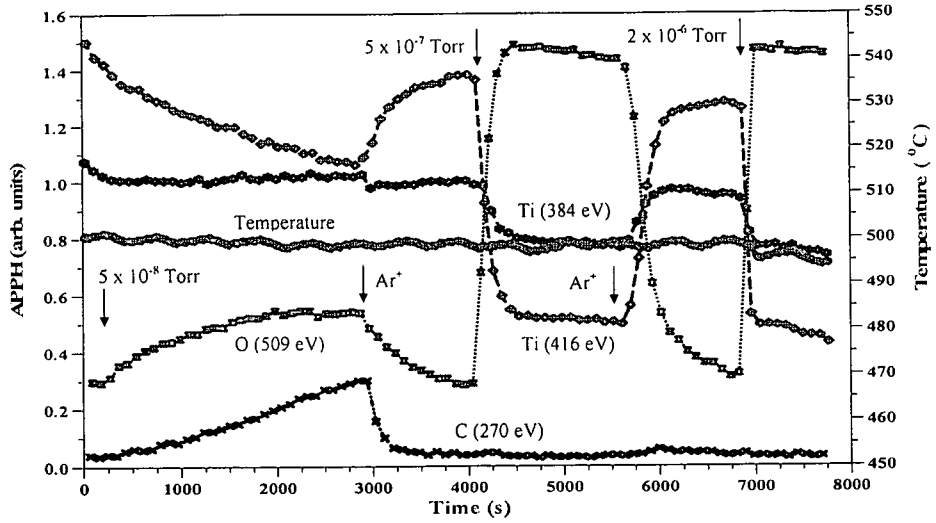

Figure 5.5: The 500 °C APPH changes during sputtering and oxidation at 5 x 10^{-8} Torr, 5 x 10^{-7} Torr and 2 x 10^{-6} Torr oxygen pressures.

Figure 5.5 shows the 500 °C APPH changes during sputtering and oxidation of a commercially pure Ti at 5 x 10^{-8} Torr, 5 x 10^{-7} Torr and 2 x 10^{-6} Torr oxygen pressures. The Ti (384 eV) showed a slight decrease at 5 x 10^{-8} Torr compared to the other lower temperatures and then increased to reach the equilibrium. After 5 x 10^{-8} Torr oxidation, during sputter cleaning, the Ti (384 eV) signal decreased. This behaviour is attributed to the formation of the TiC on the surface as discussed in the later section. The C peak showed an increase as the O peak increased at 5 x 10^{-8} Torr. The decrease in the rate of oxidation at the lower pressure (5 x 10^{-8} Torr) as the temperature increases is apparent. No increase in surface temperature was measured during the oxidation process.

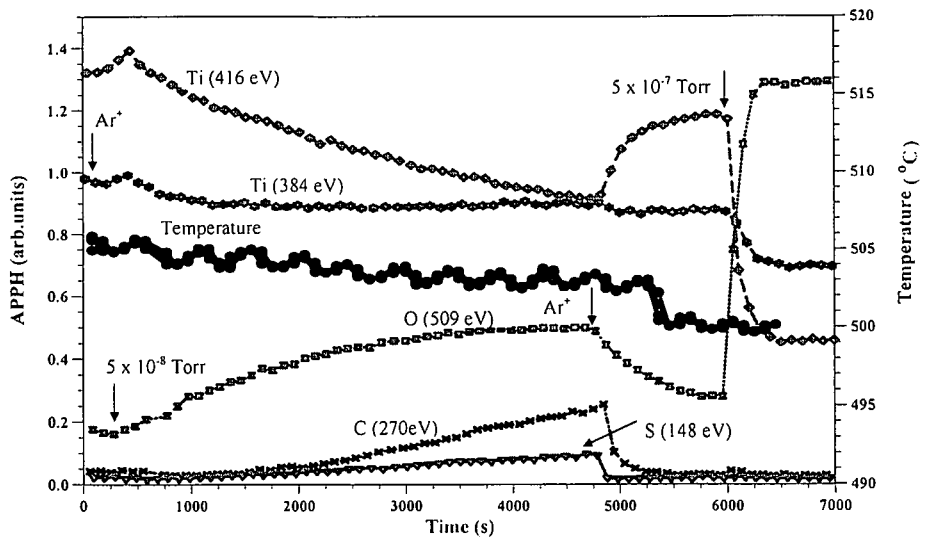

Figure 5.6: The 500 °C APPH changes during sputtering and oxidation at 5 x 10^{-8} Torr and 5 x 10^{-7} Torr oxygen pressures.

Figure 5.6 shows the 500 °C APPH changes during sputtering and oxidation at 5 x 10^{-8} Torr and 5 x 10^{-7} Torr oxygen pressures. The segregation of S and C at 5 x 10^{-8} Torr were observed, which led to site competition on the surface and as a result, the further decrease in the rate of oxidation. At the pressure of 5 x 10^{-8} Torr, the Ti (384 eV) signal decreased slightly and increased and reached equilibrium due to the formation of the TiC. During Ar^+ sputter cleaning, after 5 x 10^{-8} Torr oxidation, the Ti (384 eV) signal was observed to be decreasing which suggest the formation of titanium carbide on the surface during the oxidation process. No sulphur segregation was observed at higher pressures, 5 x 10^{-7} Torr due to the availability of O on the sample's surface.

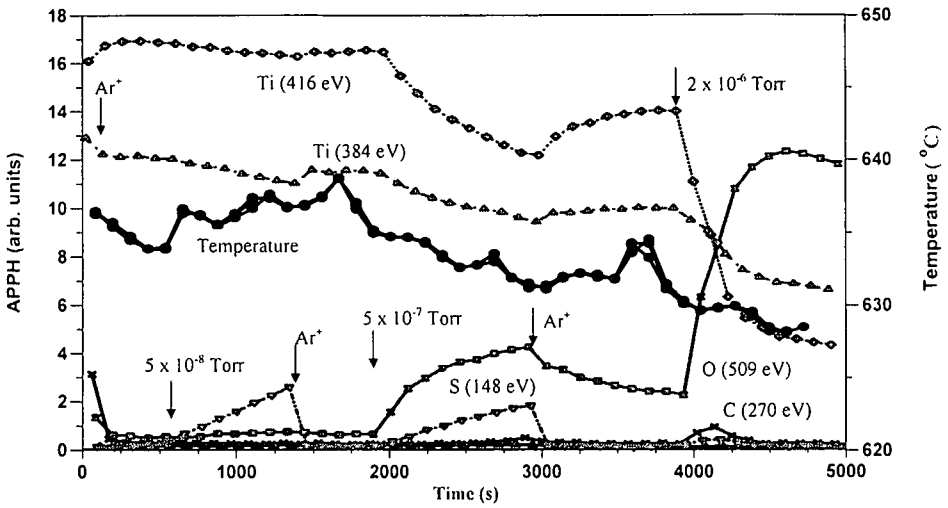

Figure 5.7: The 630 °C APPH changes during sputtering and oxidation at 5 x 10^{-8} Torr, 5 x 10^{-7} Torr and 2 x 10^{-6} Torr oxygen pressures.

It is apparent from figure 5.7 that the O peak increases slightly at 5 x 10^{-8} Torr. Both Ti (384 eV) and Ti (416 eV) signals decreased slightly at 5 x 10^{-8} Torr and decreases more as the O pressure increases. The C peak showed a slight increase as the O increases to 5 x 10^{-7} Torr and 2 x 10^{-6} Torr. The decrease in the rate of oxidation as the temperature increases is also apparent. S segregates very strongly at 5 x 10^{-8} Torr and decreases as the O pressure was increased. No S segregation was observed at 2 x 10^{-6} Torr and this is attributed to the availability of O on the surface of the sample. No increase in surface temperature was measured during the oxidation process.

5.2.3. Rate of oxidation

The results of the oxidation rate measurements for a pure commercial Ti at different temperatures and constant pressure that were performed are shown in figures 5.8 and 5.9 below. The decrease in the rate of oxidation with the increase in the oxidation temperature at lower pressures was apparent.

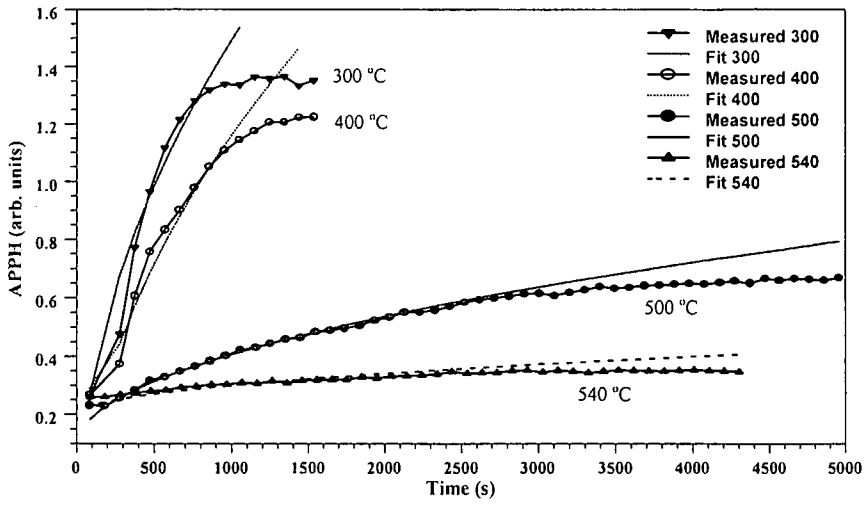

Figure 5.8: Illustration of the rate of oxidation at different temperatures and a constant oxygen pressure of 5 x 10^{-8} Torr.

At 400 °C a decrease in the rate of oxidation was observed. A further decrease in oxidation rate was observed at the temperature of 500 °C. This is attributed to the strong segregation of S and some C to the surface as seen from figure 5.6 above, which led to site competition between O and the segregating species (S and C) on the surface. The decrease is also attributed to the decrease in mean surface lifetime of the O at this pressure. A further decrease in the oxidation rate was observed at 540 °C due to the segregation rate of S which increased at higher temperatures. The initial reaction followed the parabolic rate law as seen from the parabolic fits in figure 5.8 (see section 2.3).

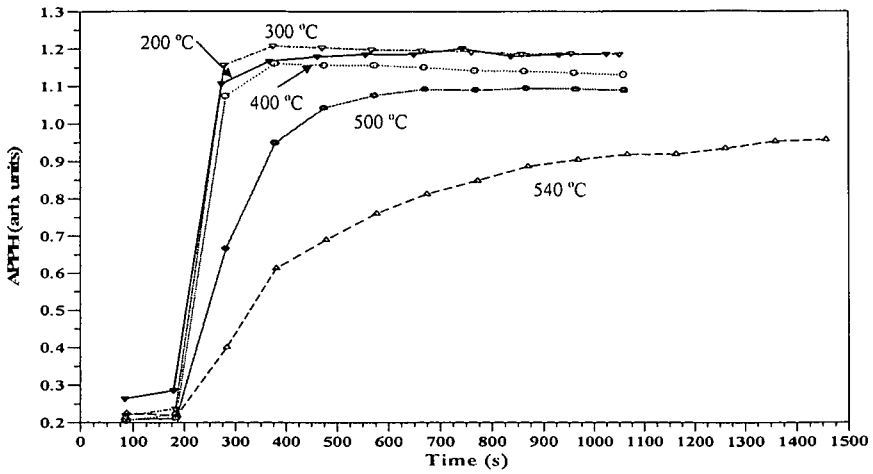

Figure 5.9: Illustration of the rate of oxidation at different temperatures and a constant oxygen pressure of 5 x 10^{-7} Torr.

The oxidation rates at 200 °C, 300 °C and 400 °C showed almost no difference due to the availability of O at this pressure. A clear decrease in the rate of oxidation was observed at 500 °C, the temperature at which strong S segregation was measured. At 540 °C the segregation rate of S increases and as a result a further decrease in the oxidation rate was observed due to the site competition between the O and the segregating S.

5.3. Oxidation of Ti6Al4V

5.3.1. Room temperature oxidation

The sample as in the case of commercially pure Ti was sputter cleaned using the parameters in Table 4.1 before exposed to the O environment. The same procedure as in the oxidation of commercially pure Ti was followed. The AES spectra before and after oxidation are shown in figure 5.10 below.

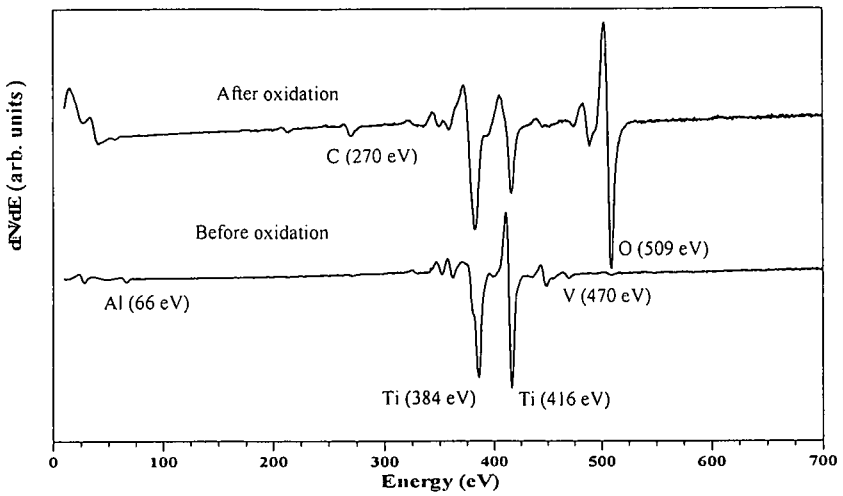

Figure 5.10: The AES spectra of Ti6Al4V before and after oxidation.

The AES spectrum after sputter cleaning (with argon Ar^+) shows the alloying elements Al and V and small contamination of O and C which could not be removed completely by sputtering due to high chemical reactivity of the alloy. There was no C on the surface after oxidation and the Al and V signals decreased greatly. The titanium peaks (20 eV-40 eV and 370 eV- 450 eV) shifted as the O signal increases and changes are also recorded.

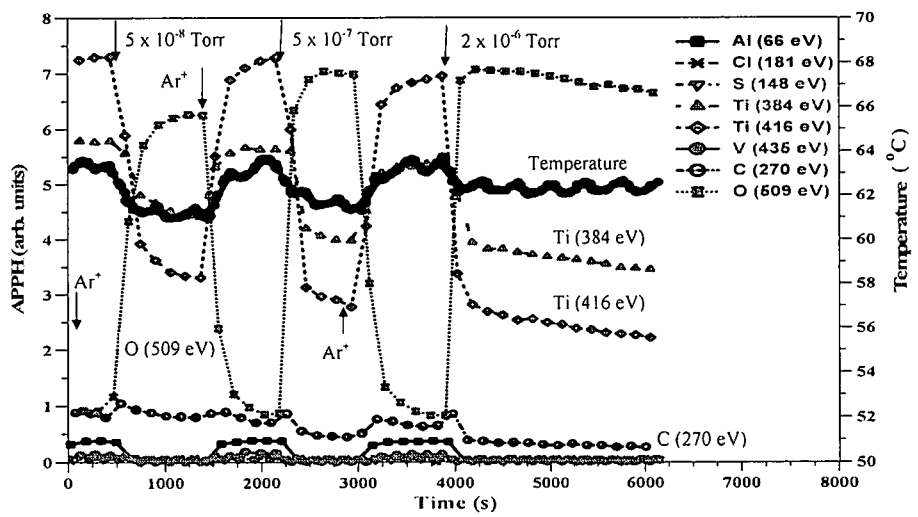

Figure 5.11: The room temperature APPH changes of Ti6Al4V during sputtering and oxidation at 5 x 10^{-8} Torr, 5 x 10^{-7} Torr and 2 x 10^{-6} Torr.

Figure 5.11 shows the room temperature APPH changes during sputter cleaning and oxidation of the Ti6Al4V alloy at 5 x 10^{-8} Torr, 5 x 10^{-7} Torr and 2 x 10^{-6} Torr oxygen pressures as a function of time. As in the case of commercially pure titanium, it was observed that the O peak increased immediately when O was leaked into the system at the different temperatures and pressures. The oxidation rate followed the parabolic rate law. Both titanium peaks, Ti (384 eV and 416 eV), followed the same trend as in the case of pure Ti as the O peak increased. The C, Al, Cl, V and S peaks showed no important features. No increase in temperature was measured.

5.3.2. Oxidation of Ti6Al4V at different temperatures as function of time

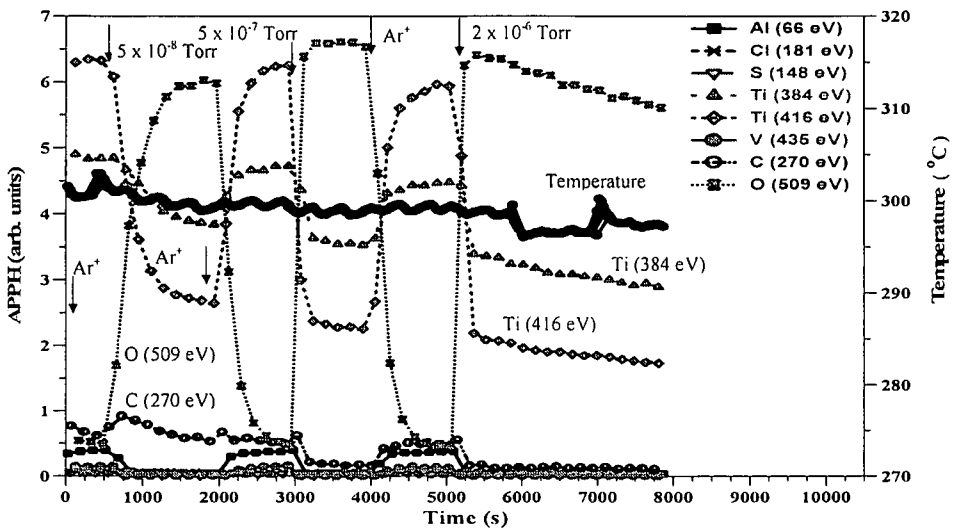

Figure 5.12: The Ti6Al4V 300 °C APPH changes during sputtering and oxidation at 5 x 10^{-8} Torr, 5 x 10^{-7} Torr and 2 x 10^{-6} Torr.

Figure 5.12 shows the 300 °C APPH changes during sputter cleaning and oxidation of the Ti6Al4V alloy at 5 x 10^{-8} Torr, 5 x 10^{-7} Torr and 2 x 10^{-6} Torr oxygen pressures. The O peak increased immediately as in the case of room temperature oxidation when O was leaked into the system at the different pressures. The rate at which the Ti peaks decrease increases with the

increase in the O pressure. The C peak showed a slight increase as the O peak increased at 5 x 10^{-8} Torr but decrease at longer exposure times. The APPH's of S, Cl, V and Al showed no important features. No increase in surface temperature was measured during the oxidation process.

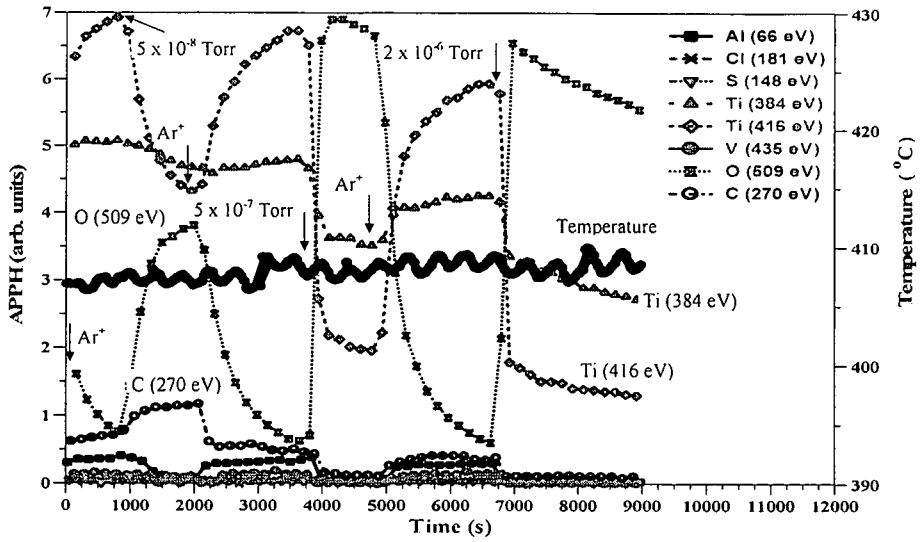

Figure 5.13: The Ti6Al4V 410 °C APPH changes during sputtering and oxidation at 5 x 10^{-8} Torr, 5 x 10^{-7} Torr and 2 x 10^{-6} Torr.

Figure 5.13 shows the 410 °C APPH changes during sputter cleaning and oxidation of the Ti6Al4V alloy at 5 x 10^{-8} Torr, 5 x 10^{-7} Torr and 2 x 10^{-6} Torr oxygen pressures. The rate at which the Ti APPH's decrease is slower at 5 x 10^{-8} Torr compared to the other lower temperatures oxidation. The C peak still showing a slight increase as the O peak increased at 5 x 10^{-8} Torr and due to the site competition between O and C at higher pressures, C ceased segregation. The Al, Cl, V and S APPH's still showing no important features. No increase in surface temperature was measured during the oxidation process.

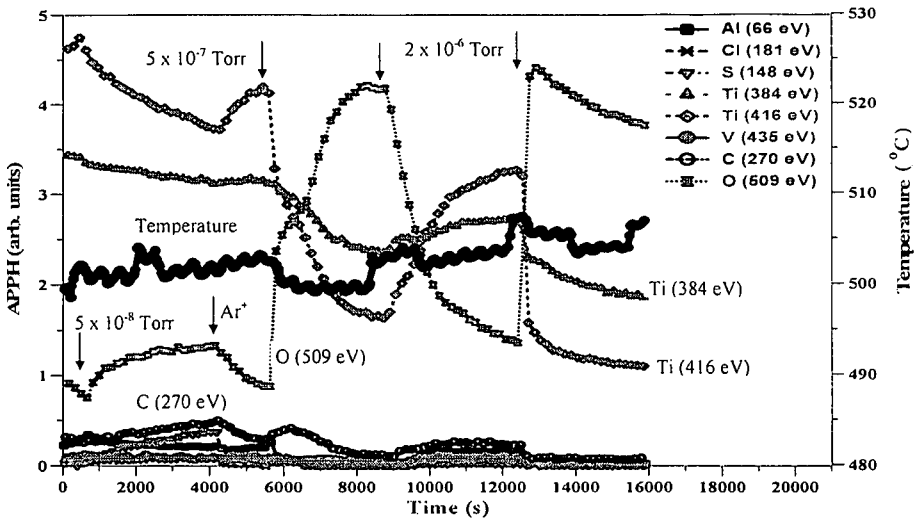

Figure 5.14: The Ti6Al4V 500 °C APPH changes during sputtering and oxidation at 5 x 10^{-8} Torr, 5 x 10^{-7} Torr and 2 x 10^{-6} Torr.

Figure 5.14 illustrates the 500 °C APPH changes during sputter cleaning and oxidation of the Ti6Al4V alloy at 5 x 10^{-8} Torr, 5 x 10^{-7} Torr and 2 x 10^{-6} Torr oxygen pressures. The changes in the Ti (384 eV) APPH showed a further decrease in oxidation rate at 5 x 10^{-8} Torr compared to the other lower temperatures oxidation and then remained constant. Segregation of S at the pressure of 5 x 10^{-8} Torr was observed and disappeared as the pressure increases. The C peak showed an increase as the O peak increased at 5 x 10^{-8} Torr. The Cl, V and Al peaks showed no important features. The decrease in the rate of oxidation at the lower pressure (5 x 10^{-8} Torr) as the temperature increases is apparent. No increase in surface temperature was measured during the oxidation process. The amount of heat generated during the reaction of Ti atoms with O_2 to form the TiO_2 layer is 939.7 KJ.

$$Ti_{(s)} + O_{2(g)} \longrightarrow TiO_{2(s)} \quad (\Delta H_f = 939.7 \text{ KJ})$$

The number of Ti atoms available for the reaction on the sputter cleaned surface of 2mm x 2mm was calculated to be 6 x 10^{13} atoms which correspond to 9.97 x 10^{-11} moles. The volume of this single surface layer (2mm x 2mm) is 1.16 x 10^{-15} m^3 and the mass of the atoms is 5.23 x 10^{-9} g. Using equation

2.13, the change in the surface temperature for this single layer due to the reaction was calculated to be 34450 °C. The increase in the thickness of the atomic layer led to the great decrease in the temperature change. This is shown in figure 5.15 below.

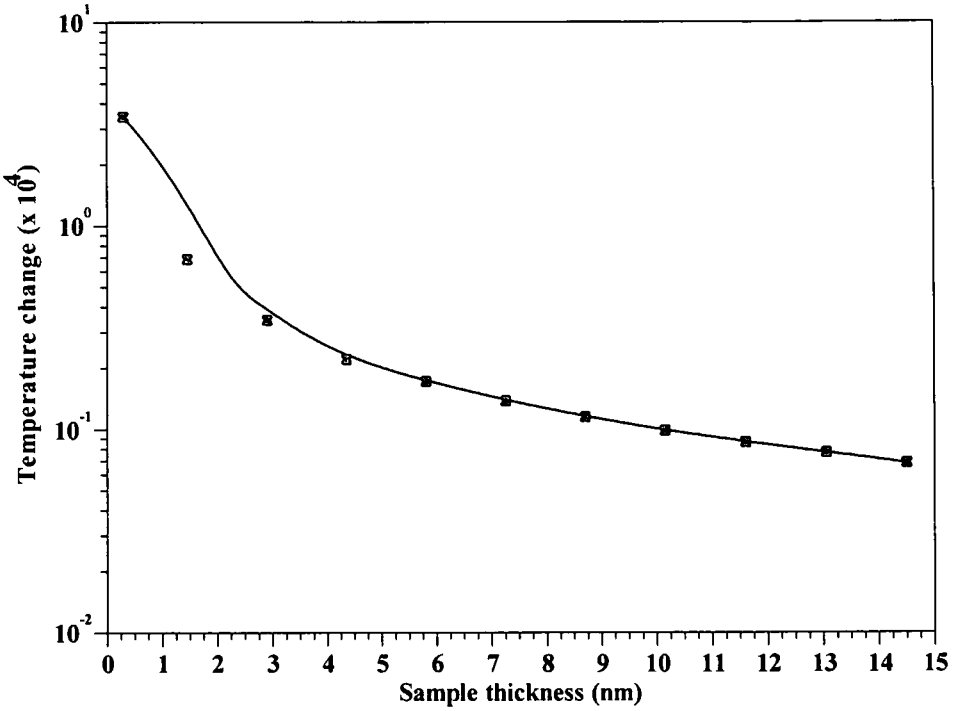

Figure 5.15: The graph of temperature change versus sample thickness.

For 0.29 nm atomic layer, 34450 °C was calculated and for 0.9 mm, 0.011 °C was calculated. But according to our setup, the shape of the sample was round and just a small area in the sputter cleaned surface (2mm x 2mm) was analysed for the change in temperature. However, certain amount of the heat generated will be transferred to other parts of the sample. As a result, the change in the surface temperature is expected to be much less than calculated.

5.4. Oxidation of Ti3Al8V6Cr4Zr4Mo

5.4.1. Room temperature oxidation

The sample was sputter cleaned using the parameters in Table 4.1 before exposed to the O environment. The same procedure as in the oxidation of the other samples was followed. The AES spectra before and after oxidation are shown in figure 5.16 below.

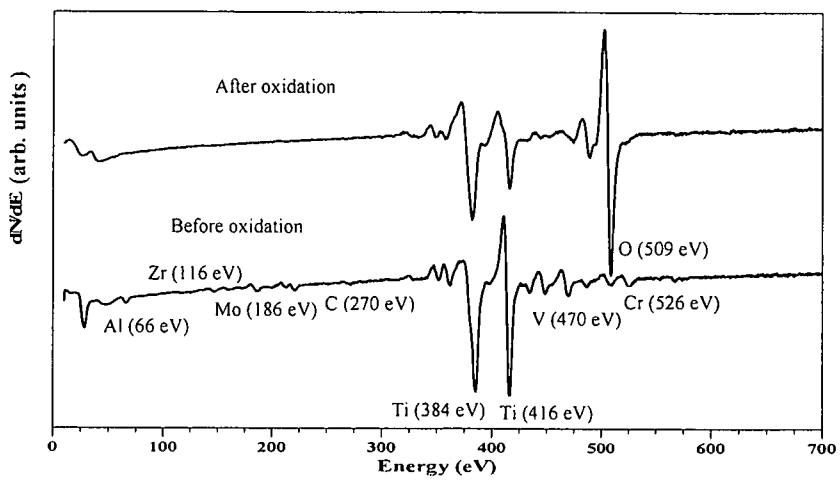

Figure 5.16: The AES spectra of Ti3Al8V6Cr4Zr4Mo before and after oxidation.

The AES spectrum after sputter cleaning (with argon Ar^+) shows the alloying elements Al, Cr, Mo, V and Zr and small contamination of O and C which could not be removed completely by sputtering due to high chemical reactivity of the alloy. There was no C on the surface after oxidation and the alloying elements signals decreased greatly. The titanium peaks (20 eV-40 eV and 370 eV- 450 eV) shifted as the O signal increases and changes are also recorded.

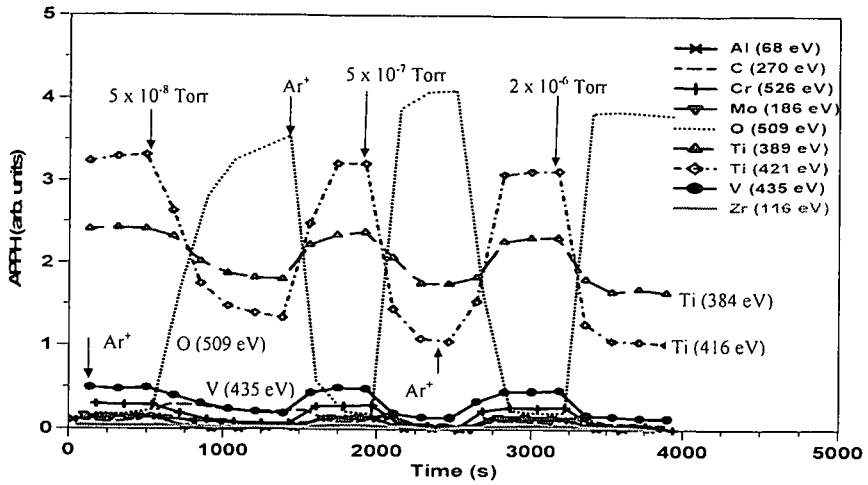

Figure 5.17: The room temperature APPH changes during sputtering and oxidation at 5 x 10^{-8} Torr, 5 x 10^{-7} Torr and 2 x 10^{-6} Torr.

Figure 5.17 shows the room temperature APPH changes during sputter cleaning and oxidation of the Ti3Al8V6Cr4Zr4Mo alloy at 5 x 10^{-8} Torr, 5 x 10^{-7} Torr and 2 x 10^{-6} Torr oxygen pressures. It was also observed, as in the previous samples that the O peak increased immediately when O was leaked into the system at the different temperatures and pressures. The oxidation rate followed the parabolic rate law. The titanium peaks followed the very same trend as the O signal increased. All the other peaks C, Al, Cr, Mo, V and Zr decreased or disappeared as the O was allowed into the system.

5.4.2. Oxidation of Ti3Al8V6Cr4Zr4Mo at different Temperatures as function of time

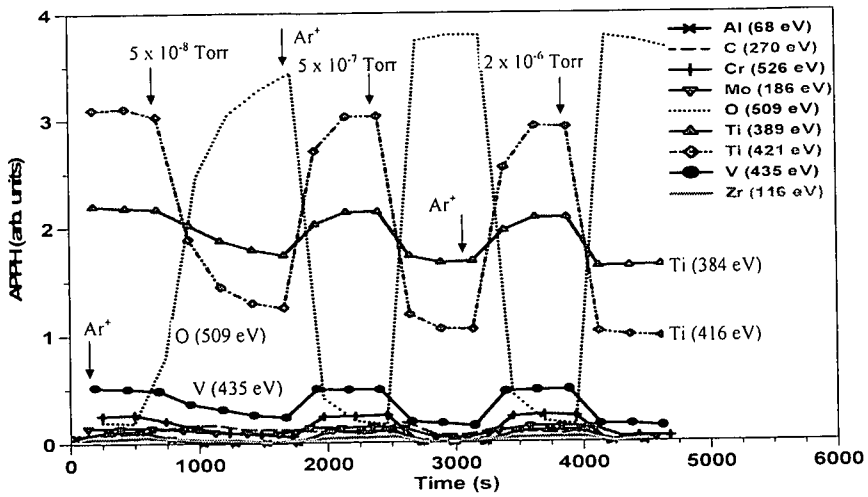

Figure 5.18: The Ti3Al8V6Cr4Zr4Mo 300 °C APPH changes during sputtering and oxidation at 5 x 10^{-8} Torr, 5 x 10^{-7} Torr and 2 x 10^{-6} Torr.

Figure 5.18 shows the 300 °C APPH changes during sputter cleaning and oxidation of the Ti3Al8V6Cr4Zr4Mo alloy at 5 x 10^{-8} Torr, 5 x 10^{-7} Torr and 2 x 10^{-6} Torr oxygen pressures. The O peak, as in the room temperature oxidation case, increased immediately when O was leaked into the system at the respective different O pressures. The rate at which the Ti peaks are decreasing increases with the increase in the O pressure. The C peak showed a slight increase as the O peak increased at 5 x 10^{-8} Torr and then remained constant later. The other APPHs showed no important features.

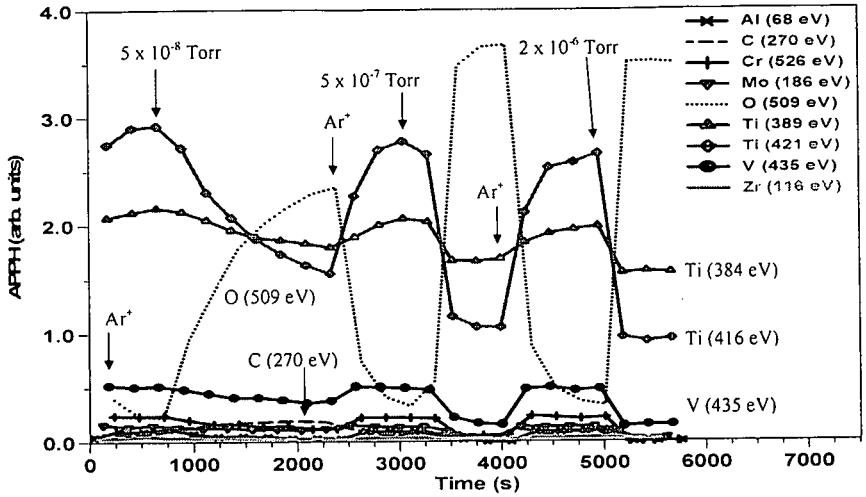

Figure 5.19: The Ti3Al8V6Cr4Zr4Mo 400 °C APPH changes during sputtering and oxidation at 5 x 10^{-8} Torr, 5 x 10^{-7} Torr and 2 x 10^{-6} Torr.

Figure 5.19 shows the 400 °C APPH changes during sputter cleaning and oxidation of the Ti3Al8V6Cr4Zr4Mo alloy at 5 x 10^{-8} Torr, 5 x 10^{-7} Torr and 2 x 10^{-6} Torr oxygen pressures. The Ti (384 eV) showed slight decrease at 5 x 10^{-8} Torr compared to the other lower temperatures oxidation. The C peak still showing a slight increase as the O peak increased at 5 x 10^{-8} Torr and then remained constant. The other APPH's still showing no important features.

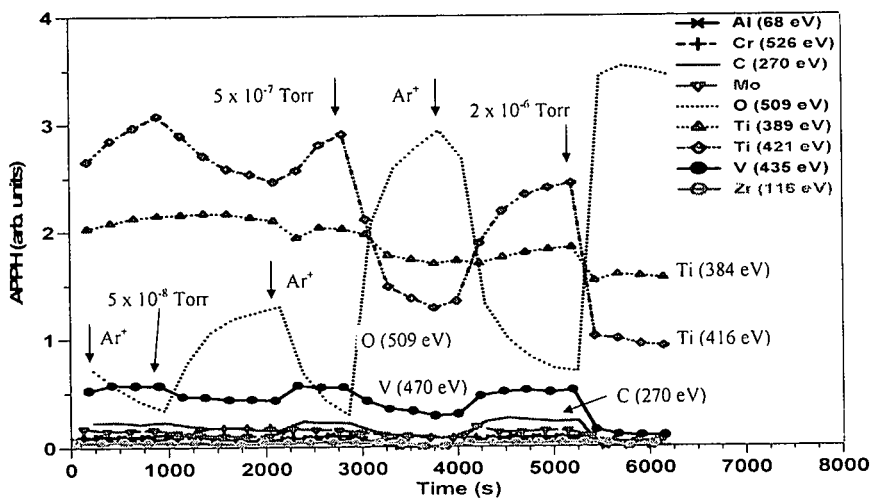

Figure 5.20: The Ti3Al8V6Cr4Zr4Mo 500 °C APPH changes during sputtering and oxidation at 5 x 10^{-8} Torr, 5 x 10^{-7} Torr and 2 x 10^{-6} Torr.

Figure 5.20 shows the 500 °C APPH changes during sputter cleaning and oxidation of the Ti3Al8V6Cr4Zr4Mo alloy at 5 x 10^{-8} Torr, 5 x 10^{-7} Torr and 2 x 10^{-6} Torr oxygen pressures. The Ti (384 eV) showed a slight increase at 5 x 10^{-8} Torr oxidation and then decreased slightly during sputter cleaning and increased to reach equilibrium again. This behaviour confirms the TiC formation as discussed later in section 5.6 on the surface at the lower O pressure oxidation. The other APPH's showed no important features. The decrease in the rate of oxidation at the lower pressure (5 x 10^{-8} Torr) as the temperature increases is apparent.

5.5. Summary of the Oxidation of Ti and its alloys

The Ti and its alloys react rapidly with the O environment at all temperatures. The Ti (416 eV) decreased more severe than the Ti (384 eV) in each oxidation run. As seen from the TiC, TiN, TiO and Ti AES spectra that were drawn from the standards the relative intensity of the two Ti (384 eV and 416 eV) peaks changes due to the different chemical environments. The peaks may therefore be used to determine which chemical specie is mainly present on the surface. It is clear that the relative intensities of the two Ti peaks changes severely during the oxidation process of all three samples. At lower pressures (5 x 10^{-8} Torr) and higher temperatures, the rate of oxidation for the pure Ti and its alloys greatly decrease due to the segregation of C, Cl and S which lead to site competition on the surface. No noticeable difference in the oxidation behaviour of the three samples was measured and the reaction rate is parabolic rate law as seen from fits in figure 5.8. The amount of heat generated during oxidation is best described as infinitesimally small and the change in temperature is immeasurably small, so no increase in temperature due to oxidation was measured.

5.6. The effect of the electron and ion beams on the surface temperature

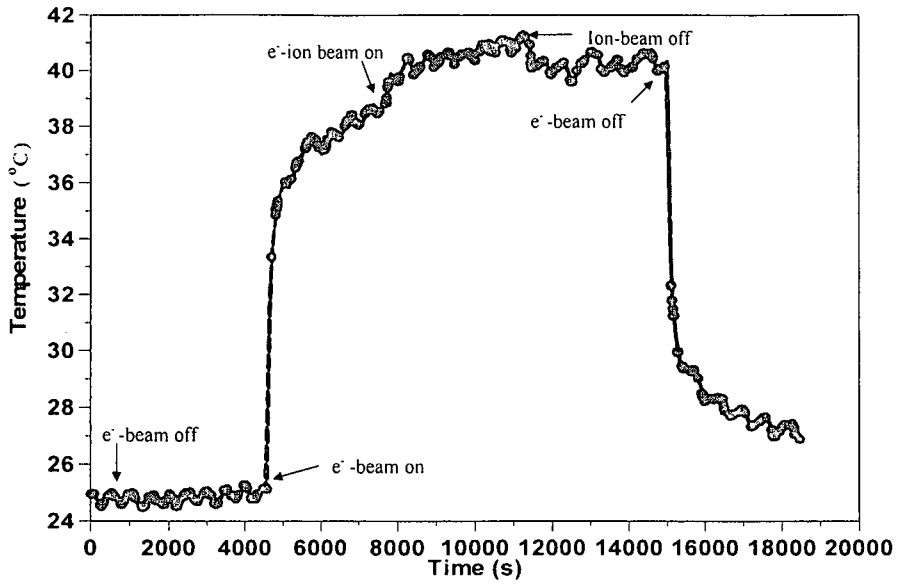

Figure 5.21: Illustration of the effect of the electron and ion beams on the surface temperature of the sample.

It was observed that the surface temperature of the samples increased dramatically when the electron and ion beams were switched on. Figure 5.21 shows the measured changes in the surface temperature due to the electron-ion beam. The experiment was allowed to run for 4800s with both electron and ion beams off and then the electron beam was switched on, followed by the ion beam after the time difference of about 4800s. There was about 16 °C - 17 °C increase in surface temperature of which 13 °C - 14 °C was due to the electron beam and 2 °C - 3 °C due to the ion beam.

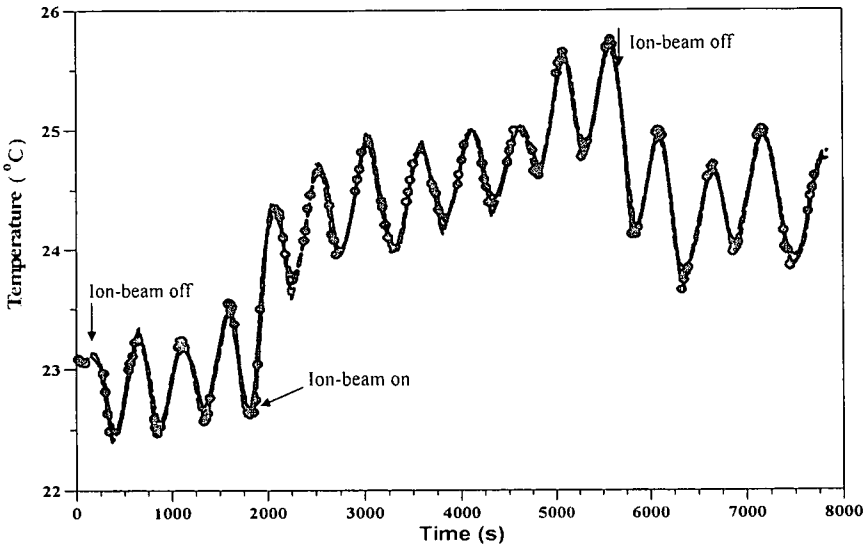

Figure 5.22: Illustration of the effect of the ion beam in the surface temperature of Ti sample.

The experiment was allowed to run for 2000s with both electron and ion beams off and then only the ion beam was switched on. There was about 2 °C - 3 °C surface temperature increase due to the ion beam. The fluctuation in the surface temperature of about 0.5 °C was also measured and this is attributed to the measured noise.

5.7. Segregation

During the oxidation processes it was observed that there was segregation of impurities from the bulk of the samples to the surface. Sulfur (S), chlorine (Cl) and carbon (C) were observed to be segregating to the surface at higher temperatures. As a result it was necessary to study the segregation behaviour of the impurities for the three samples at different constant temperatures and also by changing the temperature linearly with time.

5.7.1. Commercially pure Ti impurities segregation

The sample was sputter cleaned using the parameters in Table 4.1. The AES spectra after sputter cleaning before segregation and after segregation were taken and are shown in figure 5.23 below.

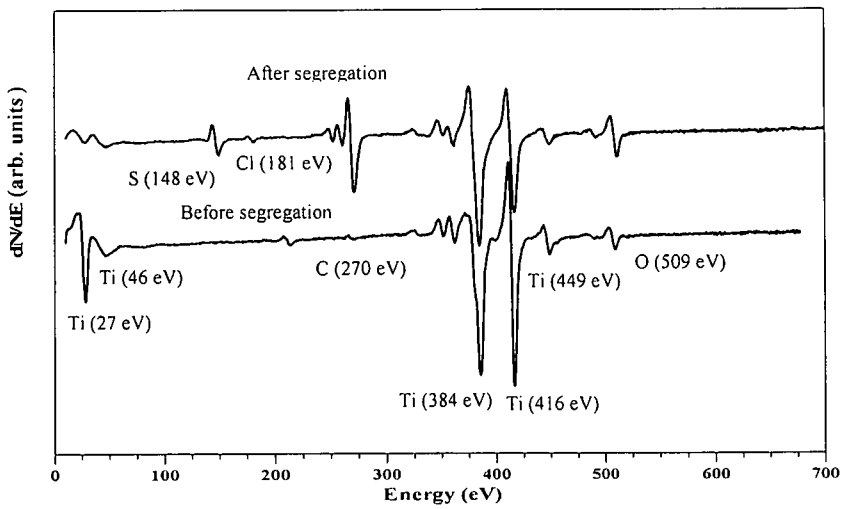

Figure 5.23: The AES spectra of Ti before and after segregation at 400 °C.

The AES spectrum after segregation shows S, C and Cl on the sample surface with some oxygen (O). The change in the respective Ti signals and C peak suggested the formation of TiC. The procedure followed is as explained in chapter 4.

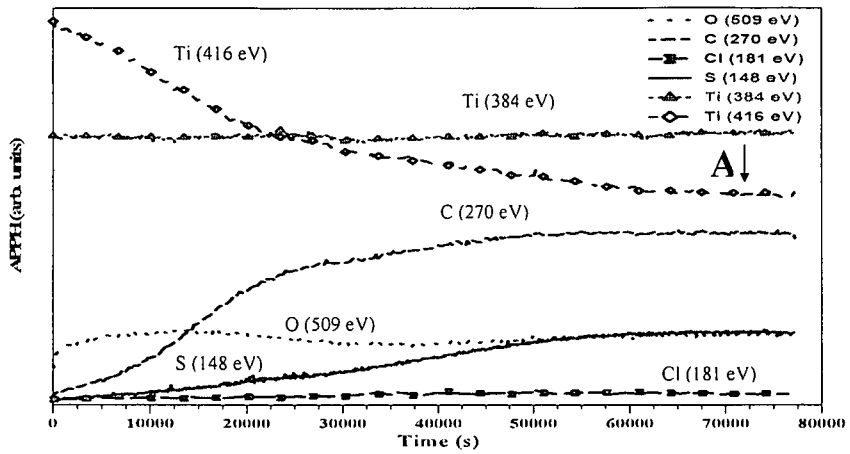

Figure 5.24: Surface segregation of S, C and Cl impurities in commercially pure grade 2 Ti at a constant temperature of 400 °C.

Figure 5.24 shows the APPH's of Ti (384 eV), Ti (416 eV), C (270 eV), O (509 eV), S (148 eV) and Cl (181 eV) that were measured as a function of the annealing time for the commercially pure Ti sample annealed at 400 °C. The APPH's of Ti (384 eV) and Ti (416 eV) decreased as S segregated to the surface. Ti (416 eV) decreased more severe than Ti (384 eV) peak which decreased partially and then increased to its maximum value and remained constant. The increase in Ti (384 eV) may be attributed to either the formation of TiC or TiO on the sample surface. The segregation, however, of C suggest the formation of TiC. Linear least square (LLS) fits of the TiC +Ti and TiO + Ti are shown in figures 5.25 and 5.26 below. It is clear from the fitted spectra that mostly TiC formed during the heating process; a relatively good fit with TiC standard was obtained. It is, however, clear that the fitted data does not correspond to TiO standard. The C signal was observed to be increasing with time until it reached the equilibrium value after 20000s. The line shapes of C changes and indicates transformation of the segregating C into carbide [57] (see figure 5.23). The Cl APPH shows no significant change during the annealing process at 400 °C.

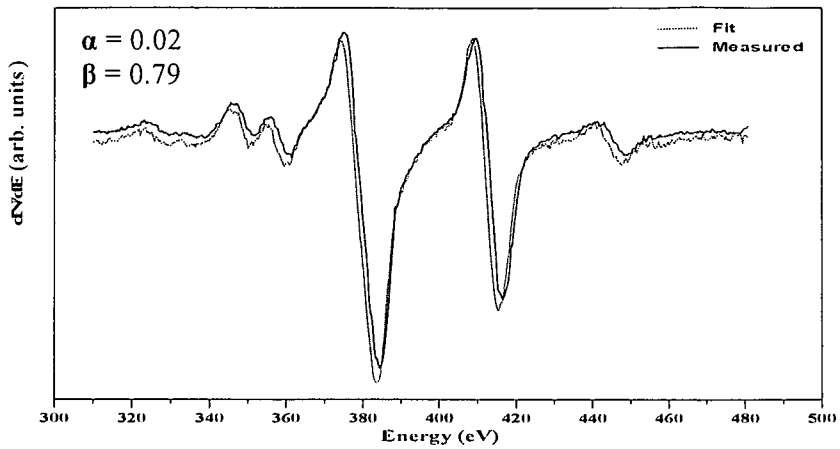

Figure 5.25: Auger spectrum to compare measured data with TiC data reconstructed using the linear least square fit at point A.

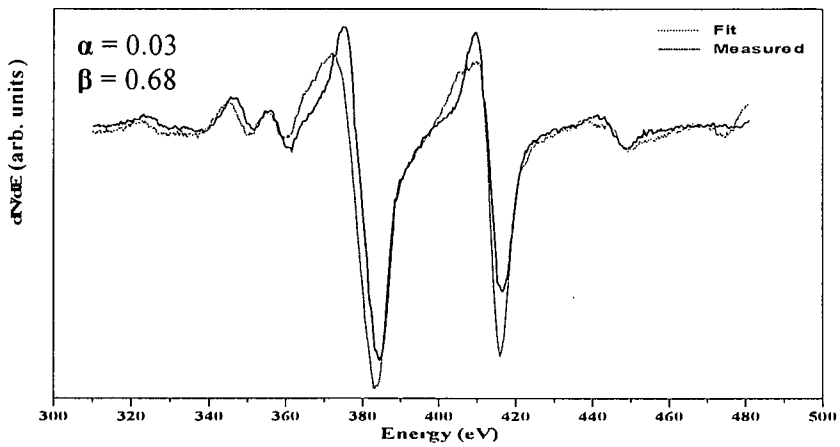

Figure 5.26: Auger spectrum to compare measured data with TiO data reconstructed using the linear least square fit at point A.

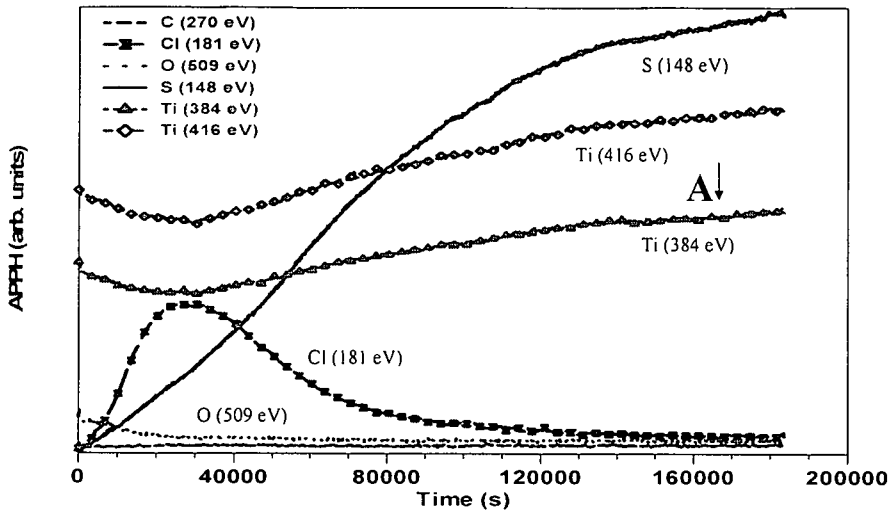

Figure 5.27: Surface segregation of S and Cl impurities in commercially pure grade 2 Ti at a constant temperature of 540 °C.

Figure 5.27 shows the APPH's of Ti (384 eV), Ti (416 eV) and the specified elements that were measured as a function of the annealing time for the pure Ti sample annealed at 540 °C. Both titanium peaks (384 eV and 416 eV) decreased instantly as Cl and S segregated to the surface. It is clear from figure 5.27 above that Cl was the first to segregate to the surface and reached the maximum equilibrium concentration after 28000s. The fast segregating Cl, however, is replaced from the surface by the slower and stronger segregating S. The segregation behaviour of Cl and S suggests that the diffusion coefficient of Cl is higher than that of S and the segregation energy of S is higher than that of Cl [56,59,58]. Further more, the activation energy of Cl is expected to be higher than that of S. Both Ti (384 eV) and Ti (416 eV) APPH's increased after 28000s as Cl begins to desegregate and O and C disappeared from the surface. After desegregating to the minimum concentration, Cl acquired equilibrium coverage. S segregated with a much higher rate at the temperature 540 °C as compared to the 400 °C. Both O and C APPH's show no important features except that O dropped sharply and reached the minimum equilibrium concentration. The AES spectrum as shown in figure 5.28 below proved that neither TiC nor TiO was formed. The

disappearance of the surface species proceeded by either dissolution into the bulk or by desorption as CO, CO_2 or SO_2 [60].

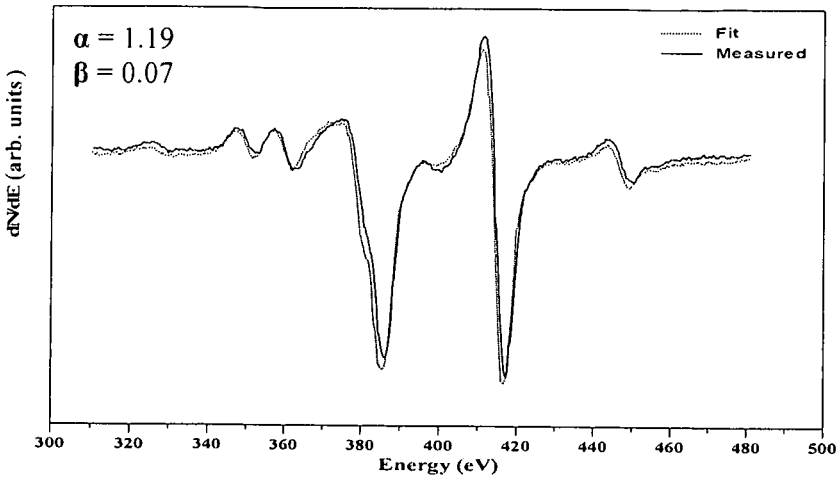

Figure 5.28: Auger spectrum to compare measured data with TiC data reconstructed using the linear least square fit at point A.

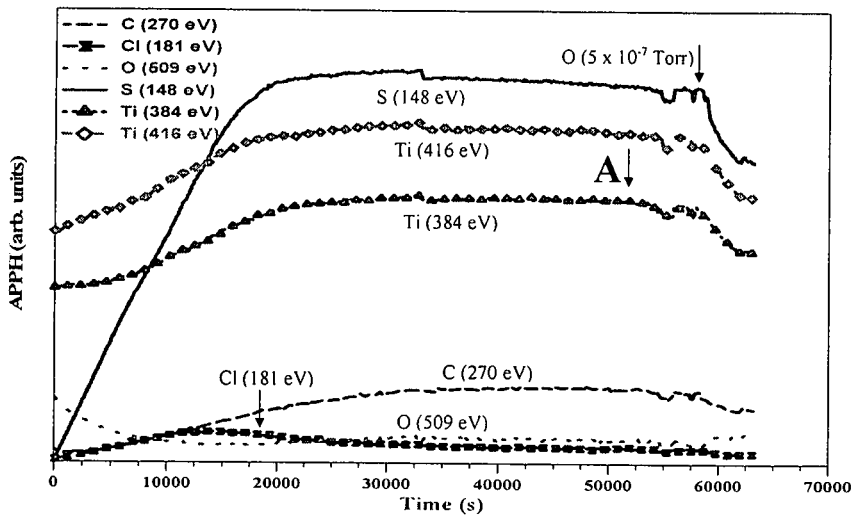

Figure 5.29: Surface segregation of S, C and Cl impurities in commercially pure grade 2 Ti at a constant temperature of 630 °C.

Figure 5.29 shows the APPHs that were measured as a function of the annealing time for the Ti sample annealed at 630 °C. At this temperature, both Ti (384 eV) and Ti (416 eV) APPH's increased instantly as S, and Cl segregated to the surface. S segregated with a much higher rate compared to

the 400 °C and 540 °C as expected. Cl segregated and reached a maximum equilibrium concentration after about 12000s and then desegregated to the minimum equilibrium concentration. The C signal was observed to be slightly increasing at 630 °C and according to the fitting in figure 5.30 below, a small amount of TiC was present on the surface. Both Ti (384 eV) and Ti (416 eV) APPH's increased slowly and reached the maximum equilibrium concentrations. The instant increase in both Ti (384 eV) and Ti (416 eV) signals is attributed to the disappearance of the surface species, O and C, at higher temperatures. It is apparent from figure 5.27 and figure 5.29 that the annealing time for both S and Cl species to reach the maximum equilibrium concentrations decreased exponentially with an increase in annealing temperature. However, Ti (384 eV) and Ti (416 eV) APPH's also show a decrease in the annealing time to reach the maximum equilibrium concentrations with an increase in the annealing temperature. The APPH's of S, Ti, Cl and C decreased as O was leaked into the system after 58000s.

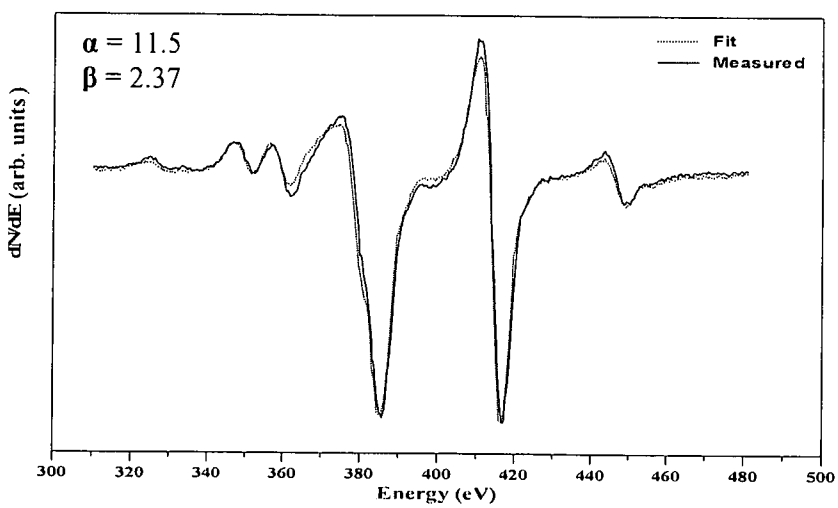

Figure 5.30: Auger spectrum to compare measured data with TiC data reconstructed using the linear least square fit at point A.

A theoretical illustration of the effect of temperature on the segregation behaviour as calculated by Swart et al [58] is given in figure 5.31. The temperature values were changed from 327 °C to 427 °C. As seen the annealing time for specie 1 to reach maximum concentration before

decreasing to equilibrium decrease exponentially with an increase in temperature as expected. The Cl and S segregation clearly shows the same type of behaviour. Different segregation energies, interaction parameters, concentration of segregating species, annealing temperature and pre-exponential factors may lead to interesting interplay amongst the different segregating species. It was, however, not the aim of this project to show and interpret the effect thereof, but a full discussion on these parameters is given by Swart et al [58].

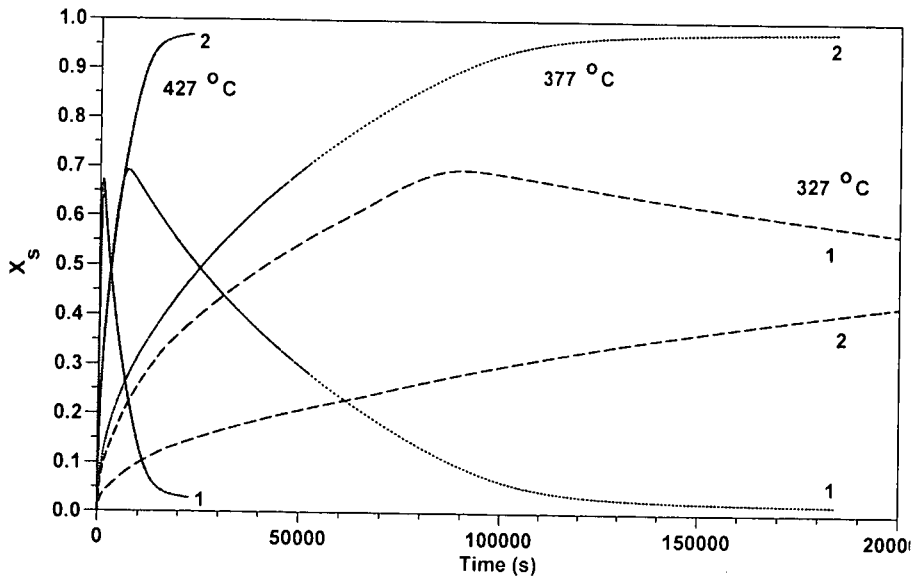

Figure 5.31: An illustration of the effect of the annealing temperature on the segregation behaviour of specie 1 and 2 from the modified Darken model [58].

5.7.2. Linear heating (Ti)

5.7.2.1 Commercially pure Ti

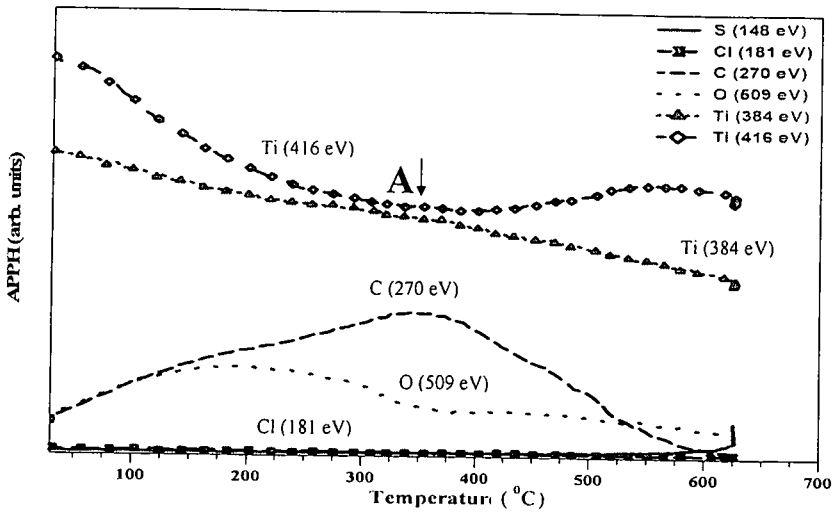

Figure 5.32: Surface segregation of the impurities during the linear heating from room temperature to 630 °C at the rate 0.05 °C/s.

Figure 5.32 shows the APPH's of Ti (384 eV), Ti (416 eV), C (270 eV), O (509 eV), S (148 eV), Cl (181 eV) during the linear heating from room temperature to 630 °C at 0.05 °C/s heating rate. At the very low temperatures only O and C are showing up on the surface and figure 5.33 shows that TiC was formed. Ti (384 eV) and Ti (416 eV) APPH's decreased as the O and C concentrations at position A on the surface increases. As the temperature increases further and approaches 200 °C, O was the first to reach the maximum equilibrium concentration and started to drop and followed by C later at about 350 °C. However, C decreases to a lower minimum equilibrium concentration than O. Segregation of S was observed after the temperature increased to 550 °C. S started segregating to the surface, as C and O disappeared from the surface, which suggests that C and O constrained the S to remain in the bulk until the dissolution of O and C occurred [59]. The Ti (416 eV) APPH showed an increase as the O and C signals dropped. Due to the heating effects, the sample's position shifted and led to loss of the elastic peak and as a result a

decrease in Ti peaks even though the surface was clean. No segregation of Cl was observed here.

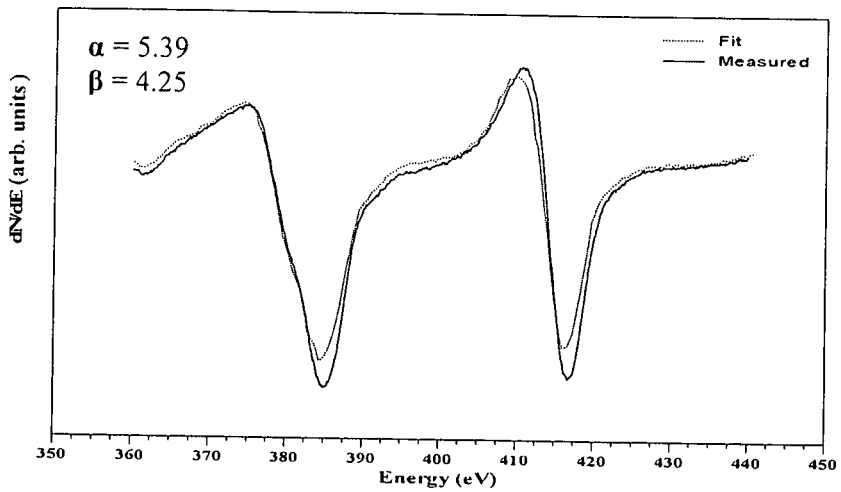

Figure 5.33: Auger spectrum to compare measured data with TiC data reconstructed using the linear least square fit at point A.

5.7.3. Ti6Al4V impurities segregation

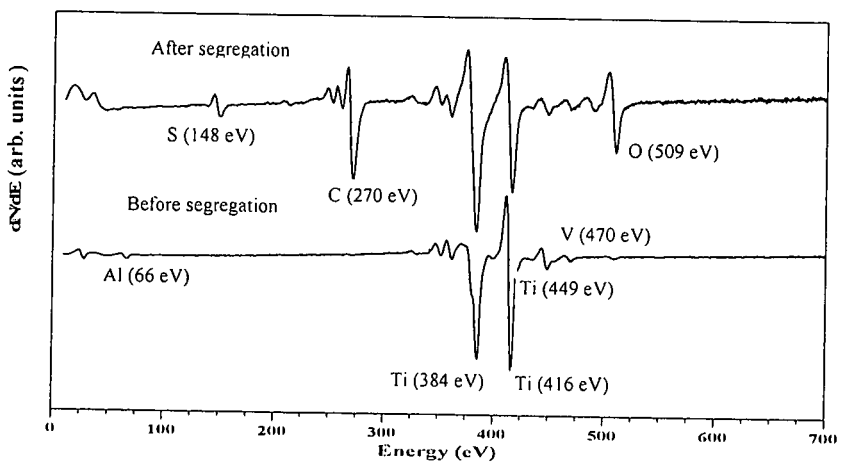

Figure 5.34: The AES spectra of Ti6Al4V before and after segregation.

Figure 5.34 shows the AES spectra after sputter cleaning before segregation and after segregation. After segregation the spectrum shows a great decrease

in the Al peak while V signal showed a slight increase and no Cl was observed. The relative change in the Ti APPH and the C peak clearly shows that TiC was formed during the annealing process. S was measured on the surface after annealing.

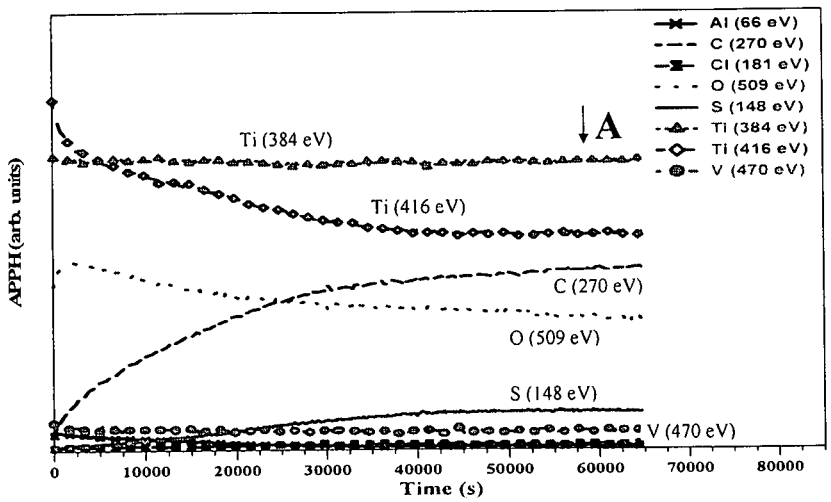

Figure 5.35: Surface segregation of S and Cl impurities in Ti6Al4V at a constant temperature of 400 °C.

Figure 5.35 shows the APPH's of Ti (384 eV), Ti (416 eV), C (270 eV), O (509 eV), S (148 eV), Cl (181 eV), Al (66 eV) and V (470 eV) that were measured as a function of the annealing time for the Ti6Al4V sample annealed at 400 °C. The APPH's of Ti (384 eV) and Ti (416 eV) decreased instantly as C and S segregated to the surface. Ti (416 eV) decreased more severe than Ti (384 eV) peak which decreased partially and then increased to its maximum value and remained constant. The oxide layer remained constant except a slight decrease in O signal at the earlier stages. The source of the high concentration of O on the surface is due to the continual uptake of the background gases such as H_2O, CO and CO_2 [60]. The peaks fitting in the figures 5.36 and 5.37 below showed that both TiC and TiO are present on the surface. The extra peak in the measured spectrum at 435 eV is attributed to V. The under estimation of the shoulder of the Ti peak at about 370 eV may be an indication of the presence of TiN on the surface [61] (see figure 5.38). The C peak was as well observed to be increasing with time until the

equilibrium was reached. The C line shapes changes confirming the transformation of the segregating C into carbide. The Cl and V APPH's showed no significant change during annealing process at this temperature.

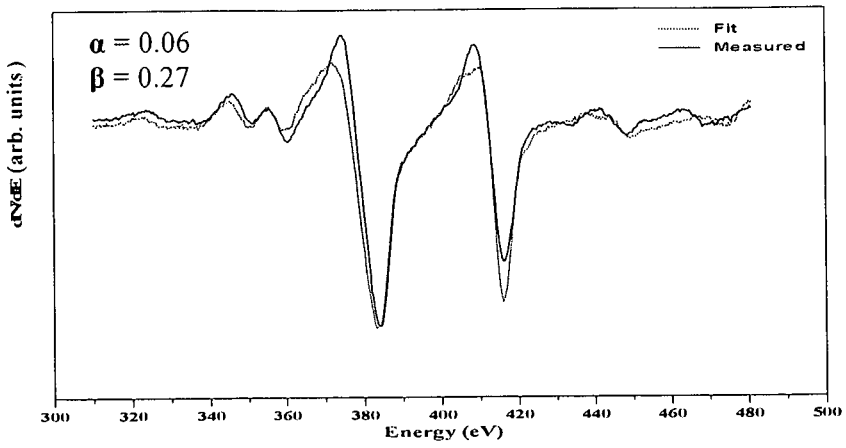

Figure 5.36: Auger spectrum to compare measured data with TiO data reconstructed using the linear least square fit at point A.

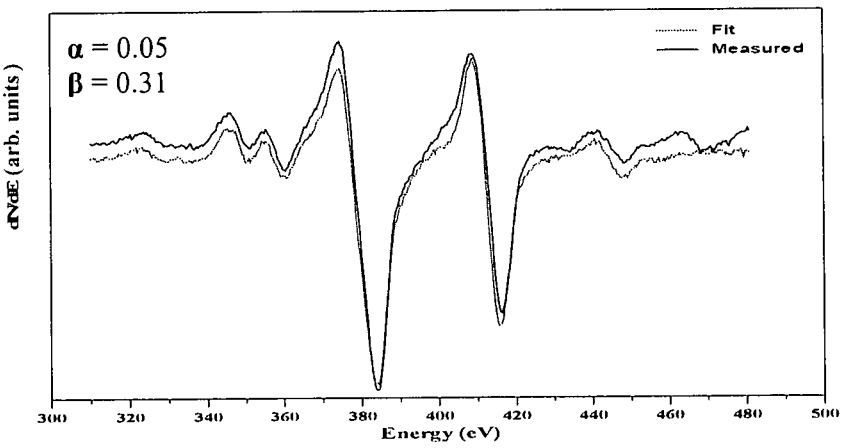

Figure 5.37: Auger spectrum to compare measured data with TiC data reconstructed using the linear least square fit at point A.

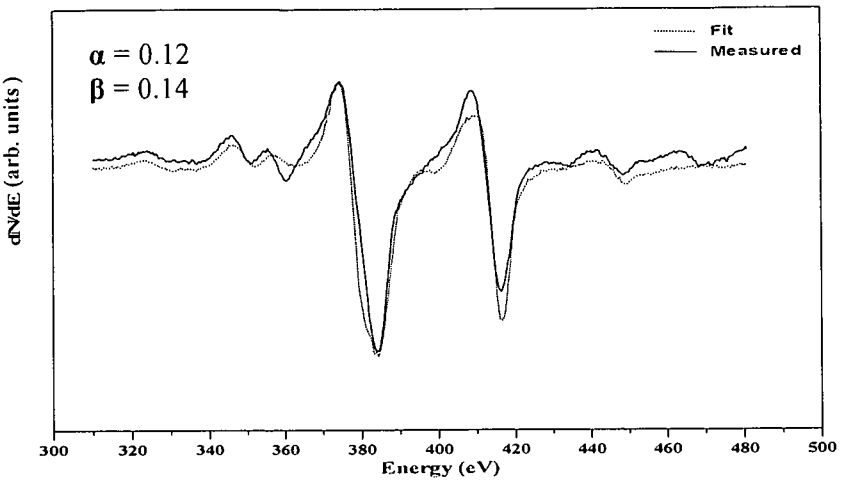

Figure 5.38: Auger spectrum to compare measured data with TiN data reconstructed using the linear least square fit.

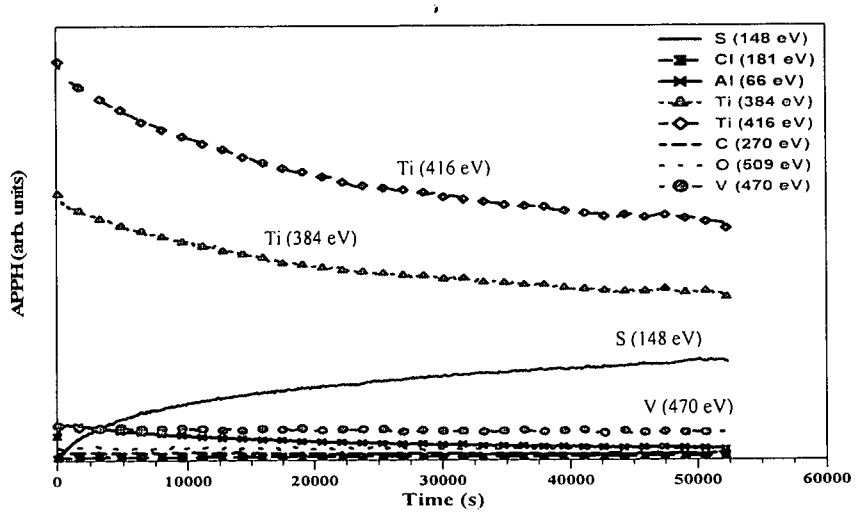

Figure 5.39: Surface segregation of impurities in Ti6Al4V at a constant temperature of 600 °C.

Figure 5.39 shows the APPH's of Ti (384 eV), Ti (416 eV) and the specified elements that were measured as a function of the annealing time for the Ti6Al4V sample annealed at 600 °C. At this temperature, both Ti (384 eV) and Ti (416 eV) APPH's decreased instantly as S segregated to the surface. S segregated with much higher rate compared to the 400 °C and 500 °C as expected. S coverage of titanium was responsible for decrease in Ti APPH

intensity. The Al peak increased slightly as S segregated to the surface and then decreased with a constant rate until the minimum equilibrium concentration. The Cl, V, O and C peaks showed no important changes.

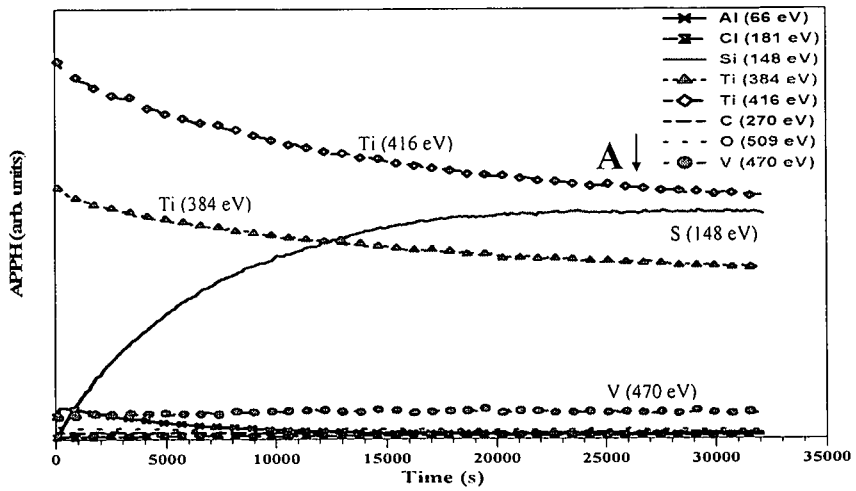

Figure 5.40: Surface segregation of impurities in Ti6Al4V at a constant temperature of 700 °C.

Figure 5.40 shows the APPHs that were measured as a function of the annealing time for the Ti6Al4V sample annealed at 700 °C. At this temperature, both Ti (384 eV) and Ti (416 eV) APPH's decreased instantly as S segregated to the surface. The segregation rate of S is much higher than at the lower temperatures as expected. The Al peak decreased as S segregated to the surface. The Cl, V, O and C peaks showed no important changes. The higher energy Ti peaks and the fittings in figure 5.41 below showed that the surface remained pure Ti.

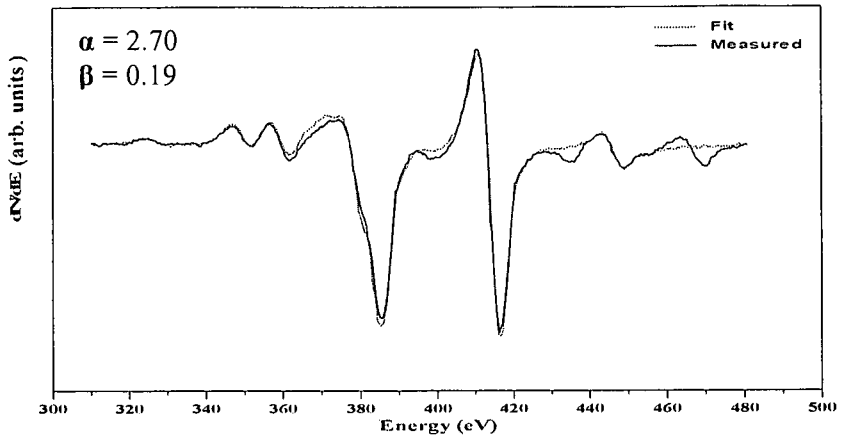

Figure 5.41: Auger spectrum to compare measured data with TiC data reconstructed using the linear least square fit at point A.

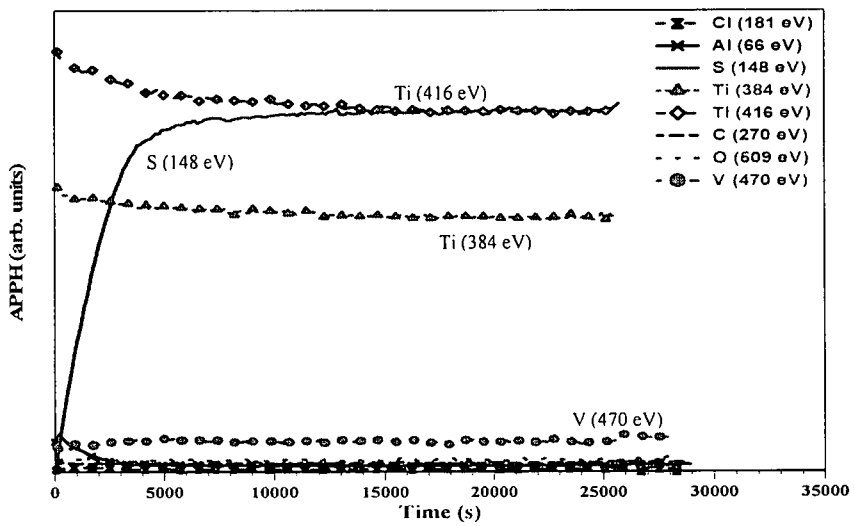

Figure 5.42: Surface segregation of impurities in Ti6Al4V at a constant temperature of 800 °C.

Figure 5.42 also shows the measured APPHs during the annealing process of Ti6Al4V sample at 800 °C. At this temperature, both Ti (384 eV) and Ti (416 eV) APPH's decreased instantly with a much slower rate as S segregated to the surface. The increase in the rate of S segregation is apparent. The Al peak also decreased as S segregated to the surface. The Cl, V, O and C peaks showed no important changes. It is apparent from figure 5.42 that the

annealing time for S specie to reach the maximum equilibrium concentration decreased exponentially with an increase in annealing temperature.

5.7.4. Linear heating (Ti6Al4V)

5.7.4.1 Grade 5 Ti (Ti6Al4V)

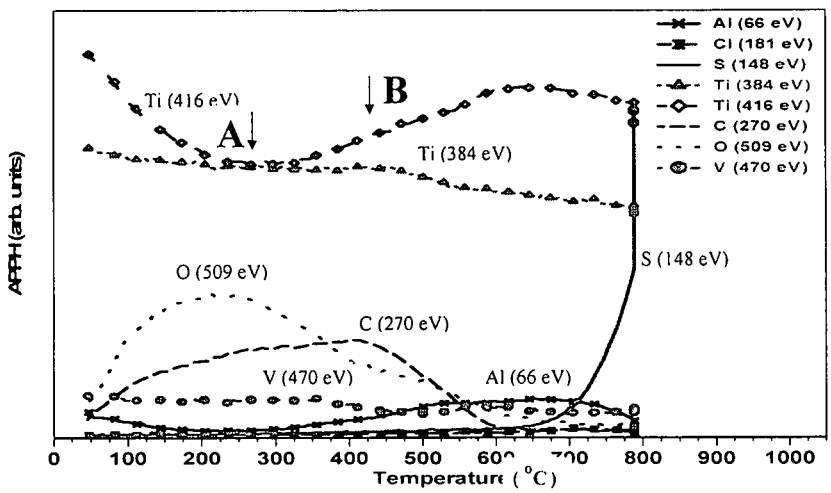

Figure 5.43: Surface segregation of the impurities during the linear heating from room temperature to 800 °C. Rate 0.05 °C/s.

Figure 5.43 shows the surface segregation of the impurities during the linear temperature run from room temperature to 800 °C. At the very low temperatures only O and C are showing up on the surface. The Ti (384 eV) and Ti (416 eV) APPH's both decreased as O and C concentrations on the surface increases and increased as they started to decrease. As the temperature increases further, O was the first to reach the maximum equilibrium concentration and started to drop and followed by C at 400 °C. The combination of TiO and TiC was formed and this is well illustrated in the AES spectra in figure 5.44 and figure 5.45 below. However, C decreases to the lower minimum equilibrium concentration than O. Segregation of S was observed after the temperature increased to 600 °C. S started segregating to the surface as C and O disappeared from the surface which confirms that C and O constrained the S to remain in the bulk until the dissolution of O and C

occurred. As S started segregating to the surface, Ti (416 eV) APPH decreases again. Aluminium was observed to be segregating and reached the equilibrium concentration after 550 °C. No segregation of Cl was observed here.

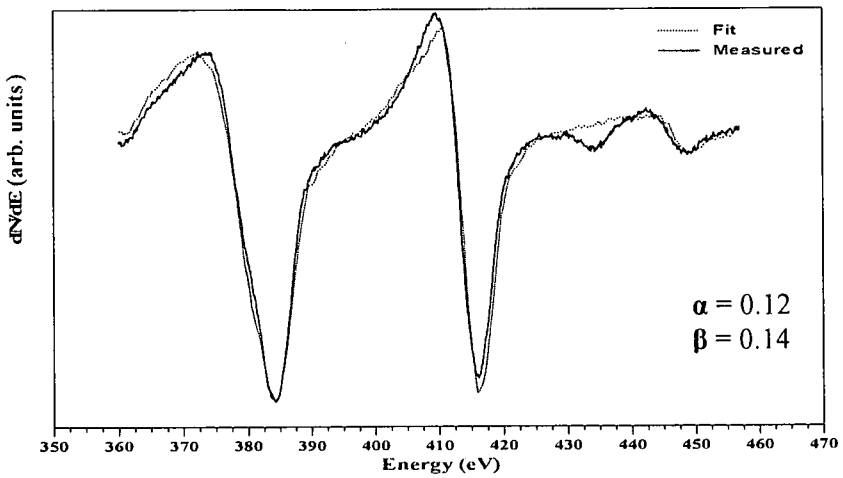

Figure 5.44: Auger spectrum to compare measured data with TiO data reconstructed using the linear least square fit at point A.

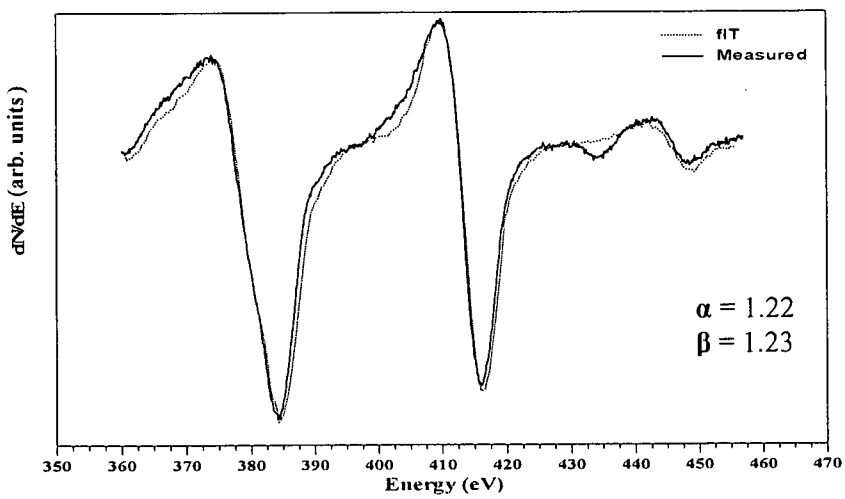

Figure 5.45: Auger spectrum to compare measured data with TiC data reconstructed using the linear least square fit at point B.

5.7.5. Ti3Al8V6Cr4Zr4Mo impurities segregation

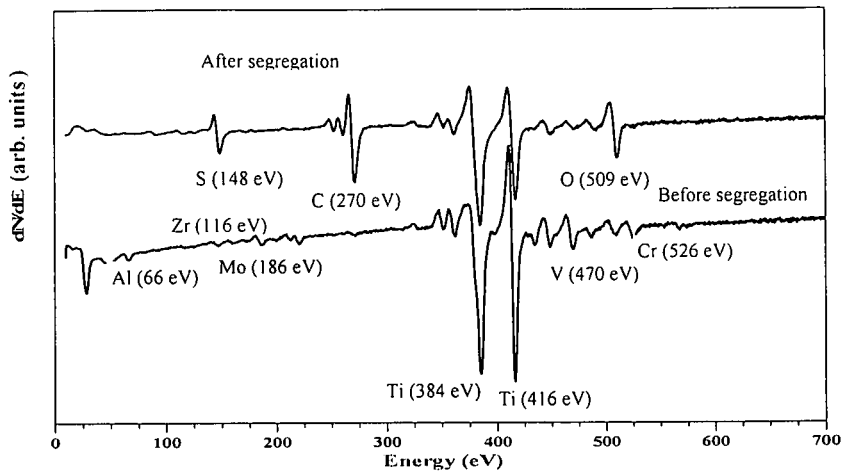

Figure 5.46: The AES spectra of Ti3Al8V6Cr4Zr4Mo before and after segregation.

Figure 5.46 above shows the AES spectra after sputter cleaning before segregation and after segregation. After segregation the spectrum shows a great decrease in the peaks of the alloying elements and the increase in the S and C peaks. The titanium peaks showed changes and this is due to the presence of S, C and O on the surface.

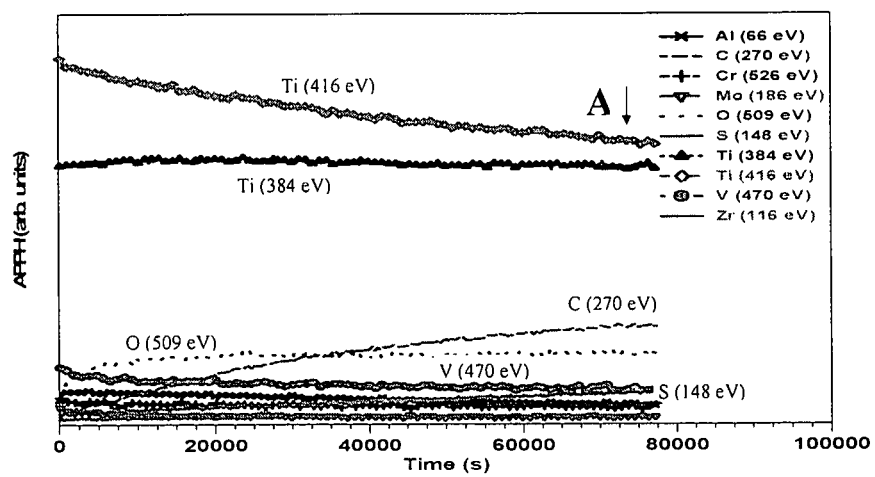

Figure 5.47: Surface segregation of impurities in Ti3Al8V6Cr4Zr4Mo at a constant temperature of 400 °C.

Figure 5.47 above shows the APPH's of Ti (384 eV), Ti (416 eV), C (270 eV), O (509 eV), S (148 eV), Cl (181 eV), Al (66 eV), V (470 eV), Cr (526 eV), Zr (116 eV) and Mo (186 eV) that were measured as a function of the annealing time for the Ti3Al8V6Cr4Zr4Mo sample annealed at 400 °C. The Ti (416 eV) APPH decreased with slower rate as C and S segregated to the surface. The Ti (384 eV) showed a slight increase and then remained constant. The oxide layer was also observed to be stable at this temperature. The C signal increased and the line shapes change, which confirms the transformation of the segregating C into carbide as shown in figure 5.46. The AES spectra in the figure 5.48 below proved the formation of TiC. S was observed to be segregating with a slower rate at 400 °C. The other APPHs showed no significant changes during the annealing process at this temperature.

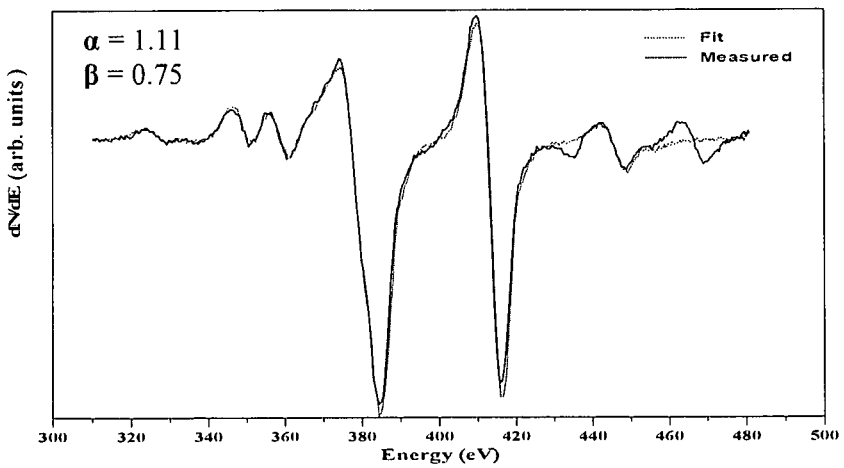

Figure 5.48: Auger spectrum to compare measured data with TiC data reconstructed using the linear least square fit at point A.

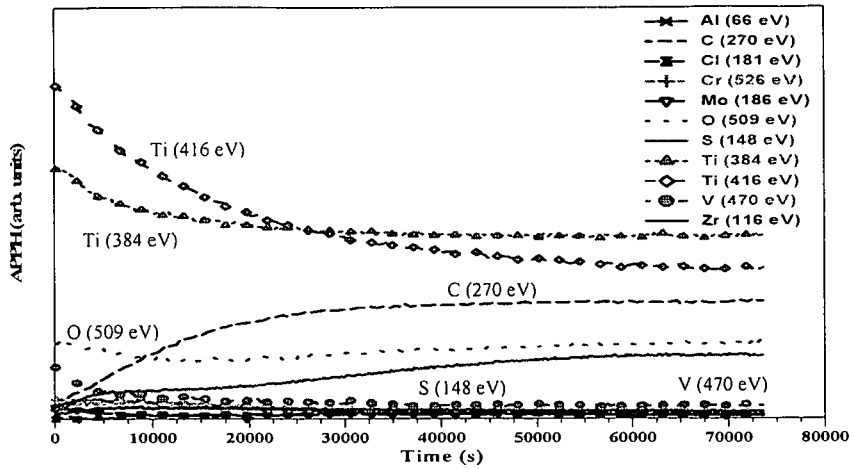

Figure 5.49: Surface segregation of impurities in Ti3Al8V6Cr4Zr4Mo at a constant temperature of 500 °C.

Figure 5.49 above shows the APPH's of Ti (384 eV), Ti (416 eV) and the specified elements that were measured as a function of the annealing time for the Ti3Al8V6Cr4Zr4Mo sample annealed at 500 °C. The APPH's of Ti (384 eV) and Ti (416 eV) decreased instantly as the impurities, S and C segregated to the surface with Ti (416 eV) showing a severe decrease. Cl showed no change in this sample measurement as compared to the pure Ti and Ti6Al4V samples which showed the segregation of Cl at 500 °C. S segregated with a much higher rate at 500 °C temperature compared to the 400 °C. C was observed to be segregating to the surface with a higher rate at 500 °C compared to 400 °C. The change in the lines shape proved the transformation of the segregating C into carbide. The oxide layer was observed to be stable again at 500 °C, and this might be due to the alloying elements which impact the retention of O and C on the surface. The other APPHs still showing no significant changes at this temperature.

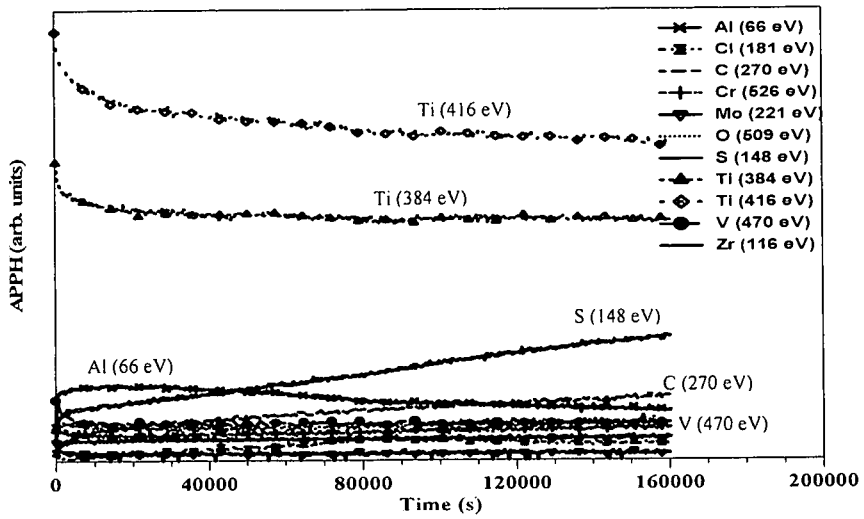

Figure 5.50: Surface segregation of impurities in Ti3Al8V6Cr4Zr4Mo at a constant temperature of 600 °C.

Figure 5.50 above shows the APPHs that were measured as a function of the annealing time for the Ti3Al8V6Cr4Zr4Mo sample annealed at 600 °C. At this temperature, both Ti (384 eV) and Ti (416 eV) APPH's decreased instantly as S and C segregated to the surface. S segregated with much higher rate compared to the 400 °C and 500 °C as expected. It was observed that the rate at which S is segregating is much lower than in the case of a pure titanium and Ti6Al4V, and the reason for this might be the alloying elements which are said to impact the retention of C and O. These two contaminants constrain the S to remain in the bulk until dissolution occurred. The O was observed to be the main factor controlling the segregation of S [59]. The Al was observed to be segregating at the beginning and decreased as S segregated to the surface. The AES fittings showed a formation of small TiC on the surface. The other APPHs showed no important changes.

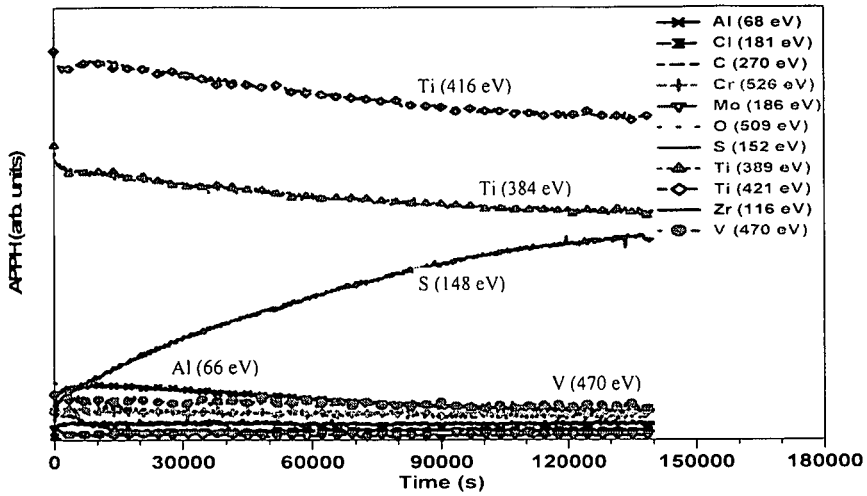

Figure 5.51: Surface segregation of impurities in Ti3Al8V6Cr4Zr4Mo at a constant temperature of 700 °C.

Figure 5.51 above shows the APPHs of the specified species that were measured as a function of the annealing time for the Ti3Al8V6Cr4Zr4Mo sample annealed at 700 °C. At this temperature, both Ti (384 eV) and Ti (416 eV) APPH's decreased instantly as S segregated to the surface. Both (Ti 384 eV and Ti 416 eV peaks) decreased with much slower rate. The segregation rate of S is much higher than at the lower temperatures as expected. No C and O signals on the surface were observed. The Al signal was observed to be slightly increasing at the beginning and decreased as S segregated to the surface. The other APPHs showed no important changes at this temperature.

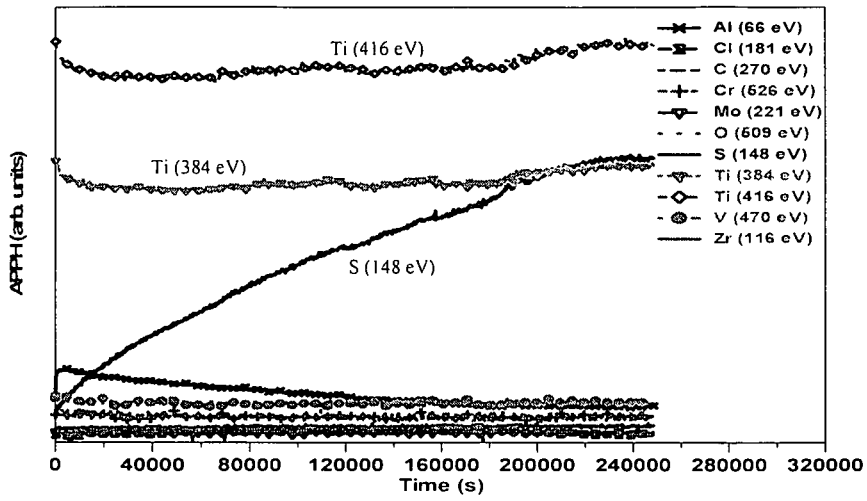

Figure 5.52: Surface segregation of impurities in Ti3Al8V6Cr4Zr4Mo at a constant temperature of 800 °C.

Figure 5.52 above shows the APPHs that were measured as a function of the annealing time for the Ti3Al8V6Cr4Zr4Mo sample annealed at 800 °C. Both Ti (384 eV) and Ti (416 eV) APPH's decreased instantly as S segregated to the surface and started to increase after 70000 s. The increase in the titanium signals confirms the disappearance of O and C species on the surface due to thermal treatment. The increase in the rate of S segregation is apparent. The Al signal was also observed to be slightly increasing at the beginning and decreased as S segregated to the surface. No O and C signals were observed at this temperature. The Cl, V, Cr, Mo and Zr peaks showed no important changes. It is apparent from figure 5.52 that the annealing time for S specie to reach the maximum equilibrium concentration decreased exponentially with an increase in annealing temperature. Neither TiC nor TiO layers were formed on the surface.

5.7.6. Linear heating (Ti3Al8V6Cr4Zr4Mo)

5.7.6.1 Ti3Al8V6Cr4Zr4Mo alloy

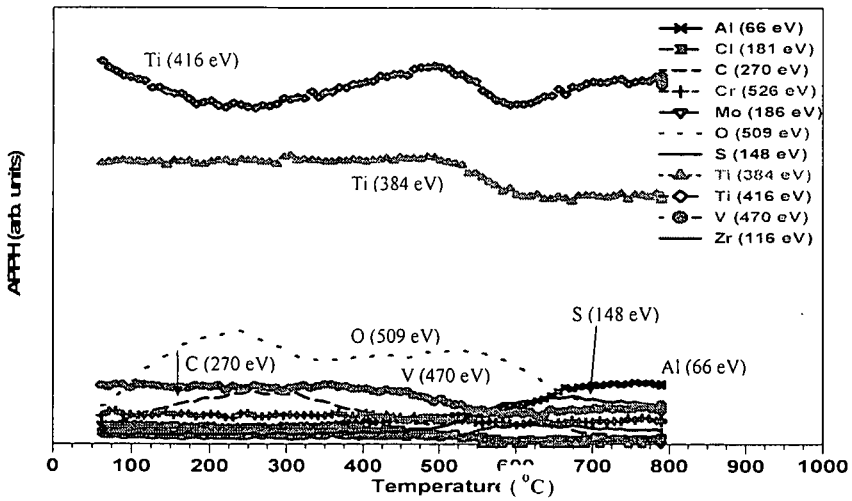

Figure 5.53: Surface segregation of the impurities during the linear heating rump from room temperature to 800 °C at 0.05 C/s rate.

Figure 5.53 shows the surface segregation of the impurities during the linear temperature run from room temperature to 800 °C. At the very low temperatures only O and C are showing up on the surface. The Ti (384 eV) and Ti (416 eV) APPHs both decreased as the concentrations of O and C on the surface increase and increased as they started to decrease. The titanium signals increased and reached equilibrium before decreasing again after 480 °C. The Ti (416 eV) increased slightly and reached equilibrium after the temperature of 600 °C while Ti (384 eV) remained constant. However, C decreases to the lower minimum equilibrium concentration as the temperature increases. Segregation of S was observed after the temperature increased to 500 °C and reached equilibrium after 650 °C. After 400 °C aluminium was also observed to be segregating and reached the equilibrium. As S segregation rate increased, both Ti (384 eV) and Ti (416 eV) APPHs were observed to be decreasing. No segregation of Cl was observed here.

5.8. Linear Least Square (LLS) Fitting

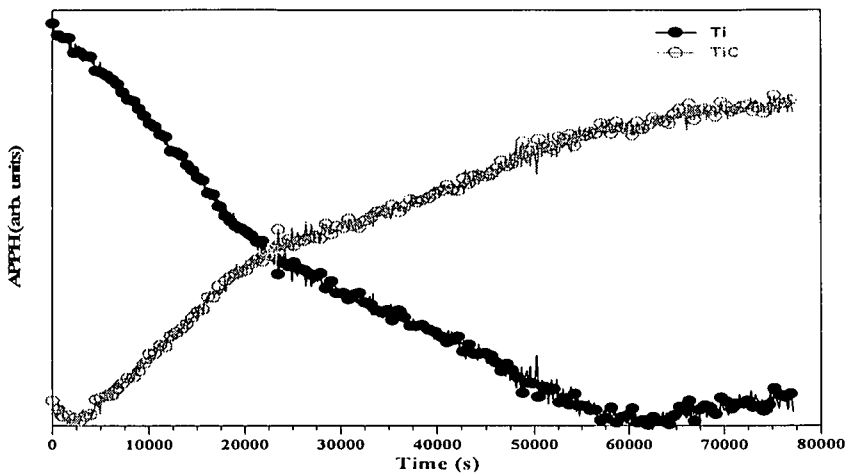

Figure 5.54: Resolved Ti and TiC normalised APPH from the commercially pure Ti.

The results of the LLS method applied to each data set in the segregation profile of figure 5.24 are shown in figure 5.54. Initially there was no TiC but it increased with time and reached the maximum equilibrium value. The Ti APPH decreased as the TiC increases. To illustrate the accuracy of the linear least square technique, the TiC, TiO and TiN Auger spectra were reconstructed at specific points A and B in each segregation profiles. The reconstructed spectra were compared with the measured spectra at a specified point. It must be pointed out that no compound in the absence of C and O on the surface was formed. The increase in the Ti APPH after reaching the minimum equilibrium might be due to the overestimated values by the programme.

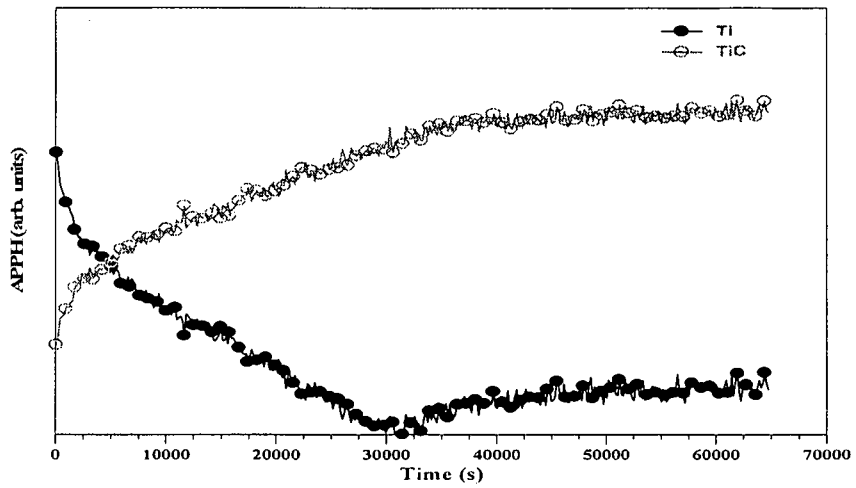

Figure 5.55: Resolved Ti and TiC normalised APPH from the Ti6Al4V sample.

Figure 5.55 illustrates the results of LLS method applied to each data set in the segregation profile of figure 5.35.

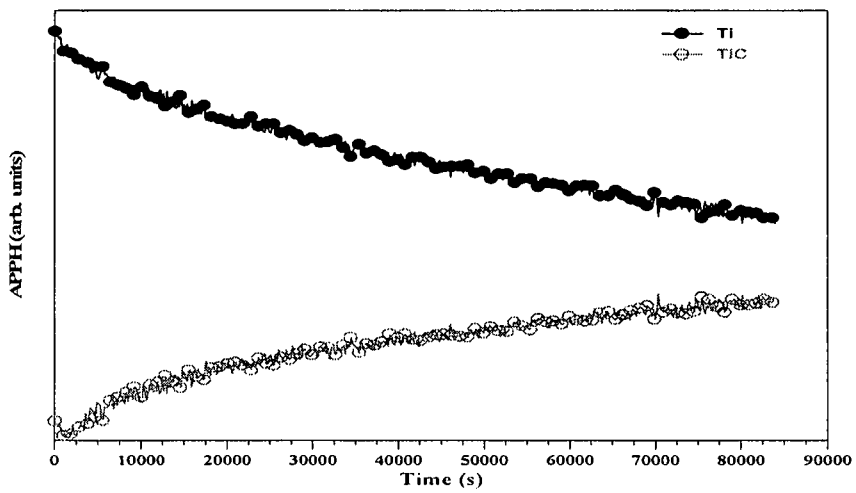

Figure 5.56: Resolved Ti and TiC normalised APPH from the Ti3Al8V6Cr4Zr4Mo sample. The results were obtained from the LLS method applied each data point in the segregation profile of figure 5.47.

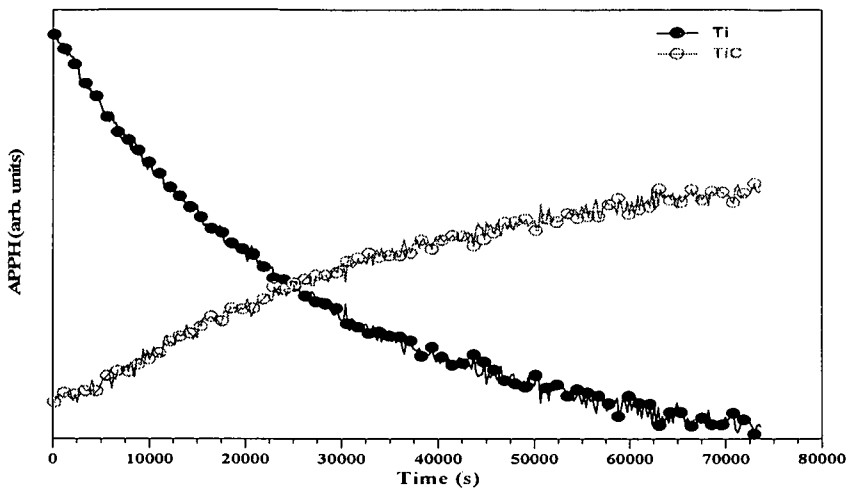

Figure 5.57: Resolved Ti and TiC normalised APPH from the Ti3Al8V6Cr4Zr4Mo sample obtained from segregation profile of figure 5.49.

5.9. Summary of the impurities segregation

The impurities C, Cl and S segregate to the surface at high temperatures. At very high temperatures, only the segregation of S was observed. The segregation rate of the impurities is temperature depended, and increases with temperature. The oxide layer at lower temperatures (400 °C – 500 °C) is very stable for all samples and C segregates at (400 °C – 500 °C) temperatures for all the three samples. O and C constrain S to remain in the bulk until the dissolution of O and C occurred, more especially O. There is no noticeable difference in the segregation behaviour of the three samples, except the decrease in the segregation rates of Cl and S in the two alloys. The linear heating ramp of the three samples confirmed that O and C control the segregation of S. The surfaces of the three species were all clean at 600 °C during the linear heating ramp. During the linear heating of Ti6Al4V and Ti3Al8V6Cr4Zr4Mo, segregation of Al at higher temperatures was observed. A unique linear least square method was used to extract the fractions that pure Ti, TiC and TiO contribute to the measured APPH. The peak shapes fittings proved the formation of the compounds TiC and TiO.

Chapter 6

Summary and Conclusions

6.1. Summary

The reaction of titanium and oxygen or any oxygen-containing medium was found to be exothermic. So the main objective of the study was to investigate if the increase in the surface temperature due to the oxidation of titanium and titanium alloys specimens is measurable. The respective samples were cut into specially designed shapes (as shown in figure 4.3) to enable the surface temperature change measurements without affecting the temperature of the sample due to other factors than exothermic reaction. Two thermocouples were used in this study and the position analysed for changes in temperature was selected to be next to the thermocouple on the surface. The two chromel-alumel thermocouples were spot-welded to each sample. There was a temperature difference of about 100 – 200 °C between the control and the surface temperatures which made it possible to monitor the change in the surface temperature.

The sample's surface was well sputter cleaned before being exposed to the oxygen environment, but due to the high chemical reactivity of titanium, there were still some oxygen and carbon contaminants on the surface which could not be removed completely because of the continual uptake of the residual gases. The segregation of C and S at the higher temperatures and lower O pressure was observed. This led to site competition on the surface between the segregates and O. Both the mean

surface lifetime of the O and the segregation of the different species influence the oxidation rate. During oxidation at 5 x 10^{-8} Torr TiC was observed to form at the temperature of about 500 °C for all three samples.

No difference in the oxidation behaviour of the three samples was observed. The effect of both the electron and ion beams on the surface temperature was monitored.

The heat generated during oxidation was infinitesimally small and the change in the surface temperature was immeasurably small, so no increase in the surface temperature was measured. However, the theoretical calculated amount of heat generated during the reaction of Ti atoms with oxygen to form TiO_2 layer is 939.7 KJ. The change in the surface temperature for the single layer due to the reaction was calculated to be 34450 °C. For the sample thickness used, 0.9 mm, the calculated amount of heat generated was 0.011°C. The impurity segregation measurements for the three samples at different constant temperatures and linear heating ramp (from room temperature to 800 °C at the rate of 0.05 °C/s) were performed. Cl, C and S as impurities were observed to be segregating at higher temperatures. The change in the line shapes of C showed the transformation of segregating C into carbide and the peak shapes (384 eV and 416 eV) after 400 °C and 500 °C (Ti3Al8V6Cr4Zr4Mo) segregation measurements confirmed. The segregation rate was found to be temperature depended as expected.

A unique linear least square method was used to extract the fraction that the pure titanium, titanium carbide and titanium oxide contribute to the measured APPH's. The peak shapes fitting was done and confirmed the formation of TiC and TiO at high temperatures (400 °C – 500 °C).

6.2. Future work

Since the AES surface technique could not function under high pressures, the use of other techniques where the surface analysis may be studied under high-pressures (1 x 10^6 Pa) might be a possible solution to determine the temperature increase. The temperature change measurements under atmospheric pressure could also be tried. From the segregation study, see the linear heating profiles as shown in figures 5.32, 543 and 5.53, it is clear that the samples may be cleaned by using linear heating. The samples may be annealed to a temperature of 600 °C – 650 °C and then cooled. It is clear that the samples were all cleaned at that temperature range. Also interesting to note that TiC may also be grown if annealed to a temperature of 350 – 400 °C for the pure Ti and Ti6Al4V samples.

References

1. *WebElements Periodic Table [online].* Professional edition. Available from http://www.webelements.com/webelements/text/Ti/key.html [Accessed October 2004].
2. J.D. Lee, *Concise Inorganic Chemistry*, 4th edition, Kin Keon Printing Co. Pte. Ltd, 1991.
3. F. Albert Cotton, Geoffrey Wilkinson, *Advanced Inorganic Chemistry, Second Edition*, John Wiley & Sons, New York, 1966.
4. Donald R. Askeland, *The Science and Engineering of Materials*, 3rd edition, Stanley Thornes Ltd, 1998.
5. http://www.grc.nasa.gov/WWW/1999/5000/51201occi.html [Accessed March 2003].
6. A.L. Yerokhin, X. Nie, A. Leyland, A. Matthews, *Surface and coatings Technology*, **130**, 2000, 195, 196.
7. K. Xia, X. Wu, J. Zhang, *Intermetallics*, **11**, 2003, 325.
8. A.L. Yerokhin, A. Leyland, A. Matthews, *Applied Surface Science*, **200**, 2002, 172, 173.
9. F. Borgioli, E. Galvanetto, F.P. Galliano, T. Bacci, *Surface and Coatings Technology*, **141**, 2001, 103, 104.
10. Young-Taeg Sul, *Biomaterials*, **24**, 2003, 3893, 3894.
11. M.V. Ribeiro, M.R.V. Morreira, J.R. Ferreira, *Journal of Materials Processing Technology* **xxx,** 2003, 1, 2.
12. E.N. Codaro, R.Z. Nakazato, A.L. Horovistiz, L.M.F. Ribeiro, R.B. Ribeiro, L.R.O. Hein, *Materials Science and Engineering,* **A341**, 2003, 202.
13. Metals and their Weldability, *Welding Handbook*, W.H. Kearns (Ed.), 7th ed., vol. 4, Miami, *American Welding Society*, Chap. 10, 1984.
14. D. Bloor, R. Brook, M. Flemings, S. Mahajan (Eds), *The Encyclopedia of Advanced Materials*, vol. 4, Elsevier Science Inc, New York 1994.
15. Zu Xiaotao, Feng Xiangdong, Wang Zhiguo, Zeng Guangting, Lin Libin, Li Yanling, Huang Xingquan, *Surface and Coating Technology,* **148**, 2001, 216, 218.
16. S. Malinov, W. Sha, Z. Guo, C.C. Tang, A.E. Long, *Materials Characterisation,* **48**, 2002, 279, 280.

17. M. Cirakoglu, S. Bhaduri, S.B. Bhaduri, *Journal of Alloys and Compounds,* **347**, 2002, 259.
18. R Felton, 2004. *Metal powder report [online].* Available from www.metal-powder.net [Accessed August 2004].
19. J.C. Huang, T.H. Chuang, *Materials Chemistry and Physics*, **57**, 1999, 203.
20. T. Albrektsson, P.-I. Branemark, H.-A. Hansson & J. Lindstrom, *Acta orthop. Scand.,* **52**, 1981, 155, 165.
21. M.F. Lopez, A. Gutierrez, J.A. Jimenez, *Surface Science,* **482 – 485**, 2001, 300, 301.
22. D.H. Kohn, P. Ducheyne, in: D.F. Williams (Ed.), *Medical and Dental Materials, Serie Materials Science and Technology,* vol. 14, Weinheim, 1992.
23. I. Milosev, M. Metikos-Hukovic, H.-H. Strehblow, *Biomaterials,* **21**, 2000, 2103, 2104, 2107.
24. S. Roessler, R. Zimmermann, D. Scharnweber, C. Werner, H. Worch, *Colloids and Surfaces B: Biointerfaces,* **26**, 2002, 387,388, 389, 390.
25. T.H. The, A. Berkani, S. Mato, P. Skeldon, G.E. Thompson, H. Habazaki, K. Shimizu, *Corrosion Science*, **xxx**, 2003, 1, 2.
26. I. Tsyganov, E. Wieser, W. Matz, H. Reuther, E. Richter, *Surface and Coatings Technology,* **158 –159**, 2002, 318,319, 320.
27. J. Komotori, B.J. Lee, H. Dong, P.A. Dearnley, *Wear,* **251**, 2001, 1239, 1240.
28. Charl Wynand Louw, *The oxidation of titanium and its alloys*, Philosophiae Doctor Thesis, University of the Free State (Bloemfontein), South Africa, 1997.
29. Limin Shao, Luning Zhang, Mohua Chen, Hao Lu, Mingfei Zhou, *Chemical Physics Letters,* **343**, 2001, 178.
30. L. Avalle, E. Santos, E. Leiva and V.A. Macagno, *Thin Solid Films*, **219**, 1992, 7, 8.
31. *Ti oxidation [online].* Available from http://www.timet.com/cor-p04.htm [Accessed June 2004].

32. M. Ask, J. Lausmaa, and B. Kasemo, *Applied Surface Science*, **35**, 1988 - 1989, 283, 293.
33. A. Bellucci, F. Di Pascasio, D. Gozzi, S. Loreti and C. Minarini, *Thin Solid Films*, **405**, 2002, 1, 2, 5, 13.
34. Ulrike Diebold, *Surface Science Reports*, **48**, 2003, 59, 65, 67, 68, 73, 155.
35. Refractory metals [online]. Available from http://www.ultramet.com/oxidation.htm [Accessed 18 May 2004].
36. 26 May 2004. *Oxidation and reduction [online]*. Available from http://www.ilpi.com/msds/ref/oxidation.html [Accessed 20July 2004].
37. J.W. Rogers, Jr., K.L. Erickson, D.N. Belton, R.W. Springer, T.N. Taylor, and J.G. Beery, *Applied Surface Science*, **35**, 1988, 137,139, 145.
38. Wenbin Xue, Chao Wang, Ruyi Chen, Zhiwei Deng, *Materials Letters*, **52**, 2002, 435.
39. Wei Zhou, K.G. Chew, *Materials Science and Engineering*, **A347**, 2003, 180.
40. Roger Nix, 8 June 2003. London. Queen Mary University of London. *An introduction to surface chemistry*. Available from http://www.chem.qmw.ac.uk/surfaces/scc/scat4_2.htm [Accessed 14 October 2003].
41. Francis W. Sears, Gerhard L. Salinger, *Thermodynamics, Kinetic Theory, and Statistical Thermodynamics*, Third Edition, Addison-Wesley, Inc.,USA, 1975.
42. J.M. Walls (Ed.), *Methods of surface analysis*: Techniques and applications, Cambridge University Press.
43. A. Atkinson, *Reviews of Modern Physics*, **57**, 1985, 437,438, 439.
44. Rochelle Concradie, *Oxidation of a segregated MoN layer grown on Fe(100) – 3.5 wt% Mo-N*, Bloemfontein (2001), M.Sc. thesis.
45. D.F. Mitchell, and K.R. Lawless, *J. Paint Tech.*, **38**, 1966, 575.
46. Zu Xiaotao, Wang Zhiguo, Feng Xiangdong, Huo Yongzhong, Lin Libin, Huang Xingquan, Li Yanling, *Surface and Coatings Technology*, **140**, 2001, 161,162, 163.

47. P. Klaus Kuhn, F. Iris Chaberny, Karl Massholder, Manfred Stickler, W. Volker Benz, Hans-Gunther Sonntag, Lothar Erdinger, *Chemosphere*, **53**, 2003, 71, 72.
48. S.H. Maron, and J.B. Lando, *Fundamentals of Physical Chemistry,* Macmillan Publishing Co., Inc.,New York, 1974, 322.
49. W. Mark Zemansky, H. Richard Dittman, *Heat and Thermodynamics*, *Sixth Edition*, McGraw-Hill Book Company, 1979.
50. J. Brindley, J.F. Griffiths, A.C. McIntosh, *Chemical Engineering Science*, **56**, 2001, 2037, 2038.
51. V.I. Bolobov, Combustion, *Explosion, and Shock Waves*, **38**, No 6, 2002, 639,643, 645.
52. R. Evans Ulick, Sc.D., F.R.S., F.I.M., *The corrosion and oxidation of metals: Scientific principles and practical applications*, Edward Arnold (Publishers) Ltd, London, 1960.
53. http://crownminerals.med.govt.nz/minerals/docs/comreports/report16-titanium.pdf.
54. D. Briggs, and J.T. Grant, *Surface Analysis by AES and XPS*, IM Publications, Chichesteter, England, 1998.
55. H.C. Swart, A.J. Jonker, C.H. Claassens, R. Chen, L.A. Venter, P. Ramoshebe, E. Wurth, J.J. Terblans, W.D. Roos, *Applied Surface Science*, **205**, 2003, 231, 233, 237, 139.
56. J.K.O. Asante, W.D. Roos and M.F. Martz, *Surf. Interface Anal*, **31**, 2001, 856, 861.
57. M. Jobin, M. Taborelli and P. Descouts, *Applied Surface Science*, **72**, 1993, 363, 372.
58. H.C. Swart, W.D. Roos, and J.J. Terblans, *Surf. Interface Anal.*, **36**, 2004, 285,287, 289.
59. Joseph Kwako Ofori Asante, *The determination of ternary segregation parameters using a linear heating metho*d, Bloemfontein (200), M.Sc. thesis.
60. R.A. Outlaw, W.S. Lee, S.J. Hoekje, S.N. Sankaran, *Applied Surface Science*, **81**, 1994, 143,145, 148, 150.
61. C.J. Terblanche, J.P. Roux, P.E. Viljoen, H.C. Swart, *Applied Surface Science*, **78**, 1994, 275, 283.